Explicit numerical simulation of non-creeping single phase flow in porous media

Susithra Lakshmanan

Doctor of Philosophy

The University of Edinburgh

2010

To the memory of my late father, Mr.V.Lakshmanan

No words are sufficient to describe his contribution to my life

I owe every bit of my existence to him.

Abstract

Porous media and transport within them play important roles across industries and beyond, including in water and pollutant transport in soils, flow in petroleum and geothermal reservoirs, and water treatment in deep bed filtration to list just a few key examples. The study of such flows has traditionally been dominated by experiment. Simulation is, however, playing an increasing role in this field both because of the advent of X-ray microtomography (XRMT), which now permits the mapping of pore structures down to sub-micrometer resolution, and the ubiquitous availability of powerful compute clusters built on cheap commodity machines. Simulation in this context involves solving for the flow field in a model of a porous solid derived from XRMT – in this sense, the simulations mimic reality and are hence termed by us as explicit numerical simulation (ENS). The particular challenge in doing ENS is correctly solving the flow problem in extremely complex geometries. This challenge has led to the use of various methods such as lattice-gas automata (LGA) and the related lattice-Boltzmann method (LBM), which are particularly suited to resolving flows in complex geometries. All of this work to date has been restricted to low velocity flows termed Darcy flows because of limitations associated with LGA, LBM and other methods. There is, however, a range of applications where higher speed flows are of relevance and hence extension of the ENS approach to higher speed flows in porous media is important. This has been done here using an LGA model that does not include the deficiency of more standard LGA models that restricts them to slow flows. The thesis first details this little-known and used LGA model before demonstrating it on a range of benchmark problems. The model is then used to predict *ab initio* the hydrodynamic properties of a random packing from the Darcy to the turbulent regime. Comparison with experiment is excellent. The approach is then used to study, for the first time to our knowledge, the interstitial flow patterns from the Darcy to turbulent regimes.

Keywords: Lattice-Gas Automata (LGA), Galilean-invariant LGA, single-phase flow, random sphere packing, porous media

Declaration

The work presented in this thesis was carried out in the School of Engineering and Electronics, the University of Edinburgh. I hereby declare that this thesis was composed by me and that the work described within is my own, except where explicitly stated otherwise.

Susithra Lakshmanan

Acknowledgements

I take this opportunity to express my heartfelt gratitude to my supervisor, Professor William J Easson, for his dedicated guidance and support throughout my PhD. Without his tireless effort and invaluable help, this research would never have seen the light of the day.

I would like thank Professor Mark Biggs, for giving the opportunity and allowing me to work in his research group. I also thank Dr. Don Glass and Dr.Jane Blackford for their encouragement and help during those challenging moments.

I wish to record my sincere thanks to all of my colleagues in this research group, especially Dr.Alex Buts for his help in generating sphere packings and helpful discussions, Dr. Milan Mijajlovic and Mr.Richard Layfield for their timely help.
My sincere thanks go to the IT support and ECDF for their technical, 'rescue and recovery' help.

Even though it is not the custom, I take this opportunity to thank my husband for his support and my special thanks go to our kids Sangami and Sudhermi who provided me with constant source of happiness. I also thank my mother and all my family members back home.

I thank all my friends during this period, especially Mr.Nishad Manerikar for his timely help and special thanks goes to Dr.Raja and Mrs Bhuvaneswari Ganeshram and Mrs. Meenakshi Sundaram for their untiring hospitality whenever I visit Edinburgh.

Contents

LIST OF TABLES

LIST OF FIGURES

NOMENCLATURE

V_p volume of pores

V_s volume of solids

V_b bulk volume

μ dynamic viscosity of the fluid

p pressure

q volumetric fluid flow through the medium

ρ macroscopic density of the lattice fluid

u macroscopic velocity

b momentum states at each node

c_i velocity of link i

d_p reduced particle density

b_r rest particles

b_m moving particles

N_i local mean particle populations

c_s speed of sound

$\nu(\rho)$ kinematic viscosity

$g(\rho)$ - Galilean invariance term

N_i local mean particle population of link i

r rate coefficient

P' pressure gradient

K permeability

A and B dimensionless constants

d mean equivalent diameter of the porous matrix

ϕ porosity

υ^f interstitial fluid velocity

Re_k Reynolds number based on the interstitial fluid velocity

ω vorticity

Abbreviations:

BC - Boundary Condition

CFD - Computational Fluid Dynamics

HPP - Hardy, de Pazzis and Pomeau (HPP Model)

FHP - Frisch, Hasslacher and Pomeau (FHP Model)

FCHC - Face Centered Hyper Cubic (FCHC model)

LGA - Lattice Gas Automata

GI-LGA - Galilean-invariant LGA

Chapter 1

Introduction

The phenomena of flow through porous medium occur in diverse environments in nature as well as in science and engineering applications. The process of fluid flow in porous media influence almost all fields of science and engineering such as agricultural, biomedical, ceramic and soil sciences, chemical and petroleum engineering, nuclear reactors and waste effluent management. The examples of relevant technological applications include packed bed and membrane reactors, filtration, high efficiency heat exchangers and porous bearings. Dullien (1992) and Sahimi (1995) presented extensive examples for these applications. The study of flow in porous media plays a crucial role in the design and construction of many state-of-art, high end technological applications like biomedical (e.g. artificial organ systems), alternate energy sources (underground geothermal wells) and nuclear technology (reactors and treatment of waste nuclear effluents).

1.1 Background

A porous medium is a material that consists of solid matrix with an interconnected void. The flow behaviour in porous media is very complex due to interactions between fluid and particles, particles and column wall and fluid and column wall. Flow hydrodynamic parameters, many of which have not yet been completely described, can play a crucial role in determining the design and performance of many

industrial applications. Consequently they gain great importance in the field of research.

1.1.1 Historical developments

In the end of 19th century, engineers and scientists were working to understand the complex interactions between the porous medium and the fluids (Darcy 1856 and Slichter 1899). Darcy's experiments in creeping flow defined the permeability as conductivity to fluid flow in porous material and it is given by the coefficient of linear response of the fluid to a non-zero pressure gradient in terms of the flux induced. This is one of the most important laws governing the flow properties in porous media.

Numerous theoretical and experimental studies have attempted to investigate the performance of fluid flow in porous media. Theoretical estimates of macroscopic rock properties often resulted in error (Bear 1972 and van Genabeek *et al.* 1996). The lack of success of these models may be due to the result of faulty flow models, inadequate representation of pore space or both. Another hurdle in this model is the difficult task of defining the interface between a porous solid and surrounding bulk fluid (Nield 1991).

It is extremely challenging to set up experiments to determine the parameters associated with these models (Vafai *et al.* 1990, Nield 1991, Vafai 1995). They are very expensive and time consuming, and these experiments do not allow us to observe the flow hydrodynamics at microscopic level.

Modelling the porous media and simulating the flow with the use of computers is an alternative means to study the phenomena. They are being increasingly employed now, mainly owing to the rapid advances in the computer technology. They are more economical and faster with the added advantage of flexibility to change the characteristics of the media, fluid or flow.

1.2 Motivation

Flow in porous media is often modelled by Darcy's Law in which the porous medium is characterised by a single transport property, the permeability. This characteristic has long been determined directly using experiments or estimated by solving the Stokes fluid flow problem on structural representations of the media. The advent of relatively inexpensive bench-top microtomography systems in the past decade means the permeability of porous media can now be predicted using the latter approach (Humby *et al.* 2002). The same cannot be said for the multiple transport properties that characterise flows beyond Darcy regime – the Forchheimer and turbulent regimes. Determination of these characteristics and the related problems of identifying the Reynolds Numbers associated with the transitions between the different flow regimes and the heat and mass transfer characteristics are still dominated by experiment.

Many different models of fluid transport in porous media have been described in the literature (Dullien 1992 and Sahimi 1995). These models may be broadly grouped into two categories; continuum and discrete approaches which are described in more detail in the next chapter.

One of the techniques in discrete modelling is Lattice Gas Automata (LGA) which has been used to simulate many different flow situations (Wolfram 1986, Frisch *et al.* 1987, Chen *et al.* 1995, Biggs *et al.* 1998). The LGA model has several advantages. It permits

- fundamental studies not possible via experiment
- identification of engineering closure models
- calculation of associated parameters without extensive experimentation

These greatly enhance the scope for low cost and rapid design of novel and innovative technologies. Biggs *et al* described the LGA as Explicit Numerical Simulation (ENS) as it models all the important phenomena explicitly rather than in a mean field or average way.

We have searched the literature for the application of LGA for flows beyond Darcy regime. Existing literature of LGA based simulation for non-creeping flow through porous medium provides limited information. There were only very few studies that could be identified in this area of research. However, they are rudimentary or simple with very limited details. One of the most advanced studies in this area is LGA model of Tiexeira (1992). Unfortunately the details surrounding the implementation of this model are not available in open literature.

The main aim of this research is to develop a LGA model which could characterise the fluid dynamics of non-Darcy flow region and extend it to study the interstitial flow phenomena. We decided to implement the LGA model of Tiexeira which gains the Galilean invariance with our own coding. The implementation of this Galilean

invariant lattice gas automata (GI-LGA) model of Tiexeira and validation with a variety of benchmark problems is described in the first part of the research. The second part is aimed at *ab initio* predictions of hydrodynamic properties of flow in random packing from Darcy to turbulent regime. The approach is then used to study, for the first time to our knowledge, the interstitial flow patterns from Darcy to turbulent regimes.

1.3 Objectives

The main objectives of the research are as follows:

- To examine the existing single speed two-dimension (2D) and three-dimension (3D) lattice gas automata models for creeping flow simulation and assess their suitability for non-creeping flows.
- Implement the multi speed GI-LGA model of Teixeria for single–phase non-creeping flows.
- Use GI-LGA model to predict ab *initio* hydrodynamic properties of porous media and compare the simulation with existing experimental results.
- Use GI-LGA to characterize non-creeping single-phase flow in porous media.

1.4 Outline of the Thesis

Models of porous media are reviewed in chapter 2. It outlines the development of various modelling approaches for single phase flows in porous materials.

Chapter 3 describes the various types of lattice gas automata methods in detail. It covers the implementation and validation of LGA simulations. The strength of LGA

models is discussed and it also outlines the significant disadvantage of this model; they are restricted to relatively slow flows due to non–Galilean invariance. The method to overcome this issue is also discussed.

Chapter 4 covers the detailed description of Galilean invariant LGA model and its implementation. Validation of GI-LGA simulation is presented. This model is applied to fluid dynamics experiments such as flow between parallel plates and flow past a circular cylinder to validate the system. The results are analysed and compared with literature.

In chapter 5, the GI-LGA model is applied for simulation of single-phase flow in random packing of spheres. Correlations between macroscopic parameters of transport phenomena in porous media are determined. Comparisons of the simulation results with existing literature are presented.

We have attempted to characterize the interstitial flow field for the above simulations (flow in a random packing of spheres) in chapter 6. The study focuses on Darcy, Forchhemier, and turbulent regimes. The effect of averaging and sub-volume size is analyzed.

Chapter 7 summarises all the findings from the above chapters and the conclusions based on the findings of this research is discussed. The areas of improvements and potential extensions of this study is also identified and discussed.

Summary

LGA based explicit numerical simulations (ENS) has been developed substantially and used in the study of fluid flow in porous media. They are often very useful for the fundamental study of systems. It may eliminate the need for extensive experimentation; this will be replaced by ENS simulation and a small targeted experimentation for the purposes of model validation. It will also help to establish the performance of the system at the process level. This ENS method shows a promising future for use in simulation systems with a great potential capability to predict the performance.

Chapter 2

Literature Review

Introduction

The complexity of porous media and the varying properties of fluids flowing through them make it challenging to model such systems and arrive at an analytical solution. Modelling of solid-fluid flows requires methods that adequately define the discrete nature of the solid phase and the interaction between solids and fluids. Numerous models of fluid flow in porous media can be developed from either microscopic or macroscopic properties. This chapter begins with a synopsis of hydrodynamic parameters and brief review of continuum and discrete approaches followed by a review of various models in flow through porous media.

2.1 Hydrodynamic parameters

Properties such as porosity and permeability constitute fundamental macroscopic parameters by which a porous media can be quantitatively described. Other properties and concepts can be developed from these fundamental parameters. Porosity is defined as the ratio of the void space to the bulk volume of the rock multiplied by 100 to express in percent (Craft *et al.* 1997) and it is written as

$$\phi = \frac{V_p}{V_b} = \frac{V_b - V_s}{V_b} \tag{2.1}$$

Where V_p is the volume of pores, V_s is the volume of solids and V_b is the bulk volume.

Permeability is more complex to define. An understanding of fluid flow through porous medium will help to define this property. The motion of fluid can take a variety of forms ranging from simple flows such as laminar flow in a pipe to more complex flows and turbulence. It is described by the basic hydrodynamic formula, the continuity equation

$$\frac{\partial \rho}{\partial t} + \nabla.(\rho u) = 0 \qquad (2.2)$$

and the Navier-Stokes equation

$$\frac{\partial(\rho u)}{\partial t} + \nabla.(\rho uu) = -\nabla p + \mu \nabla^2 u + \rho g \qquad (2.3)$$

where μ is the dynamic viscosity of the fluid, velocity u, density ρ, pressure p and g is the acceleration due to gravity. In the case of stationary flow with very low inertial forces, the left-hand side of equation (2.3) is negligible, and it can be simplified as follows

$$\nabla p - \rho g = \mu \nabla^2 u \qquad (2.4)$$

This relation has great value in theoretical and experimental work related to fluid flows in porous media, where fluid velocities are low.

In the flow systems described by the Stokes equation, the pressure drop is directly proportional to the fluid velocity. The fluid motion is also smooth and regular, i.e. the flow is laminar. In 1856, Darcy first demonstrated the characteristics of fluid conductivity of porous media. The following equation which defines permeability in terms of measurable quantities is called Darcy's law (Dullien *et al.*, 1989; Craft *et al.* 1997, Ramaswamy *et al.* 2004)

$$q = -\frac{k}{\mu} \nabla p \qquad (2.5)$$

where q is the volumetric fluid flow through the medium and k is the permeability coefficient. This permeability is a measure of the capacity of the media to transmit fluids.

The importance of Darcy's law (equation 2.5) is that it governs the Stokesian flow through a porous material and the permeability coefficient, k, contains all the material dependencies. The drag is linearly proportional to the velocity.

By increasing the flow velocity, the flow begins to have instabilities and enters the 'transition' regime. Further increase in flow velocity finally turns the flow into turbulent, in which case it is dominated by inertial forces that produce eddies, vortices and other dynamical fluctuations.

At higher flow velocities, the ratio of pressure drop to velocity gradually deviates from Darcy's law. Any deviation from the Darcy flow is termed non-Darcy flow. To account for the nonlinear behaviour of the flow in porous media, Forchheimer (1901) hypothesized that the pressure drop for flow in a packed bed is a direct result from the viscous (linear in origin) and the inertial (quadratic) effects. The total pressure drop is thus given by Forchheimer empirical flow model is described as

$$\nabla p = au + bu^2 \qquad (2.6)$$

where a and b are constants. Forchheimer's hypothesis has been generally accepted as an extension to Darcy's law for high flow rates (Liu *et al.* 1996).

2.2 Modelling approaches

Continuum modelling is a macroscopic approach. All complexities and fine details of the microscopic pore structure are absorbed into bulk terms like permeability that reflect the average properties of the medium. Sahimi (1990) describes the continuum approach as a model of solving classical equations of transport and reaction, supplemented with constitutive equations describing the effect of structural changes on reaction and transport parameters.

Continuum models are convenient to use and provide a relatively simple way of modelling macroscopic domains and are typically used in the applied analysis and design capabilities. However, accurate solutions to the differential equations only exist for very simplistic systems such as array of spheres (Sangani *et al.* 1982, Schwartz *et al.* 1993), capillary networks (Adler *et al.* 1985) and array of square rods (Alshare *et al.* 2010). This limits the ability of continuum models to accurately study the transport properties of complex porous media.

Discrete models do not have these limitations. The continuum fluid is replaced by discrete fluid elements and the transport behaviour of the continuum fluid is applied to each fluid element. They model the pore space explicitly to a greater or lesser extent. The best known examples include pore network models in 2D (Dadvar *et al.* 2001) and 3D (Dadvar *et al.* 2002), full simulation flow on digitised or reconstructed pore space (Ferreol *et al.* 1995, Okabe *et al.* 2004, Dong *et al.* 2009) and explicit numerical simulation (Biggs *et al.* 2003) .

2.3 Models of porous media

2.3.1 Capillary models

This model defines pore space as collection of tubes. It can be in a series manner or a parallel-flow bundle of capillary tubes. This is the first model to explicitly capture geometric features of the pore space (Spielman et *al.* 1970 and Yao *et al.* 1971). The radius of the tubes can be the same for all or selected from a pore size distribution. The capillaries may be polygonal (Constantinides *et al.* 2000) or chamber-and-throat type segments (Avraam *et al.* 1995). In order to develop relations between permeability and some gross parameters of medium geometry, enormous effort has gone into assigning the pore size distributions of real samples to the capillaries (Indakm *et al.* 1991).

Capillary models are popular because fluid transport within them is easily modelled using classic continuum equations such as the Hagen-Poiseuille equation (Bryant *et al.* 1993). These models are being increasingly employed in wide variety of situations. Holm *et al.* (2010) developed a pore-scale model comprising of a bundle of cylindrical capillary tubes in a three phase system. They have used two different approaches to simulate the fluid flow. On the pore-scale they studied the fluid displacement and relative permeability whereas the capillary pressure functions were derived by continuum scale.

In general, capillary models have limitations in addressing the important parameters of porous media like interconnectivity of the pores, the existence of pore loops of various extents, etc. As a result, these models are not widely used to simulate complex fluid flow in porous media.

2.3.2 Spatially-periodic models

In these models, the pore space is represented by a periodic structure which is repeatedly transposed onto a lattice.

Periodic structures that have been used include spheres (Zick *et al.* 1982, Nitsche *et al.* 1989 and Ogata *et al.* 2010), cylinders (Sangani *et al.* 1982, Graham *et al.* 2002 and Krish, 2006), elliptic rods (Saito *et al.* 2006) and other more sophisticated structures such as Menger sponges and grooved channels (Bekri *et al.* 1995 and Chen *et al.* 2004). These models attempt to mimic the properties of the system in some average way and the transport properties are analysed.

Spatially-periodic models were extensively reviewed by Nitsche *et al.* (1989) and Sahimi (1993). They have two major disadvantages. The first is the fact that they model flow around objects rather than through pores. The second is that regular arrays of spheres are limited to achieve relatively low solid fractions; hence, they have difficulty in representing consolidated media.

2.3.3 Bethe lattice models

These are branching network models. Bethe lattices have been used routinely in the statistical mechanics literature for investigating critical phenomena in the mean-field approximation. Bethe lattices for modelling transport in porous media were first used by Liao *et al.* (1969) and Torelli *et al.* (1972). Others have also used it to model transport and reactions in porous catalysts (Sahimi *et al.* 1990), transport properties of porous polymer membranes (Quartarone *et al.*

2002) and phase equilibrium of fluids in porous media (Sokolovskii *et al.* 2003). Even though Bethe lattice models contain interconnected branching network spaces that can mimic pore space, they have a few shortcomings in terms of modelling flow in porous media.

Firstly, they lack closed loops of spaces. The distribution of pores and connectivity are not truly random, both of which are very important element in the topology of porous media. Secondly, the void space appears to increase from the centre to the external surface. This sometimes leads to anomalous phenomena such as those discussed by Hughes *et al.* (1982) who investigated diffusion processes on a Bethe lattice.

2.3.4 Network models

In network models, fluid paths in porous medium may branch and later, join one another. These paths, which represent either pore bodies or pore constrictions, connect pore spaces of negligible volume. Different kinds of network have been implemented including regular polyhedron (Ameri *et al.* 1993), irregular, random networks such as Voronoi network (Jerauld *et al.* 1984), random percolation lattices (Adler *et al.* 2000), cubic net work (Lock *et al.* 2002) and sphere (Øren *et al.* 2002).

The network models are used in computer simulations of flow phenomena in porous media. Transport in network models is usually solved analytically, for example, the etched glass network model to study displacement processes in

porous media (Davis *et al.* 1968) and effective medium approximation (Sahimi 1992, Andrade *et al.* 1995 and Beyne *et al.* 2001).

Various techniques of 2D and 3D network models of porous media were reviewed in detail by Dullien (1992). Indakm *et al.* (1991) and Burganos *et al.* (1992) have solved transport in network models numerically by resolving the motion of individual fluid particles. These network models are very good tools for prediction of percolation properties of macroscopic systems, for example solute transport in porous media (Goldsztein, 2007). However, they offer little physical information regarding interactions at a microscopic level.

2.3.5 Computational fluid dynamics (CFD)

CFD has been developed mainly around using numerical techniques to solve the Navier-Stokes equation. These equations do not directly describe the actual real gas of particles but rather the mean dynamics of the mass, momentum and energy densities.

Finite difference and finite element methods have been extensively used for simulating single-phase and two-phase flow in porous media. In the standard CFD technique, given a set of suitable boundary conditions it is possible to solve the Navier-Stokes equations on a grid. This approach starts from governing partial differential equations (PDE's) discretizing them by finite difference, finite volume or finite element methods.

Once the finite difference equations are set up, they are usually solved by an iterative method and all iterative techniques have to solve a large set of linear

equations. Finding an adequate approximation to the Navier-Stokes equations has proved to be an extremely difficult one (Roache, 1976). This leads to a diverse array of numerical instabilities and artefacts which often make it difficult to assess the accuracy of the simulation results.

These methods use floating point numbers to describe the properties and hence, the required computer memory for a realistic simulation will be large. Therefore, most applications of the finite difference method to flow through microscopic porous media have been limited to solving time-independent Stokes equation in single-phase systems (van Genabeek *et al.* 1996).

$$\nabla . u = 0$$

$$\nabla P = \mu \nabla^2 u$$

where u is the local velocity of the fluid at any particular point within the pore space and P is the pressure.

Manwart *et al.* (2002) studied flow through three-dimensional porous medium on a microscopic level for slow laminar flow. Stokes equation for straight tubes and cubic arrays were used and the Reynolds numbers were smaller than unity in their analysis. Time-dependent Stokes problem using an iterative pressure-correction algorithm was used. Calculated transport parameters were compared with the experimental results that are obtained from computerized tomographic imaging and found to be in good agreement with the experimental value.

Saenger *et al.* (2007) used the finite difference method for pore-scale simulation of elastic wave propagation in digital rock samples. Digital rock methodology is used to

combine the modern microscopic imaging and numerical simulation of the physical properties of rocks. Slow wave propagation in a porous medium saturated with a viscous fluid is analyzed and demonstrated as an alternating solid and viscous fluid layers.

Kim *et al.* (2009) investigated the momentum transfer parameters in laminar pulsating flow through porous media. The porous media were made of periodic arrays of squares and cylinders. Two-dimensional velocity and pressure variations were obtained by solving the Navier–Stokes using the computational fluid dynamics tool, CFD code FLUENT 6.3

2.3.6 Molecular dynamic simulations (MD)

At the molecular scale, the discrete atoms or molecules make up a fluid and this is one of the obvious ways to simulate a small-scale fluid system on a computer. Then, with correct descriptions of the inter-molecular interactions, the system should behave as a fluid (Dupuy *et al.* 1978). This approach is called molecular dynamics and is often used in many research areas like material science (Herzyk *et al.* 1991, Rapaport, 1997, Rapaport, 2003); biological processes(investigation of the physical mechanisms at atomic level, Grayson *et al.* 2003); and in nanotechnology(biological activities such as transportation of water across the nanochannels, Fang *et al.* 2008). The significant advantage of MD simulation is that different situations can be handled by changing the average energy of the molecules and their separation.

The MD approach obviously requires extremely large computer resources. At every time-step, the new position and velocity of all particles is calculated from the

knowledge of previous position and velocity, taking into account any external forces which are acting on them. In order to calculate the particles new trajectories, any particles which are collided during the previous time-step have to be identified first. The complexity of this interactions in MD can be restrictively time consuming even for a very small volume of fluid. Therefore, the MD approach to macro scale porous medium flow is prohibitive. Even if we consider gas, which contains fewer molecules than fluid, with larger time-step, still the number of molecules for simulation and the required memory in computer makes this model too restrictive to employ it in a large scale.

2.3.7. Lattice gas and lattice Boltzmann methods

Cellular Automaton initially developed by Ulam and Neumann (Schrandt *et al.* 1970) at Los Alamos National Laboratory, was first successfully used to simulate fluid dynamics by Hardy *et al.* in 1976. Lattice gas automata models consists of a lattice whose sites, the intersection points of the lattice can take a finite number of states (Wolfram 1986, Wolf-Gladrow 2000). The lattice is populated by particles. The presence or absence of particles is described by Boolean variables (its value is 1 if there is a particle and 0 if not). The evolution of the particles consists of two steps: (1) set of collision rules, the particles collide and the total number of particles and the momentum do not change (2) a propagation step, each particle hops to a neighbouring site in the direction of its velocity.

Lattice gas methods solve microscopic equations for moving and interacting fluid particles on a discrete lattice. Microscopic model with the appropriate choices of

parameters can recover the desired macroscopic PDE's by using multi-scale analysis (Frisch *et al.* 1986).

Initial lattice gas methods suffer two important disadvantages in the simulation of fluid flow: statistical noise due to Boolean operations and lack of Galilean invariance. Galilean invariance, in general terms, is a principle which states that the fundamental laws of physics are the same in all inertial frames of reference. For fluids it means that a frame of reference moving at a constant velocity υ is equivalent to inducing a uniform flow of $-\upsilon$ in the observed flow filed u. In practice, the lack of Galilean invariance results in vorticity moving in opposite direction to the bulk movement of fluid. The problem of Galilean invariance is discussed in section 3.4

Lattice Boltzmann methods (LBM) were developed to overcome the disadvantages of LGA. McNamara *et al.* (1988) introduced LBM for simulating complex flow problems. This model is updated in the same manner as the lattice gas model except that, instead of working with individual particles, it works with its mean value which is no longer a Boolean variable.

Due to the following remarkable characteristics of the LGA (Rothman *et al.* 1997; Biggs *et al.* 1998) and LBM (Chen *et al.* 1998), they are suited for more complex problems.

- The algorithm is completely stable, a feature derived from the absence of round-off. If a semi-detailed balance is satisfied in some sense, a free system initially not in equilibrium will always relax towards equilibrium in a monotonic manner and remains steady (Frisch *et al.* 1987).
- Unlike most continuum approaches, LGA naturally includes spontaneous mesoscopic fluctuations which are known to be important in many processes

including turbulence (Frisch *et al.*1990), phase change (Karapiperis, 1995) and reaction (Boon *et al.* 1996).

- Initial LGA models were restricted to slow flows. However, advances in LGA models overcome this problem by gaining Galilean invariance and therefore can be used to explore the inertia and turbulent regimes.
- The implementation of the solid-fluid boundary conditions is particularly straightforward and it does not increase the computation cost significantly. Hence these models are much more suitable for simulation of flow in porous media than conventional CFD methods.
- They can run faster on a computer than a MD simulation due to the local nature of the collision rules. The state of the fluid needs to be known only at the lattice sites and only at discrete times. They have another advantage over MD that these methods are highly parallel (Buick, 1997).
- They can be easily extended to multiphase flow simulations (Rothman *et al.* 1988, 1994; Appert *et al.* 1990). A second or more fluid component can be added to the model by the addition of fluid particles that posses different fluid properties.

LGA has been applied to a wide range of problems including single and multiphase flow (Rothman *et al.* 1994), within complex geometries such as porous media (van Genabeek *et al.* 1996), chemically reacting flows (Boon *et al.* 1996 and Chen *et al.* 1995) and heat transfer (Chen *et al.* 1989).

Frisch, Hasslacher and Pomeau (1986) developed the LGA model using the hexagonal lattice (FHP model). This was soon followed by 3D LGA model

(d'Humières *et al.* 1986) and several studies confirming LGA's ability to reproduce the correct hydrodynamic behaviour both qualitatively and quantitatively (d'Humières *et al.* 1986a, 1987 and Shimomura *et al.* 1987).

2.4 Application of LGA to flow through porous media

Flow through porous media is one of the most popular classes of problem to which LGA has been applied. This is primarily because Lattice gas methods can easily handle very complicated geometry and boundary conditions. Furthermore, unlike many other methods it solves the full Navier-Stokes equations rather than some potentially restrictive subset such as Stokes law (Adler *et al.* 1990) or Hagen-Poiseuille flow (Bryant *et al.* 1993). The majority of studies have concentrated on the development of LGA as a tool for permeability prediction. These studies were motivated by the fact that experimental determination of permeability can be extremely time consuming and limited to relatively small samples compared to the real-world applications (van Genabeek *et al.* 1996).

Advances in fluid mechanics and computer technology made it possible for accurate calculations of microscopic flow to be practicable in arbitrarily complex pore-space geometry. This heralded the application of LGA techniques to flow through porous media (Rothman 1988 and Margolus *et al.* 1986).

The potential application of LGA to model flow through porous media were first examined by Balasubramanian *et al.* (1987), obtaining Darcy's law from flow in a 2-D channel in the presence of randomly-distributed point scatterers. Rothman (1988) studied single-phase flow in what could be truly termed 2-D porous media,

comprising distributions of rectangular blocks of solid. The complex geometry of the porous media was simulated by placing solid obstacles of specific shapes in the fluid and imposing a no-slip boundary condition on all nodes within this boundary. He confirmed that Darcy's equation can be applied and verified on a more realistic two dimensional porous media and visualisation of his simulations showed excellent qualitative flow characteristics.

Following Rothman's findings, several works focused attention on demonstrating LGA's suitability for single-phase flow in 2-D porous media, using a variety of representations of porous media: arrays of cylinders (Brosa *et al.* 1991 and Sahimi *et al.* 1991), constricted channels (Kohring,1991a-b), arrays of rhomboids (Kohring,1992) and arrays of cruciforms (McCarthy, 1994). Gao *et al.* (1994) manipulated the location and density of point scatterers (similar to the technique used by Balasubramanian *et al.* 1987) to simulate flow through 2-D heterogeneous porous media.

The first 3-D studies of flow through porous media were carried out by Chen *et al.* (1991). They applied a basic Face centered hypercubic (FCHC) model to simulate flow through randomly-generated porous media having a fractal distribution of small to intermediate scale features (less than $\approx$ 100 μm) and a log-normal distribution of larger features. They reported only qualitative findings that both the pressure and velocity distributions within the media were typical of real systems. Later, Knackstedt *et al.* (1994) studied the effect of the pore structure on the flow properties of 3-D porous media using LGA.

Chen *et al.* (1991) combined LGA simulations with an accurate representation of a porous medium and compare permeability with experimental results to provide a realistic measure of the LGA technique's performance. They simulated flow through 2-D porous media generated from digitized photographs of 2-D sections of sandstones. The LGA results were within 5% of the experimental data which itself had associated with a 10% uncertainty.

Chen *et al.* (1991b) used the 2-D LGA model for hydrodynamic calculations. This method employed interactions of discrete fluids on a regular lattice analogous to microscopic molecular dynamics. It demonstrated that a complex system can be simulated by simple rules of particle interactions at a lattice. By averaging over a spatial and temporal space, macroscopic variables are recovered.

Chen *et al.* (1991c) studied the variation of the Forchheimer equation parameters as a function of Reynolds number using the 2-D LGA model.

Summary

This chapter provides an overview of the development of various models of fluid flow in porous media. The most popular models reported in the literature are summarised. The reviews highlight the advantages and disadvantages of current models of porous media and fluid transport within them. Numerical simulations are increasingly used in the study of fluid flow in porous media. They demonstrate that the models selected for use in this study, namely the LGA simulation techniques for fluid transport, offer several advantages over the other methods discussed here.

Advantages of the LGA technique:

- "Costly" floating-point calculations may be replaced by fewer Boolean and/or table-lookup operations.
- Each point in space demands significantly less memory than traditional numerical techniques.
- Boundary conditions are easily and simply applied even for complex geometries such as those found within porous solids.
- Provided physical laws are correctly modelled, LGA resolves and tracks interfaces between different phases without any special or extra effort.
- The algorithm is completely stable.
- Spontaneous mesoscopic fluctuations are naturally included.

Further description of these LGA models and their implementation is discussed in the following chapter.

Chapter 3

Lattice Gas Automata models

Introduction

Lattice gas automata (LGA) are a class of cellular automata that have been applied to a wide range of problems in materials science and physics. The first LGA based fluid flow simulation was developed by Hardy *et al* (1976) which used square lattice. The fundamental principle governing the LGA model is that the particles are restricted to move on the nodes of a regular lattice and the automaton updates the state of particles in discrete time-steps. Zanetti (1989) defined lattice gas automata as the state of particles of gas that occupy a node in a regular lattice; the state of each node at any time is determined by its own state and the state of a set of neighbouring nodes at previous time step.

In this chapter the first section describes the details of standard LGA which covers the evolution of particles on the lattice gas models and various types of lattice gas models. The next section details the implementation of LGA and the advantages of LGA based explicit numerical simulation (ENS) modelling of flow in porous media. The third section provides discussion of a significant restriction of LGA model and how to overcome this issue by extending the LGA to gain Galilean invariance.

3.1 Description of the LGA model

In modern hydrodynamic lattice gas models, mesoscopic particles of unit mass and velocity move between the nodes of a regular lattice in discrete time-steps. As all the particles move with unit speed, mass and energy conservation are therefore

synonymous. The basic automaton evolves in two stages, the collision and propagation, each of which is implemented at each time-step.

During the collision stage, the lattice particles arriving at each node collide and exchange momentum according to pre-set rules in which the total mass and momentum of the lattice particles at each node are conserved. These collisions occur simultaneously at all nodes on the lattice. The local nature of the rules means that a node needs to "know" its own state prior to collision to update. In the propagation stage, the particles move with their new post-collision momentums to neighbouring nodes on the lattice in preparation for the next time step.

The collision phase of each time step is the process of transformation between the input and output states of the lattice nodes under a set of collision rules (Frisch *et al.* 1987). The collision rules are expressed by the Boolean variable. They define the relationship between the input and output states of a node and satisfy the requirements of collision rules, i.e.

- conserve mass and momentum
- avoid spurious conservation of mass and momentum
- be invariant under all transformations that preserve the velocity set
- conserve the probability of collisions; the probabilistic collision procedure obey semi-detailed balance, with each outgoing state allowed by the conservation laws sampled with equal probability.

The basic collision rules and its implementation can be better explained by a 2D FHP (Frisch, Hasslacher and Pomeau) model of lattice gas automata (described in detail below). This model is made up of hexagonal lattice. Each node has 6 non-zero

momentum directions and each link of the hexagonal lattice may at most carry one particle (of a given mass/momentum/energy state) at any one time. This is called the exclusion principle. An exclusion principle is usually imposed; insisting only one particle is allowed to travel in each direction along a link. As a consequence, each direction of the node on the lattice can be described by a single bit (0 for no particle, 1 for a particle) giving $2^6 = 64$ possible input configurations per node of lattice. It helps in reducing the memory requirements. The particles of fluid on a hexagonal lattice are shown in Figure 3.1

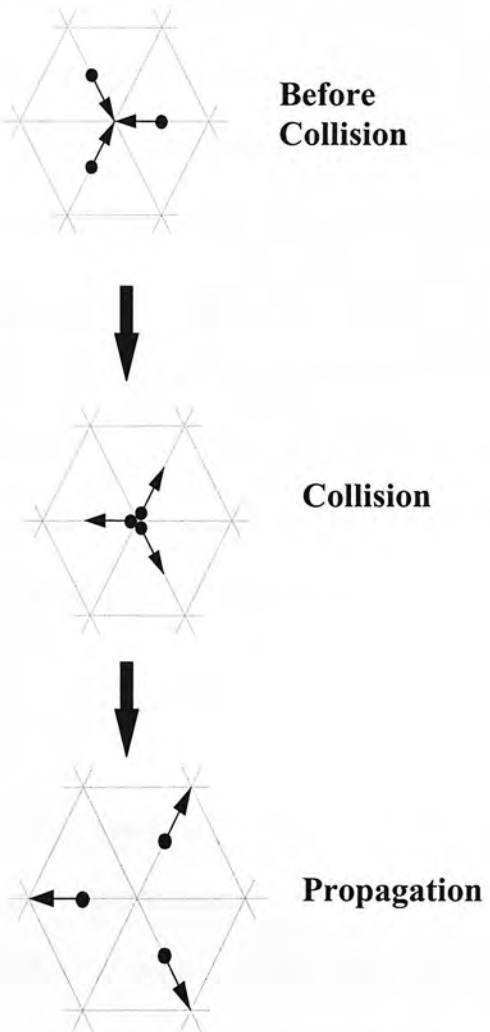

Figure 3.1. One time-step in FHP model (based on Frisch *et al.* 1987).

In the above figure, each arrow represents a particle of unit mass moving in the direction of the arrow. In collision stage, the particles arriving at a node collide according to collision rules (illustrated by figure 3.1). Next is the propagation stage in which the particles emerging from collision move along their momentum directions to neighbouring nodes of the lattice, in preparation for the next time-step.

3.2 Types of Lattice Gas Models

In the bulk phase of a simple fluid, the particles in the fluid are free to move in any direction with equal probability at the microscopic level (Biggs *et al.* 1998). In order to recover similar behaviour in simulations, the lattice must be a regular and must have sufficient rotational symmetry. There are only two types of lattices used in a two dimensional model; regular square and hexagonal lattice.

Lattice gas models are characterized by the structure of the lattice, particle velocities and collision rules. The following are the examples of the 2D models, most of them are named after their developers, the HPP model (Hardy, de Pazzis and Pomeau), the FHP models (Frisch, Hasslacher and Pomeau) which consists of FHP-I, FHP-II and FHP –III, and Face-Centred hypercubic (FCHC) model.

3.2.1 HPP Model

The first lattice gas model was introduced by Hardy, De Pazzis and Pomeau (HPP, 1976).This model is built on a square lattice. The exclusion principle is applied so that no more than one particle is allowed to travel in each direction along a link. This means that a maximum four particles per node can arrive at any time step which is shown in the following figure

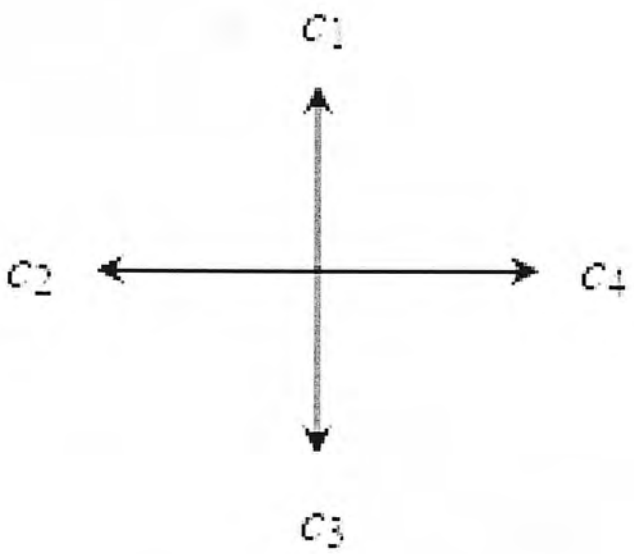

Figure 3.2. Velocity vectors in HPP model (Hardy *et al.* 1976).

The particles are restricted to travel on the links, $c_i, i = 1,....4$, as shown in Figure 3.2, which are represented numerically as follows

$$c_i = \sin[\frac{\pi}{2}(i-1)]i + \cos[\frac{\pi}{2}(i-1)]j$$

The particles entering a node collide according to the collision rules as shown in figure 3.3. It may be noted that all the incoming configurations are shown on the left hand side of the figure, the particles then collide and their velocity vectors are rearranged in such a way to conserve mass and momentum to give the outgoing configuration as shown in the right hand side of the figure. This means the sum of the momentum within any row or column of the square lattice is conserved.

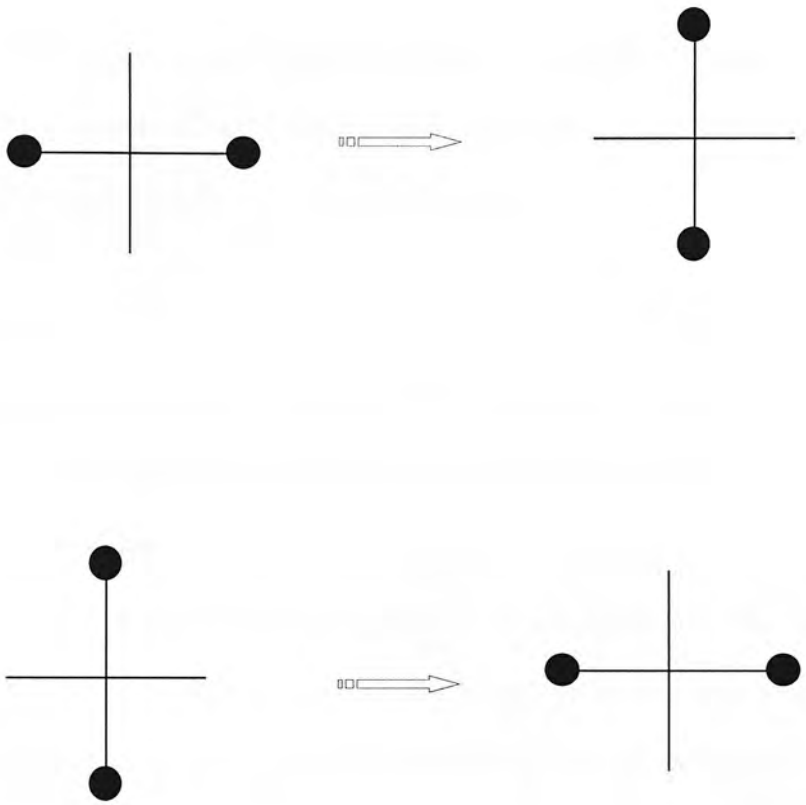

Figure 3.3. HPP model: Collision rules.

For any other configuration, the particles retain their incoming velocities and continue travelling in a straight line. Hence only two out of the sixteen (2^4) pre-collisional state results in different post-collisional state and this is not very effective from the point of momentum transfer. They also yield anisotropic hydrodynamic equations that are not invariant under global spatial rotation (Rivet *et al.* 2001).

This HPP model does not possess sufficient symmetry for the fluid dynamical equations to be isotropic. The number of particles parallel and orthogonal to a lattice axis does not change by collisions or propagation. This creates additional artefact by

spuriously conserving momentum along each row and column of the lattice which limits its usefulness in the study of real fluids (Frisch *et al.* 1987). This anisotropy is unacceptable for a model of fluid dynamics and it necessitates the use of different lattice for simulation of fluid flow in most circumstances.

3.2.2 FHP models

In 1986, Frisch Hasslacher and Pomeau (FHP) introduced a variant of the HPP model using a regular hexagonal lattice. The main innovation of this FHP model was the change of underlying lattice to a 2D triangular lattice which has sufficient symmetry. The fundamental principle of FHP is six possible non-zero particle momentums at each node in a hexagonal lattice and governing collision rules. Another great advantage in this model is introduction of 'rest particles'; a zero velocity particle can be added in the hexagon and this is able to take part in a collision with the particles arriving at the node. The basic FHP models are classified as FHP-1, FHP-II and FHP-III depends on the number of rest particles.

The non-zero momenta corresponds to the six link directions $c_i, i = 1,....6$, shown in figure 3.4 which are represented as

$$c_i = [\cos\frac{\pi}{3}i, \sin\frac{\pi}{3}j]$$

As with the HPP model each of the particles travels with unit speed and the exclusion principle is applied to allow each link to carry only one particle at any one time step.

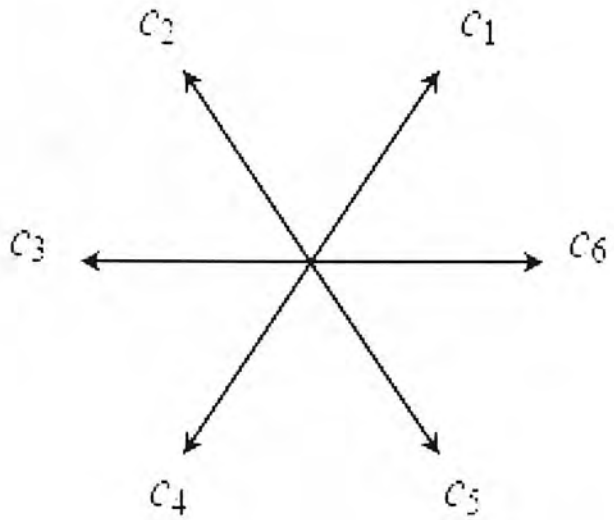

Figure 3.4. Velocity vectors in FHP model (Frisch *et al.* 1986).

A set of collision rules on a hexagonal lattice is shown in figure 3.5 and 3.6, where small filled circles represent the non-zero momentum particle and large empty circles represent a rest particle at the node. The collision rule conserves both particle number and momentum at each node.

FHP-I model

The simplest of the FHP models is FHP-I (Frisch *et al.* 1986) in which each node have six possible moving particles. The collision rules for this model are illustrated in figure 3.5 (a) and (b). This gives a total of 5 collisions among the $2^6 = 64$ possible in-states.

Two particles coming from opposite directions in figure 3.5(a) undergo a binary collision with outgoing configurations rotated by $\pm 60^\circ$.

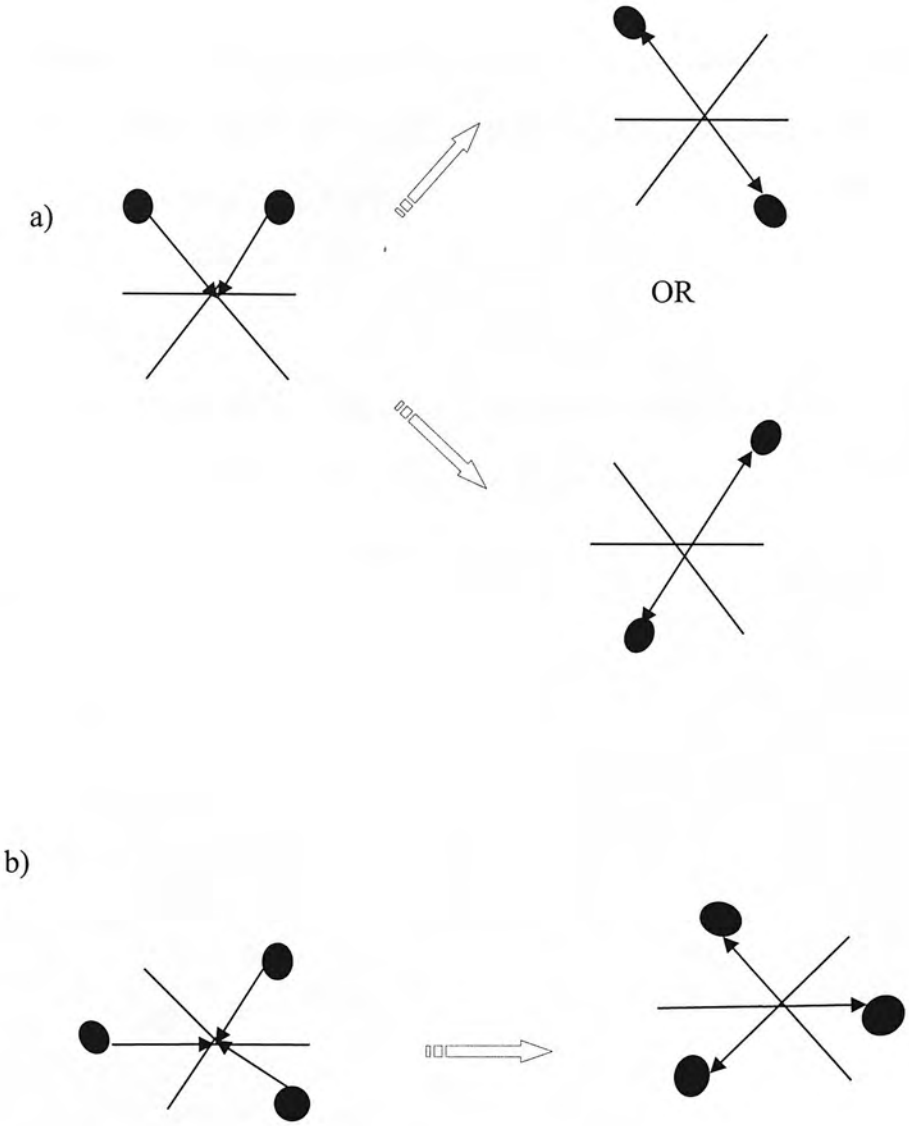

Figure 3.5. Collision rules for FHP-I model.

This is similar in the case of symmetric three-body collisions which are shown in figure 3.5(b) and also it should be noted that there are two possible outcomes of the binary head-on collisions, each selected with equal probability. If the selection process is done using a random number generator, then the collision rules are called non-deterministic.

Although the FHP-I model had been used in the past (Frisch *et al.* 1986), variations on this model with an additional rest particle have proved far more popular models (d'Humieres *et al.* 1986, 1987) .

FHP-II Model

The FHP-II model is a variant of the FHP-I model in which a rest particle is introduced in addition to six moving particles of FHP-I. The additional collisions are explained in the following figure.

c)

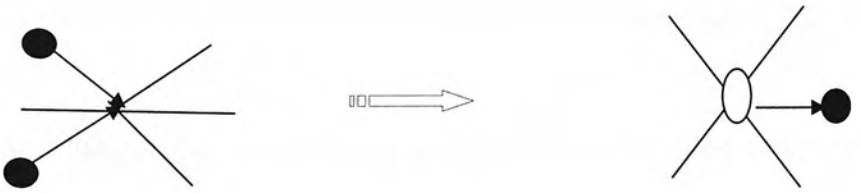

d)

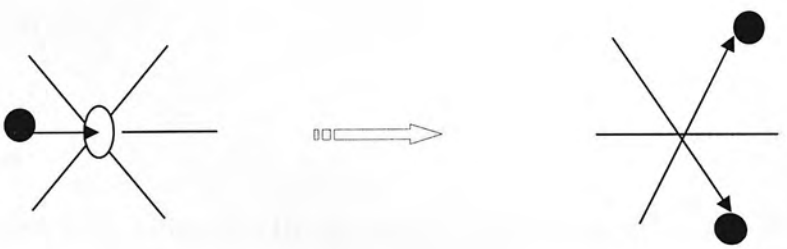

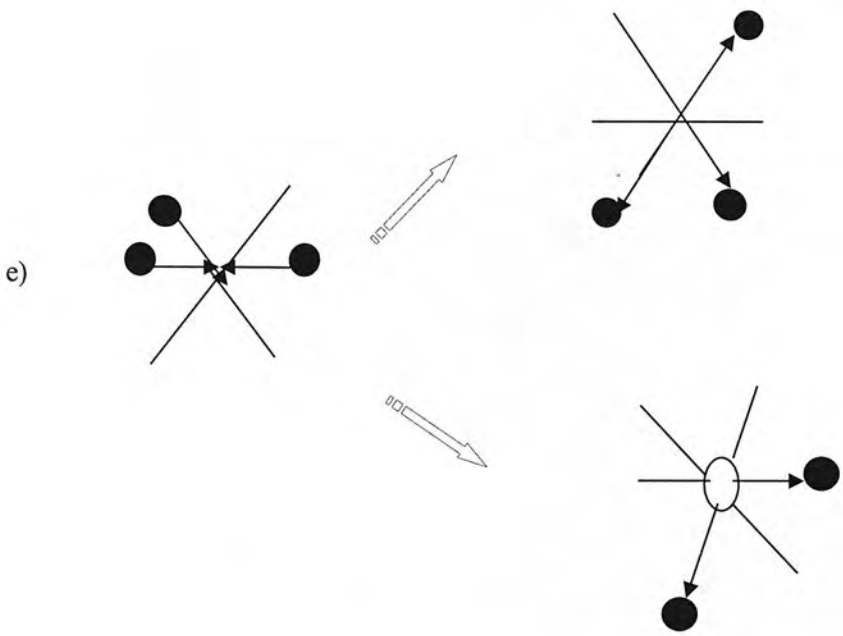

Figure 3.6. Additional collision rules for FHP-II model.

The collision rules for this model result in the following possible collisions; five FHP-I collisions (figure 3.5 a & b); six rest particle creation collisions (figure 3.6c), six rest particle destruction collisions (figure 3.6d) and the five FHP-I rules with spectator rest particle (figure 3.6e). This gives 22 possible interactions out of a possible total of 128.

FHP-III Model

A further variant in this class is FHP-III model (Frisch *et al.* 1986, D.d'Humieres *et al.* 1987) which allows as many collisions as possible under the constraint of mass and momentum conservation at each node. This model has all the FHP-II collisions

with additional collisions that are shown in Figure 3.7. This gives 76 possible collisions out of 128 possible states.

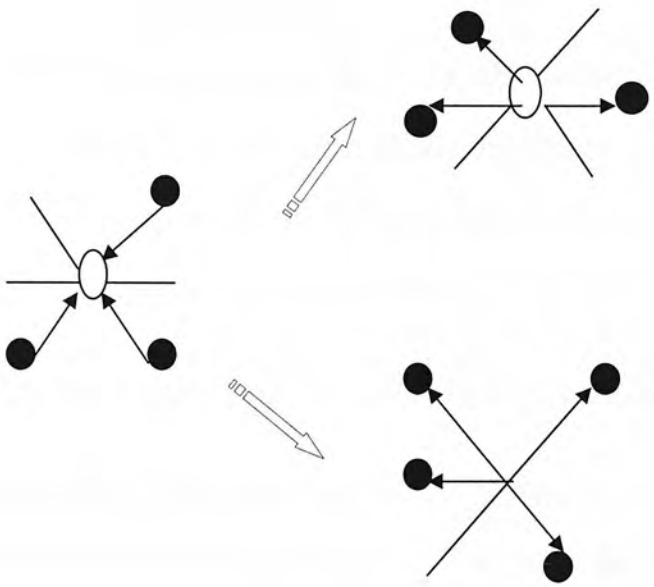

Figure 3.7. Additional collision rules for the FHP-III model.

3.2.3 Three-Dimensional Models

Many phenomena of fluid dynamics are not amenable to a two dimensional description (e.g the onset of three-dimensional turbulent flow) which created the need for lattice gas models with higher dimensionality (Rivet *et al.* 2001). In three-dimensional models there are three regular lattices named simple cubic, body-centred cubic and face-centred cubic. However, none of these models have enough rotational

symmetry to ensure macroscopic isotropy (Frisch *et al.* 1986). This problem was overcome by d'Humieres et al (1986) who modelled 3D fluid dynamics on a 4D face-centred hyper cubic (FCHC) lattice, projected into 3D space.

FCHC Model

The FCHC model resides on an ordinary 3D cubic lattice with the velocity structure is maintained with unit periodicity in the fourth direction. Such a lattice is shown in figure 3.8. Each node is connected to its 24 nearest neighbours by the set of vectors $c_i, i \in \{0,1,..,23\}$ and this can be represented as

$$(\pm1,\pm1,0,0),(\pm1,0,\pm1,0),(\pm1,0,0,\pm1),(0,\pm1,\pm1,0),(0,\pm1,0,\pm1),(0,0,\pm1,\pm1).$$

This model gives two groups of eight totalling 16 vectors for regular four-dimensional hypercube and the third group 8 vectors in the direction of the centres of the faces of that hypercube (hence, it is called FCHC).

The larger number of possible states for each site ($2^{24} = 16 \times 10^6$ configurations) leads to much smoother (less noisy) hydrodynamics than the 2D models. Unfortunately this also makes the generation of the collision rules much harder. This is the only available hypercube for LGA simulations which posses good rotational symmetry and yields microscopic isotropy.

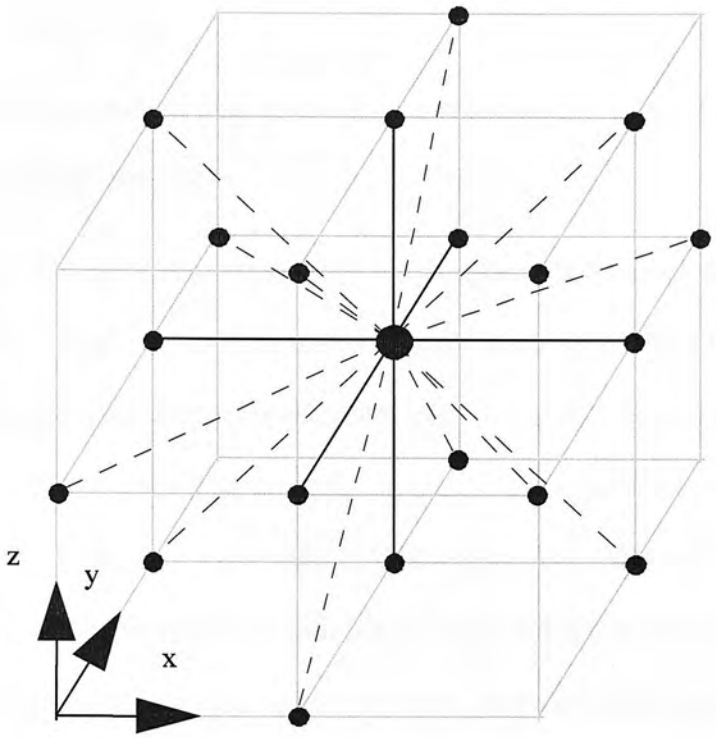

Figure 3.8. Connectivity of pseudo-4 dimensional FCHC lattice (after Frisch *et al.* 1987).

3.3 Implementation of the LGA algorithm

Our LGA algorithm is coded using C++ and it is written in an object-oriented manner. Both the 2D and 3D LGA algorithms were implemented. The 2D simulations were carried out using the FHP-II and FHP-III models. In 3D, the 24bit FCHC model was used. The code produced is easily reusable and some part of the code written for the FHP models has been reused in the FCHC code.

The following section discusses the key issues surrounding the implementation of 2D and 3D LGA model.

3.3.1 Storage of information

There are two strategies which may be adopted for storing the state of each node; site-per-word and bit-per-word storage.

The site-per-word strategy (Brosa et *al.* 1989 and Stauffer, 1991) uses one complete integer variable (or "word") to store the information for each node, so a FCHC lattice of side L will require L^3 words to store the states of all the nodes. The collision stage for site-per-word strategy uses look-up collision tables; each possible configuration for a node will have a unique integer word to describe it. As all the information for one node is stored as one integer, deterministic collision rules may be implemented by the use of a simple array containing pre-generated post-collision states for every possible node configuration. The collision stage is implemented by simply "looking-up" the post-collision state for each node. The propagation stage however necessitates large numbers of bit shifting and masking operations to extract bits relating to particle momentum states and pass them to neighbouring nodes, thus increasing the time required for simulation.

This means of storage is also inefficient in terms of the memory required to store the whole lattice. For the single phase FHP-III implementation 11 bits (7 particle momentum states, 3 kohring algorithm bits, and 1 bit for the solid state) are required to completely store the information for a node and this is stored as a C++ short integer variable which is 16 bits long. For every 11 bits required to store node information, 5 bits are unused and are therefore wasted. For FCHC model, 25 bits are required (24 particle momentum states, and 1 for the solid state), and this is stored as

a long integer variable which is 32 bits long, wasting 7 bits of storage for every node on the lattice.

The alternative strategy is bit-per-word storage where the complete description for each node is spread bit-wise across a number of words, with each word being part of an array designed to hold only one particular momentum state or piece of information. This utilises every bit of every word and is therefore far more efficient in terms of total memory required to store the lattice. In addition the propagation stage simply becomes a matter of shifting the addresses in each array which is faster than the operations required for the same stage using site-per-word storage.

However, the collision stage may not be implemented by simple collision tables; Boolean operations are required to generate the post-collision states. This has been shown to be very fast and efficient for simple 2D lattice gases (Kohring, 1991a-b, 1992), but a prohibitively large number of Boolean operations are required to calculate collisions outcome in 3D models (Biggs et *al.* 1998).

This leaves site-per-word storage as the only realistic method of storing the lattice with the FCHC models. The computational advances in recent years have provided massively larger amounts of memory; hence inefficient memory usage is not as important problem as it was a few years ago. To ensure homogeneity between the 2D and 3D models, site-per-word storage method is used in all our simulations.

3.3.2 Initialisation of the lattice

The macroscopic density ρ of the lattice fluid with b momentum states at each node is related to the local mean particle populations N_i with corresponding velocity c_i by

$$\rho = bd_p = \sum_i N_i \tag{3.1}$$

where d_p reduced particle density.

The macroscopic momentum of the lattice fluid is related to the following:

$$\rho u = ubd_p = \sum_i N_i c_i \tag{3.2}$$

The distribution of these N_i at equilibrium is described by the Fermi-Dirac distribution (d'Humieres *et al.* 1987 and Frisch *et al.* 1987):

$$\mathrm{N_i} = \frac{1}{1+\exp(\mathrm{h}+\mathrm{q}\cdot\mathrm{c_i})} \tag{3.3}$$

where h and q are non-linear functions of u and ρ. If we take the case with rest particles, b_r and moving particles, b_m such that

$$b = b_r + b_m, \quad \rho_m = d_p b_m, \quad \rho_r = d_p b_r, \quad \rho = \rho_r + \rho_m.$$

A first order expansion of (equation 3.1 and 3.2) for small value of u yields:

$$N^{eq}{}_i = d\left(1 + \frac{D}{c^2}\frac{\rho}{\rho_m} c_i \cdot u\right) \tag{3.4}$$

Where D is the dimension and c is the macroscopic velocity and c_i is the velocity at microscopic level. From this result, the equilibrium distributions of particles in a FCHC and FHP LGA are described as follows

for zero velocity rest particles $N_i^{eq} = d_p$ (3.5)

for unit velocity moving particles $N^{eq}{}_i = d\left(1 + 2\frac{\rho}{\rho_m} c_i \cdot u\right)$ (3.6)

For a given initial velocity distribution (e.g. a Poiseuille profile for laminar flow), these equations are used to initialise the configuration of lattice particles at each of the nodes on the lattice based on the calculated mean velocity of the fluid at the coordinate of that node.

3.3.3 Addition of solid surfaces

Certain lattice sites are labelled as a solid surface in the model. To assign a node as a solid state an additional bit is used to store the corresponding node information. It denotes whether the node is part of a solid surface or not.

Depending on the level of shear stresses experienced between the LGA fluid and the solid surface, a slip or no-slip boundary condition is assigned to the solid surface (Thompson *et al.* 1990). This is done by using specular reflection or bounce-back collision rules respectively implemented at solid nodes or a mixture of the two (Lavallée *et al.* 1989 and 1991, Hayot *et al.* 1989, Gao *et al.* 1994). These are shown in Figure 3.9a and Figure 3.9b.

Figure 3.9a. Bounce-back collision at a solid node.

Figure 3.9b. Specular reflection collision at a solid node.

For simulations of fluid flow in porous media, a no-slip boundary condition would be normal and use of bounce-back collisions provides the best means of representing this. Lavallée *et al.* (1989) has shown that use of a mixture of bounce-back and specular reflection rules will also produce a no-slip boundary condition, but will require greater computation time for the flow field to reach equilibrium. Bounce-back reflections are used in our implementation and these collisions are generated before the execution of the simulation and stored in the collision table.

3.3.4 Periodic boundaries

Simulation domains have been coded with default periodic boundary conditions, i.e. any particles leaving one side of the simulation domain will re-enter on the opposite side. To encode this into the current models, an additional plane of lattice nodes outside of the simulation domain is included on each side of the lattice (corresponding to columns 0 and x-1 in figure 3.10). These nodes contain the same information as the plane of nodes on the opposite side of the lattice (corresponding to columns x-2 and 1, see figure 3.10). This information is copied across once in each time-step before the propagation stage, to allow the propagation of particles to nodes on the edge of the lattice (1 and x-2).

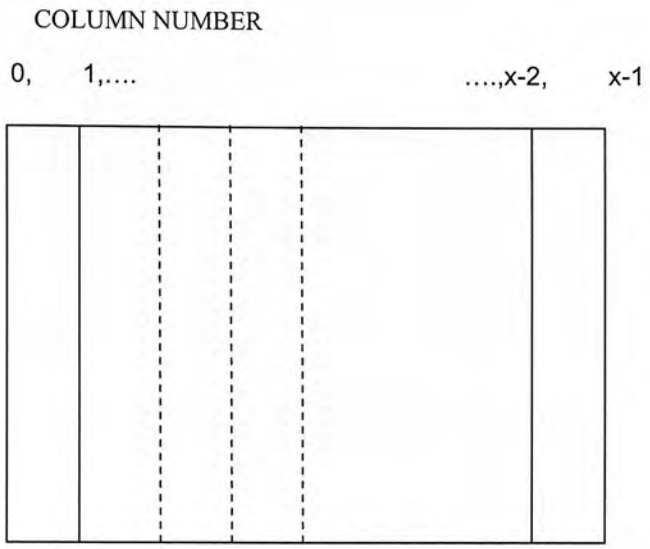

Figure 3.10. Periodic boundaries.

3.3.5 Applying force

There are three different ways that have been used to drive flows through simulation domains in LGA: applying a body force to the fluid (Kadanoff et *al.* 1987, Rothman 1988, Rybka 1993), using a pressure difference to drive the flow (Gao *et al.* 1994, Chen 1991) or by overwriting the planes of nodes at the inlet and outlet sites of the simulation domain with a pre generated velocity distribution (d'Humieres 1986a, 1987, Stauffer 1991).

Of these, the use of a pressure difference is unsuitable for simulations of quasi-infinite length using periodic boundaries, like single-phase flow in a pipe, as it produces unphysical walls of fluid (Gao *et al.* 1994). Overwriting the inlet and outlet sites may not be suitable for flow around objects (Eissler *et al.* 1992) as an outflow

flux might cause a non-physical suction and also the system will tend to achieve lower equilibration (Jeulin, 1992) over the course of a simulation.

Body force is applied in LGA by introducing an additional "forcing" stage to the automaton's updating algorithm. A force may be thought of as a rate of change of momentum. Hence a force is applied by changing the momentum states of a set number of lattice particles at each time state. In this process, known as "flipping", a random site is chosen from the region in which the force is being applied and a check performed to see if this site is a potential candidate. This will require a particle be present in a momentum state from which it may be moved and a corresponding "hole" to move it into. If these conditions are met, the particle is moved into its new momentum state. Another node is then chosen and this operation repeated until the required force has been applied. An example of some of the x-direction forcing rules for the FHP-II and FHP-III models are shown in figure 3.11.

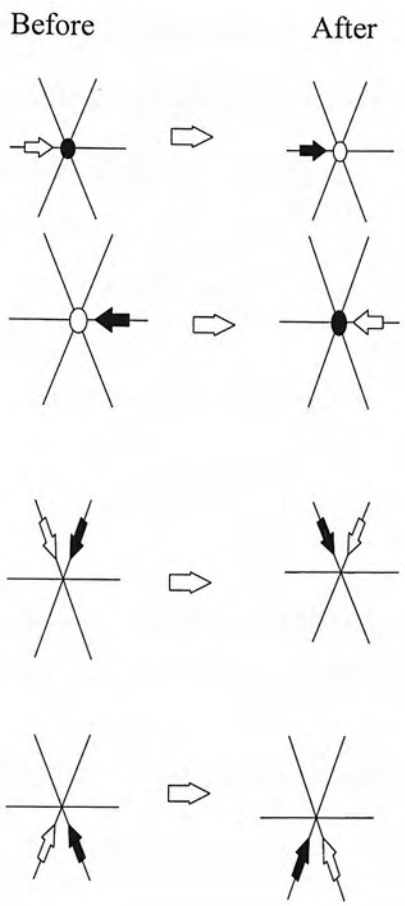

Figure 3.11. Forcing rules (Kadanoff *et al.*1987).
—— or ¯ unoccupied ; ⟶ or ● occupied

3.3.6 The Navier–Stokes Equation of Lattice Gas Automata

Frisch *et al.* (1987) showed that with suitable collision rules and other moderating conditions such as density in place, the collective motion of the particles should yield behaviour similar to that predicted by the incompressible Navier-Stokes equations with the presence of density dependent factor. The complete derivation has been discussed by various authors (Frisch *et al.* 1987 and Rothman *et al.*1994).

In summary, they used the principles of kinetic theory to derive a Boltzmann-like equation for the LGA particle dynamics and solved it using a Chapman-Enskog approach to yield the following hydrodynamic equations (equations 3.7, 3.8) and equation of state (equation 3.9) for the LGA fluid.

$$\frac{\partial \rho}{\partial t} + \nabla \cdot (\rho u) = 0 \tag{3.7}$$

$$\frac{\partial (\rho u)}{\partial t} + \nabla \cdot [\rho g(\rho) uu] = -\nabla p + \gamma(\rho) \nabla^2 (\rho u) \tag{3.8}$$

$$p = c_s^2 \rho \left(1 - g(\rho) \mathrm{u}^2\right) \tag{3.9}$$

(ρ and u are the macroscopic density and velocity, g(ρ) is the Galilean invariance term, c_s and ν(ρ) are the speed of sound and kinematic viscosity)

The above are calculated from a property of the lattice d_p (reduced particle density) which is defined as the mean probability of finding a lattice particle in any momentum state on the lattice. The momentum equation 3.8 is almost identical to the incompressible Navier-Stokes equations, save for the presence of g(ρ), the Galilean invariance factor. This g(ρ) is defined in the equations from 3.10 to 3.12 for 2D and 3D LGA models. It can be seen from the equations that this *g* factor is dependent on the density ρ which reflects the lack of Galilean invariance in LGA models. This is caused by the discretisation of the particle velocities and the limited number of directions in which particles may travel. The problem of Galilean invariance in LGA will be discussed in detail later in this chapter.

The transport coefficients for the FHP-I model are

$$\rho = 6d_p, \qquad c_s = \frac{1}{\sqrt{2}}, \qquad g(\rho) = \frac{(\rho - 3)}{(\rho - 6)} \tag{3.10}$$

And for the FHP-II and FHP-III models

$$\rho = 7d_p, \qquad c_s = \sqrt{\frac{3}{7}}, \qquad g(\rho) = \frac{7}{12}\frac{(7-2\rho)}{(7-\rho)} \tag{3.11}$$

And for the FCHC model

$$\rho = 24d_p \qquad c_s = \frac{1}{\sqrt{2}} \qquad g(\rho) = \frac{2}{3}\frac{1-2d_p}{1-d_p} \tag{3.12}$$

3.3.7 Units in Lattice Gas Model

The following are the standard units in the lattice gas simulations:

The basic unit of time is one time-step, the basic unit of length is lattice unit (lu) which is the distance between two neighbouring nodes on the grid. The basic unit of mass is the mass of a particle which is taken to be unity. Other quantities, such as velocity, are measured in units derived from these basic units. Velocity is expressed as lattice unit per time-step.

3.3.8 Validation of LGA model

This section reports the results of various tests that were applied to the LGA programming code to ensure that they were conceptually correct and properly written. The 2D and 3D LGA fluid transport codes were applied to the well known engineering problem; flow in a duct.

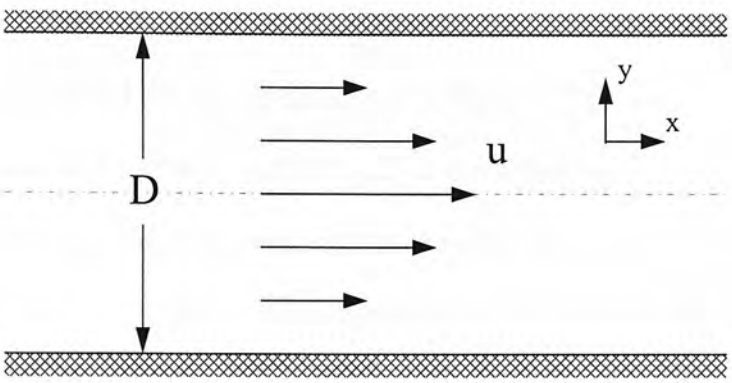

Figure 3.12. Geometry of 2D flow in a channel.

The LGA fluid transport model was first applied to simple flow in a 2D channel. The no-slip boundary condition at the solid walls should impose frictional drag upon the fluid resulting in the development of the well-known parabolic Poiseuille flow distribution across the channel. This is due to the nature of fluid flowing faster in the centre of the channel and approaching zero at the walls (Henon 1987). The analytical solution to the Poiseuille distribution of flow is given by

$$u_x = \frac{\Delta P}{2\mu}\left(\frac{D^2}{4} - y^2\right) \tag{3.13}$$

where u_x is the fluid velocity parallel to flow at a distance y from the channel centerline, ΔP is the pressure drop across the system, μ is the fluid dynamic viscosity and D is the channel width or distance between plates; the corresponding system geometry is shown in figure 3.12.

The flow is forced by adding momentum in the positive x direction of the system at a constant rate. After each time step, we randomly select a number of lattice nodes and apply one of the microscopic forcing rules (Kadanoff *et al.* 1987). Each successful application of a forcing rule adds one unit of momentum to the system. The forcing process is repeated until the desired amount of momentum has been transferred to the fluid. The overall effect of this process results in a constant body force applied to the fluid uniformly across the width and length of the channel.

The force imparted to the system is dissipated due to the pressure gradient and from there the pressure drop down the length of the channel was calculated.

A number of simulations as described above were carried out to test the ability of the 2D and 3D codes to reproduce the analytical distribution described in the above equation. Fluid velocities (max) of 0.20 to 0.30 lattice units per update (l.u./t) were simulated and the results are shown below for FHP-II and FHP-III and FCHC models in Figure 3.13 -3.15.

Simulation of the channel flow gives the expected parabolic profile to a good degree of accuracy. The results confirm that the program codes are implemented properly and LGA model is correctly represented in the coding.

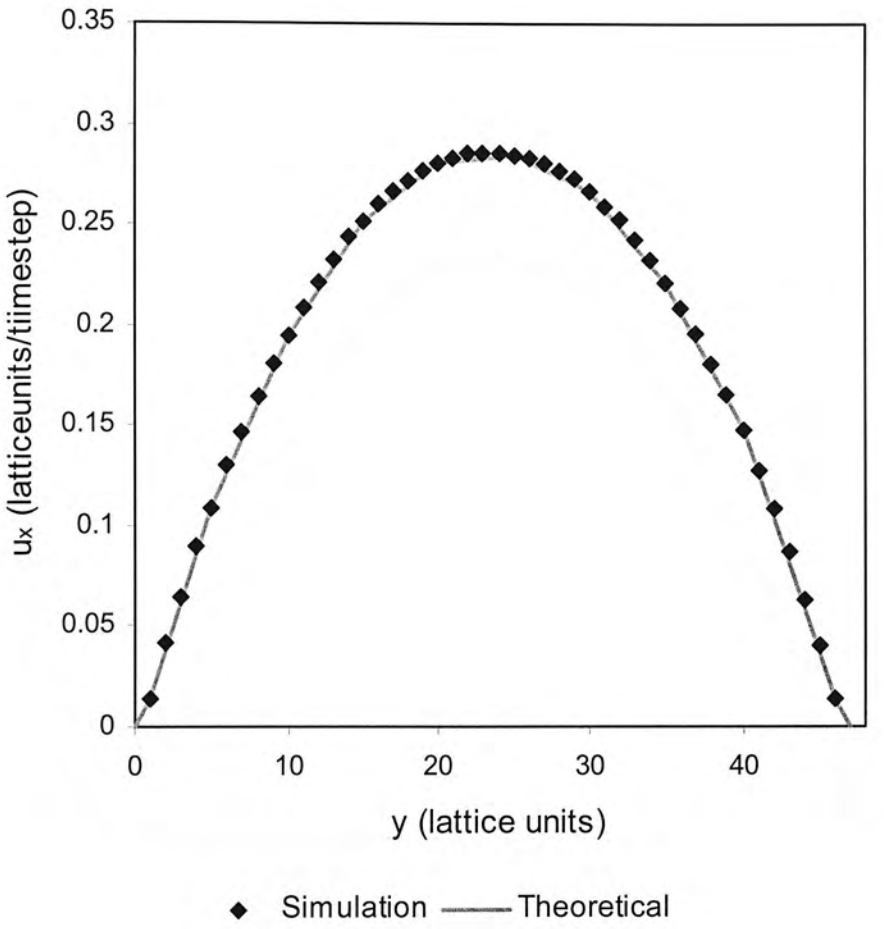

Figure 3.13. Flow distribution across a channel: Comparison of simulation with theoretical Poiseuille flow profile for FHP-II model.

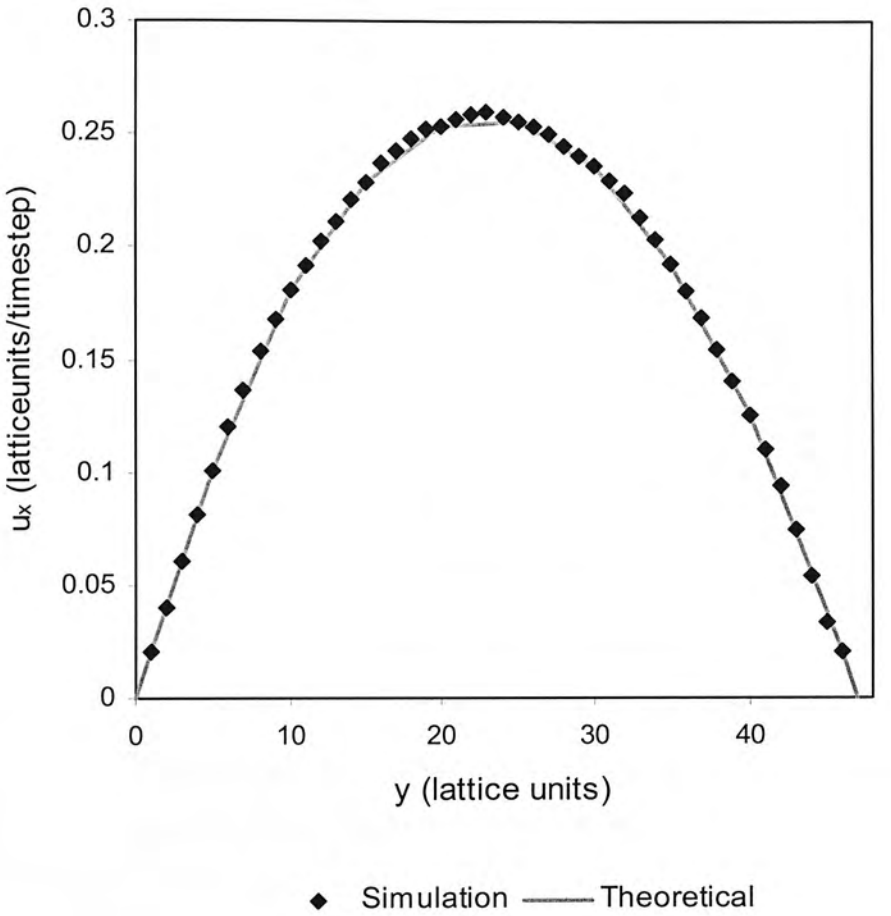

Figure 3.14. Flow distribution across a channel: Comparison of simulation with theoretical Poiseuille flow profile for FHP-III model.

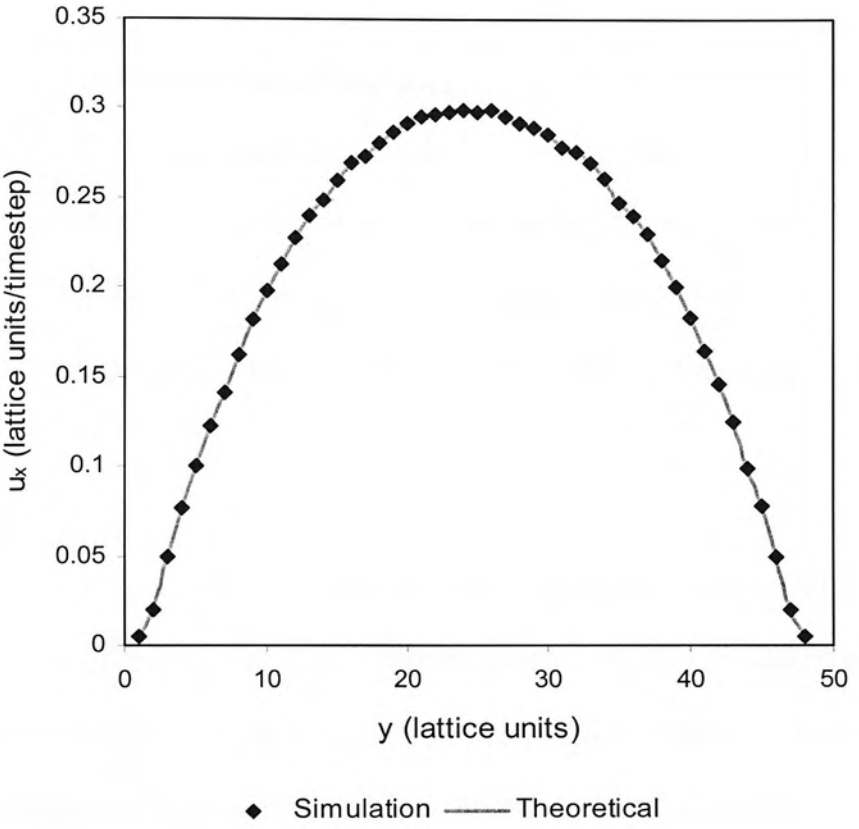

Figure 3.15 Flow distribution across a channel. Comparison of simulation with theoretical Poiseuille flow profile for FCHC model.

3.4 The problem of Galilean invariance

Lattice gas automata methods have been used to simulate many different flow situations (Wolfram 1986, Frisch *et al.* 1986 and 1987, Chen *et al.* 1995, Biggs *et al.* 1998). One of the advantages of LGA is that they model the pore space explicitly to a greater or lesser extent. However they are restricted to relatively slow flows due to non-Galilean invariance.

The Galilean invariance factor present in the hydrodynamic equations (equation 3.8) is an artefact introduced by the limited number of particle momentums and the discrete lattice used. If this Galilean invariance factor is not 1 (i.e. the lattice fluid is non-Galilean invariant), this manifests as the vorticity advecting with a different velocity to the bulk movement of the fluid (d'Humeieres *et al.* 1987). This factor is a density dependent term (the density in turn depending only on d_p). A quick consideration of equations 3.10, 3.11 and 3.12 will show that this factor will be zero for $d_p = 0.5$ and negative for $d_p > 0.5$. Physically this would be seen as the vorticity moving in the opposite direction to the bulk movement of the fluid. This has been demonstrated through simulation of the motion of a shear wave through the lattice gas fluid (Rothman *et al.* 1994).

This lack of Galilean invariance is one of the well-documented problems with LGA but it is possible to reduce or control its effects. In a single-phase LGA it is possible to remove the $g(\rho)$ term from the Navier-Stokes equations by rescaling the velocity

by a factor $g(\rho)$ ($u' = g(\rho)u$). This does not remove it from the equation of state, but its effect may be considered negligible as long as u $<< c_s$.

In order to exactly recover the Navier-Stokes equations in immiscible lattice gas automata (ILGA), it is possible to modify the model to ensure that g(ρ)=1. This may be done by adding a large number of possible rest particles at every node. For example with an FHP LGA, it may be noted that the Galilean-invariance term depends on the number of rest particles. The relationship can be described in the following equation (Rothman *et al.* 1994).

$$g(\rho) = \frac{M}{6}\left(\frac{\frac{1}{2}M - \rho}{M - \rho}\right)$$

(where is M is the number of rest particles)

This may then be solved for the M required to give $g(\rho) = 1$ for any given value of ρ and the model recovers the Navier-Stokes equations exactly. However, the closer the $g(\rho) = 1$, the greater the error in the equation of state. This leads to problems for instance at higher velocity, the pressure would be abnormally low, which would lead to spurious flows and compressibility effects.

There is a class of LGA models known as multi-speed LGA which use multiple lattice particle speeds and controls the rate for the direct and inverse collision process (Tiexera, 1992). The more elaborate of these models remove all the artefacts of the lattice from the hydrodynamic equations and recover continuum hydrodynamics exactly. In this multi-speed model particles with several speeds are included so that energy becomes an independent variable. The structure of the underlying 4D FCHC lattice allows these particles of different speeds to exist independently on sufficiently

symmetric sub lattices while also allowing particles of different speeds to interact via energy exchange collisions. These energy exchange collisions force the lattice artefacts to have the continuum values necessary for correct hydrodynamic behaviour. Full details of this model will be discussed in the following chapter.

Summary

Details of the fundamental theory of the lattice gas automata (LGA) are described in this chapter. LGA is an alternative numerical description of flow dynamics where the physical state of the particles are represented in terms of Boolean variables, particles move and interact in a lockstep manner on a regular lattice and obtaining macroscopic variables of the particles motion. The results reported in this chapter demonstrate that the 2D and 3D LGA fluid transport codes written for this study are capable of reproducing correct hydrodynamic behaviour of fluids.

LGA is ideal for the fundamental study of the systems involving fluid flow and transport within porous media. However this single speed LGA models are restricted to relatively slow flows due to non-Galilean invariance. The next chapter discusses the implementation of Galilean-invariant LGA (GI-LGA) model and this new model will address this problem directly.

Chapter 4

The Galilean-invariant LGA model of Teixeira

Introduction

As outlined earlier, a variety of methods have been proposed to remove the various non-hydrodynamic artefacts from LGA (d'Humieres 1986, Frisch *et al.* 1987, Rothman *et al.* 1994, Teixeira 1992). Perhaps the most advanced is Teixeira model (1992) which recovers Galilean invariance in three-dimensions by allowing particles to take on one of a small number (*e.g.* three) speeds and then controlling the density of each over small sub-volumes (e.g. 5×5×5 lattice units). Unfortunately, the details of the method have not been published in the open literature; the few papers that have discussed this issue (Molvig,K *et al.* 1990, Mujica, 1991), reported only the results with very few details. The thesis of Teixeira (1992) has not covered many details surrounding its implementation. This chapter, therefore, provides a comprehensive summary of the method and its implementation, including the influence of the various control parameters for which Teixeira provides virtually no details, and results for a variety of benchmark problems to demonstrate that the model produces correct results whilst recovering Galilean invariance.

The method of Teixeira is first described in detail followed by its implementation. The results of studies aimed at elucidating the influence of the various control parameters of the method on its accuracy are then discussed. To my knowledge the results presented here are unique. This is finally followed by detailed comparison of

our implementation of the Teixeira method against several standard benchmark problems.

4.1. Summary of Teixeira model

In Teixeira's thesis a three-speed model that removes the discreteness artefact is implemented using the FCHC lattice. This is the only regular lattice available with properties required to remove the artefact. This lattice permits all the integral energies and allows interaction among them.

Teixeira, using a super computer, developed a three speed model; two types of particles with different energies and momenta along with rest particle were used. Total of 54 particles in which 24 belong to energy1, other 24 belong to energy2 and 6 energy0 particles were used in this model. There was no explicit explanation available in the thesis for this particular particle number and distribution. We think this is the model with probably minimum number of particles that was necessary to remove artefacts. The exclusion principle is imposed during the simulation as described previously.

Momentum contributions for these two energy levels are tabulated in Table 4.1 and the particle projection of each energy level is illustrated in figures 4.1 and 4.2. Modelling of temperature equilibrium and particle interactions producing energy exchange are constructed in this model. The Galilean invariance factor 'g' is directly affected by the rate of energy exchange collisions. By regulating the number of energy transfer collisions the model is forced to exhibit Galilean invariance. The full detail of the implementation is discussed in the following section.

Momentum contributions for energy level one particles	Momentum contributions for energy level two particles
{ 1, 0, 0, 1 }	{ 2, 0, 0, 0 }
{ 1, 0, 0,-1 }	{ 0, 2, 0, 0 }
{ -1, 0, 0, 1 }	{ 0, -2, 0, 0 }
{ -1, 0, 0,-1 }	{ -2, 0, 0, 0 }
{ 0, 1, 1, 0 }	{ 0, 0, 2, 0}
{ 0, 1,-1, 0 }	{ 0, 0, 0, 2 }
{ 0,-1, 1, 0 }	{ 0, 0, 0, -2 }
{ 0,-1,-1, 0 }	{ 0, 0, -2, 0 }
{ 0, 1, 0, 1 }	{ 1, 1, 1, 1 }
{ 0, 1, 0,-1 }	{ -1, 1, 1, 1 }
{ 0,-1, 0, 1 }	{ 1, -1, -1, -1 }
{ 0,-1, 0,-1 }	{ -1, -1, -1, -1 }
{ 1, 0, 1, 0 }	{ 1, -1, 1, 1 }
{ 1, 0,-1, 0 }	{ 1, 1, -1, 1 }
{ -1, 0, 1, 0 }	{ -1, -1, 1, -1 }
{ -1, 0,-1, 0 }	{ -1, 1, -1, -1 }
{ 0, 0, 1, 1 }	{ 1, 1, 1, -1 }
{ 0, 0, 1,-1 }	{ -1, -1, 1, 1 }
{ 0, 0,-1, 1 }	{ 1, 1, -1, -1 }
{ 0, 0,-1,-1 }	{ -1, -1, -1, 1 }
{ 1, 1, 0, 0 }	{ -1, 1, -1, 1 }
{ 1,-1, 0, 0 }	{ -1, 1, 1, -1 }
{ -1, 1, 0, 0 }	{ 1, -1, -1, 1 }
{ -1,-1, 0, 0 }	{ 1, -1, 1, -1 }

Table 4.1. FCHC particle momentum contributions for energy level 1 and 2.

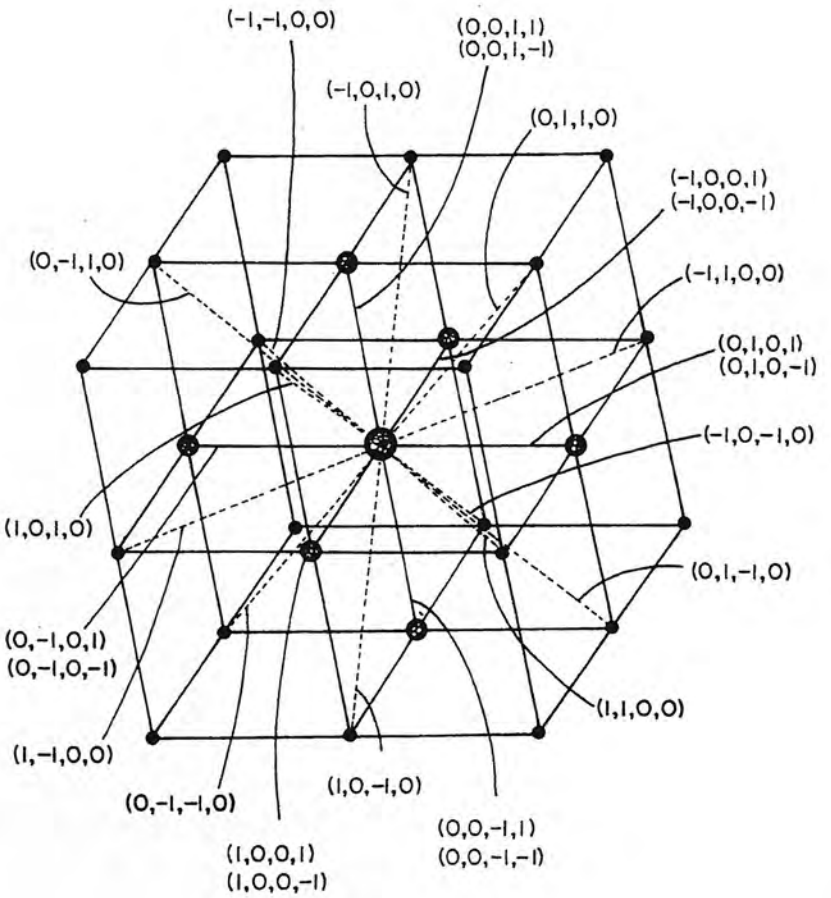

Figure 4.1. FCHC particle momentums-energy level 1(Molving,1994).

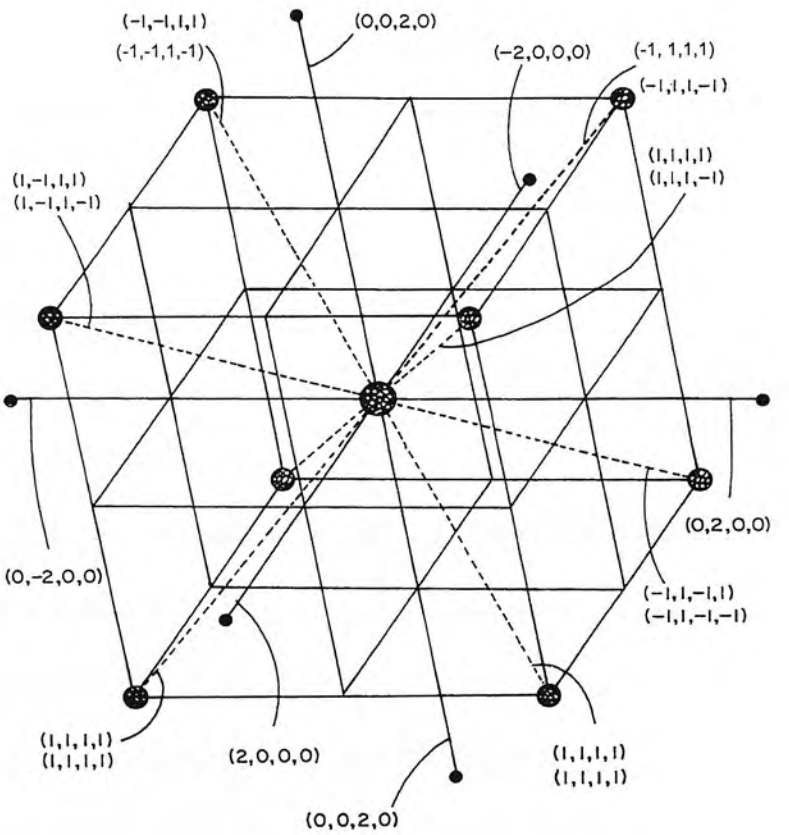

Figure 4.2. FCHC particle momentums-energy level 2(Molving, 1994).

4.2 Implementation

The flow of LGA code is grouped into three sections; initialization, updating the lattice from time-step to time-step which has two steps - collision and the propagation stage and the final output routine.

The initialization part sets up the geometry on the entire lattice according to a user-defined function. The particles are then seeded in the lattice with the probabilities equal to the equilibrium (Fermi-Dirac distribution function) which is derived from the following section.

4.2.1 Equilibrium distribution

The following equilibrium derivation is based on the thesis (Continuum limit of Lattice gas fluid dynamics) of Teixeria

When simulating a lattice gas model, we like to specify the density and temperature of the equilibrium fluid. This means that we will treat density, ρ, and a temperature related variable, z, as input parameters while, the fugacity, y, is a variable that must be tuned to give the desired density. The equilibrium distribution is done by seeding the particles with the probabilities equal to the equilibrium Fermi-Dirac distribution function. This ensures not only the conserved quantities of mass, momentum and energy, but also allows the Galilean invariant factor '*g*' to be set at 1, i.e. $g=1$ as well. The relation for g is in terms of moments of the equilibrium distribution function as

$$N_j = \frac{yr_j}{yr_j + z^j} \qquad (4.1)$$

Where y and z are quantities related to density and temperature. Using equation 4.1, the equilibrium distributions for this model could be calculated as following:

$$N_0 = \frac{yr}{yr+1}$$

$$N_1 = \frac{y}{y+z} \qquad (4.2)$$

$$N_2 = \frac{y}{y+z^2}$$

The equations defining the density and energy together with the Galilean invariance condition (g =1) form three equations which in principle allow determination of the Lagrange multipliers, α0, β0, as well as the rate coefficient 'r'.

The density and energy relations for the three speed model are

$$f = \frac{1}{4}N_0 + N_1 + N_2 = f(y,r,z) \qquad (4.3)$$

$$U_p = 24(N_1 + 2N_2) \qquad (4.4)$$

Using the above equations, the Galilean invariance condition can be written in the following equation for this model

$$g = \frac{2}{3}\left[\frac{N_1(1-N_1)(1-2N_1)+4N_2(1-N_2)(1-2N_2)}{(N_1(1-N_1)+2N_2(1-N_2))^2}\right]f = 1 \qquad (4.5)$$

The above may be rewritten as a function of *gcond (y ,z, f)* = 0

$$0 = f[N_1(1-N_1((1-2N_1)+4N_2(1-N_2)(1-2N_2)] - \frac{3}{2}[N_1(1-N_1)+2N_2(1-N_2)]^2 \qquad (4.6)$$

Equation 4.6 allows us to solve for y as a function of the input parameters f and z. Knowing $y(f,z)$ will allow us to find $r(f,z)$ from equation 4.3.

The expansion is established by developing the fugacity (y) in a power series

$$y = y_1 f + y_2 f^2 + y_3 f^3 + y_4 f^4 + \ldots\ldots \qquad (4.7)$$

Plugging this relation into equation 4.5 and setting the result equal to zero order by order in f, the coefficients $y_j(z)$ may be calculated as rational polynomials. If the corresponding power series for the rate coefficient 'r' is developed from equation 4.3, it can be solved exactly for r as a rational function of the f and z and the accurate series for y through fourth order in f may be substituted.

$$r = \frac{-4(-2y^2 + fy^2 - yz + fyz - yz^2 + fyz^2 + fz^3)}{y(-9y^2 + 4fy^2 - 5yz + 4fyz - 5yz^2 + 4fyz^2 - z^3 + 4fz^3)} \qquad (4.8)$$

This will provide an accurate expression for the rate coefficient for all usable densities. To maintain an even temperature within the flow r can not be too large or too small and allowed values should be in the range $0.1 < r < 10$ when f is less than 0.56 with the number of rest particles we used in the system. This gives a positive solution for r over the range of z which is $0.5 \leq z \leq 10$ (Teixeira, 1992).

One way of assuring r remains at the appropriate value is to create a feedback system that can sense the local density and temperature related variable (z) and then alter the collisions accordingly.

The equilibrium temperature T is determined by the fluid variables, density and energy and the $g = 1$ condition; z can be calculated from the expressions for N_1 and N_2 in equations 4.2

$$z = \frac{\hat{N}_1}{\hat{N}_2} \tag{4.9}$$

Where $\hat{N}_j = \frac{N_j}{1 - N_j}$ and z is defined as

$$z = \frac{2(2 - 3T)}{3T - 1} \tag{4.10}$$

T is calculated by inverting equation 4.10

$$T = \frac{z + 4}{3(z + 2)} \tag{4.11}$$

To determine the equilibrium temperature of the system, optimization studies has been carried out. This is the necessary foundation for simulating a thermal process. The entire lattice is divided into small sub-volumes and the temperature is defined with an upper and lower temperature range. We have looked at the effect they have on performance and the details of this study are presented in the next section.

4.2.2 Collision Types

Each collision is a binary collision occurring between two sets of paired particles. The collisions are classified into two groups of collisions:

- self collisions
- energy exchange collisions

In the self collisions there are two possibilities: self collisions between energy1 particles and self collisions between energy2 particles.

$$\text{energy1} + \text{energy1} \Leftrightarrow \text{energy1} + \text{energy1}$$

$$\text{energy2} + \text{energy 2} \Leftrightarrow \text{energy2} + \text{energy2}$$

These self collisions are grouped into three equivalence classes:

For the pairs whose net velocity vectors have a magnitude of zero is classified as *first equivalence.* There are 12 pairs of particles that belong to this group and out of these a few of them are shown here as an example.

$$\begin{cases} (0, 1, 0, 1) \\ (0, -1, 0, -1) \end{cases} \qquad \begin{cases} (0, 1, 1, 0) \\ (0, -1, -1, 0) \end{cases} \qquad \begin{cases} (1, 0, 0, 1) \\ (-1, 0, 0, -1) \end{cases}$$

The *second equivalence class* can be produced by 3 pairs of particles. two sets of three pairings that may produce the net velocity vectors of (2,0,0,0) and (1,1,1,1). There are 72 pairings in this group and an example for the net velocity vector (2, 0, 0, 0) is shown here.

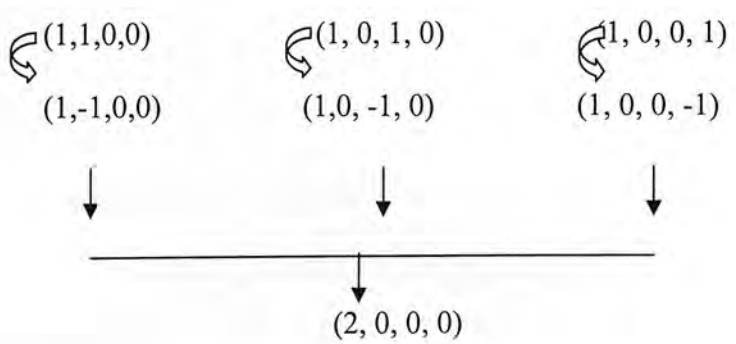

The *third equivalence class* is made of those pairs of particles which produce a net velocity vector having the same magnitude as each of the velocity vectors of the particles. There are 96 particle pairs in this group. An example for the net velocity vector (1, 0, 1, 0) is shown below.

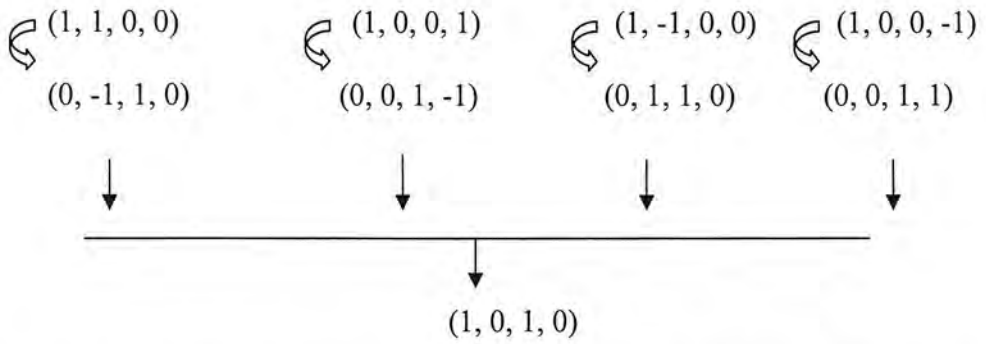

These three equivalence classes give 180 pairings in which self-collisions are possible.

Apart from the above collisions, other types of collisions are also possible in this model. These are energy exchange collisions. There are 72 possible pairings that bring about such a collision when the particles are present. This is shown as an example here

$$\text{energy1} + \text{energy1} \Leftrightarrow \text{energy2} + \text{energy0}$$

Energy exchange collisions occur when two energy1 particles collide to form an energy2 particle and an energy0 particle as illustrated in figure 4.3 below along with its inverse process.

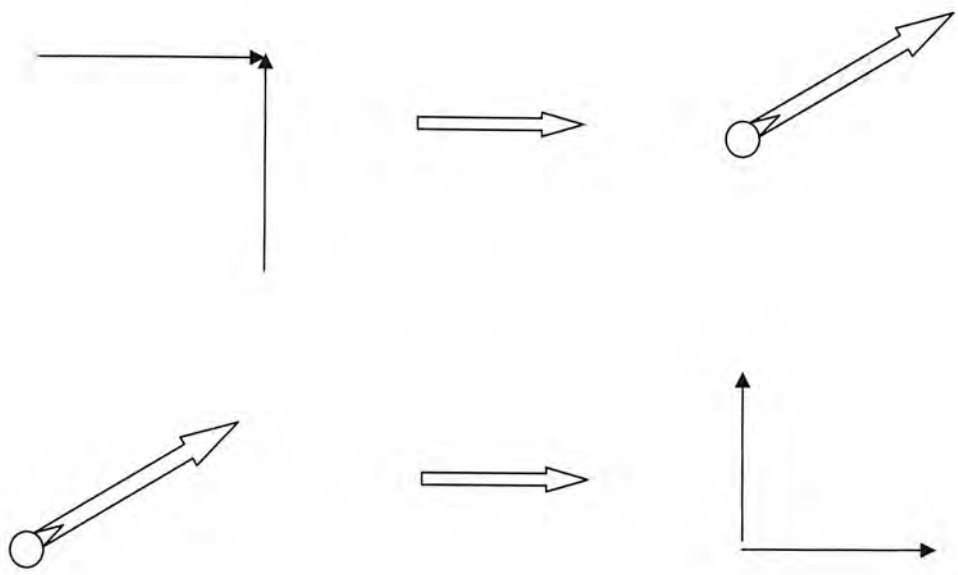

Figure 4.3. Example of energy exchanging interactions among particles: energy1 particle ⟶ , energy 2 particle ⟹ , energy 0 particle ○

The inclusion of energy exchange collisions adds an additional degree of freedom to the system in order to simulate the true fluid behaviour.

4.2.3 Collision Mechanism

During the collision stage, the collisions are performed by cycling through each of the possible particle pairings. It begins with the first equivalence class of particle pairings. The system looks at the first pairing in the first equivalence class to check to see whether both of the particles for the pairing are present or not. If both particles are present then the system proceeds to check for the hole pair. If this hole pair is present then the collision is performed. Once the collision process is completed for

the first equivalence class the subsequent equivalence classes are examined in a similar manner. Once the self collisions are completed, the energy exchange collision (or the inverse energy exchange collision) is performed.

The energy exchange collision happens in forward direction from the energy1 particles and a backward direction from the energy2 and energy0 particles. These collisions rates are dependent on the temperature of the system. A feed back system is created to sense the local density and temperature and then alter the collisions accordingly. This feedback technique was used successfully to maintain the removal of the 'g' artefact in simulations where local values of the density and temperature changed significantly.

The only other type of collision which may occur is when a particle collides with a solid boundary. We require that the boundary does not create or destroy particles and that particles can not propagate through the boundary. 'bounce-back' rule is applied at the boundary to ensure that particles arrive at a node that are marked as a solid simply reverse their direction.

The final step in the entire algorithm is the calculation of macroscopic properties of the flow for all 54 particles. At any node the local value of fluid density, momentum or any other macroscopic flow variable is calculated by taking appropriate bits of the microscopic distribution. For instance

$$\rho(x) = \sum_{i=1}^{54} ni(x) \qquad (4.12)$$

$$\rho u(x) = \sum_{i=1}^{54} c_i ni(x) \qquad (4.13)$$

calculates the local values of density and momentum respectively accumulated over a sub-volume. It is divided by the size of sub-volume to get an average quantity per lattice node. This sub-volume size is one of the controlling parameters apart from temperature difference in the simulation and the detail of this study is discussed in further below.

4.3 Effect of model control parameters on performance

As outlined earlier the simulations were designed to find out the influence of sub volume size and temperature difference (deltaT). Poiseuille flow experiments were used in this study. One of the aims of this experiment is to find the optimum conditions for further simulations. The effects of sub-volume size and temperature difference were examined and the results are discussed in this section. Both factors are very important in deciding the outcome of the process.

4.3.1 Effect of sub-volume size

It is important to predict the sub-volume size which is independent of viscosity for further simulations. The resolution of the lattice is selected based on the viscosity of the flow. Sub-volumes are grouped as micro blocks in to various volume size. The following for sub-volume sizes, (4,4,4), (6,4,4), (12,4,4) and (29,4,4), were used in the simulations. The nodes in the sub-volume is defined as $N_i(n)$, where n represents the relative position of the lattice node within the sub-volume and $n \in \{0,1,2,.....63\}$ for the sub-volume of dimensions X=4, Y=4, Z=4 as grouped as (4, 4, 4). Simulations were carried out by varying the sub-volume sizes for constant

temperature difference (deltaT) range. Viscosity fluctuation as a function of sub-volume size (in terms of total number of nodes) is plotted in figure 4.4.

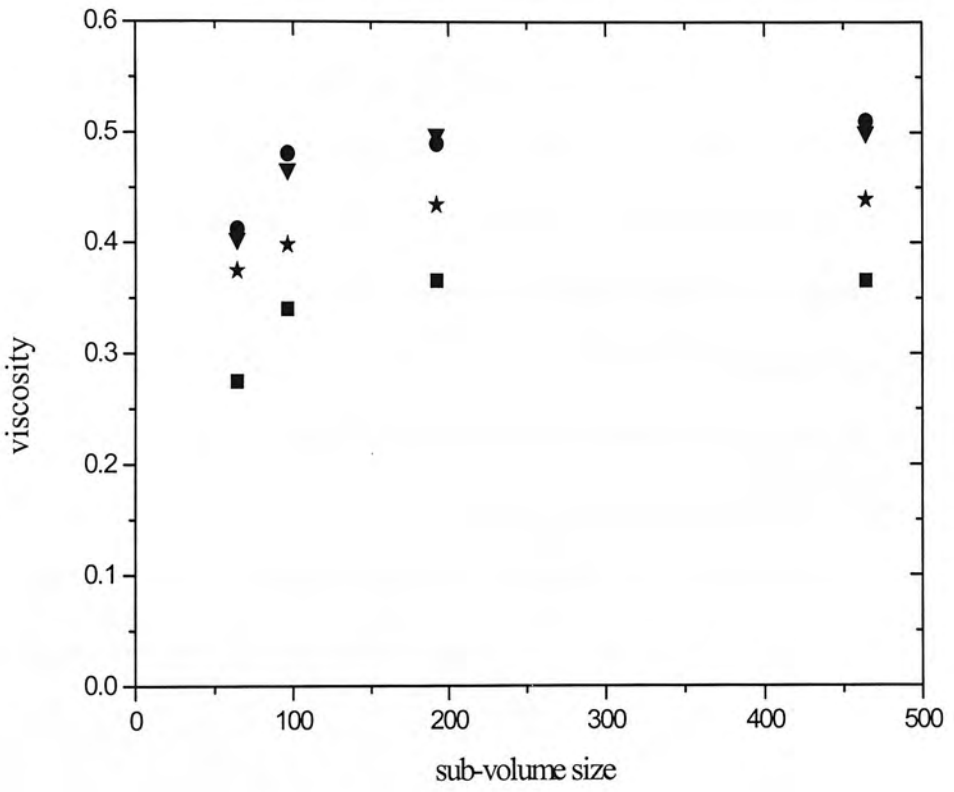

Figure 4.4. Viscosity fluctuation as a function of sub-volume size.
■ deltaT 0.015, ★ deltaT 0.0165, ▼ deltaT 0.0175, ● deltaT 0.0185.

Keeping the deltaT at 0.015, 0.0165, 0.0175 and 0.0185, various sub-volume sizes were analysed. The results showed a trend of initial increase in viscosity before it become constant with increasing sub-volume size. Increasing the sub-volume size beyond (12, 4, 4) did not influence the viscosity. This is probably because the system gets saturated with regard to the collisions rules as it is pre defined in the model.

4.3.2 Effect of temperature difference range

Further simulations were carried out for various temperature differences while keeping the sub-volume size constant to see the viscosity changes. This will also enable us to verify the accuracy of previous simulation results. For each of the sub-volume size (4,4,4), (6,4,4), (12,4,4), (29,4,4) simulations were carried out with different deltaT values. Viscosity fluctuation as a function of temperature difference (deltaT) range is plotted in figure 4.5. The change in viscosity pattern was similar with initial increase before it become constant at 0.0175. As before the predetermined model parameters make the system saturated with maximum number of collisions.

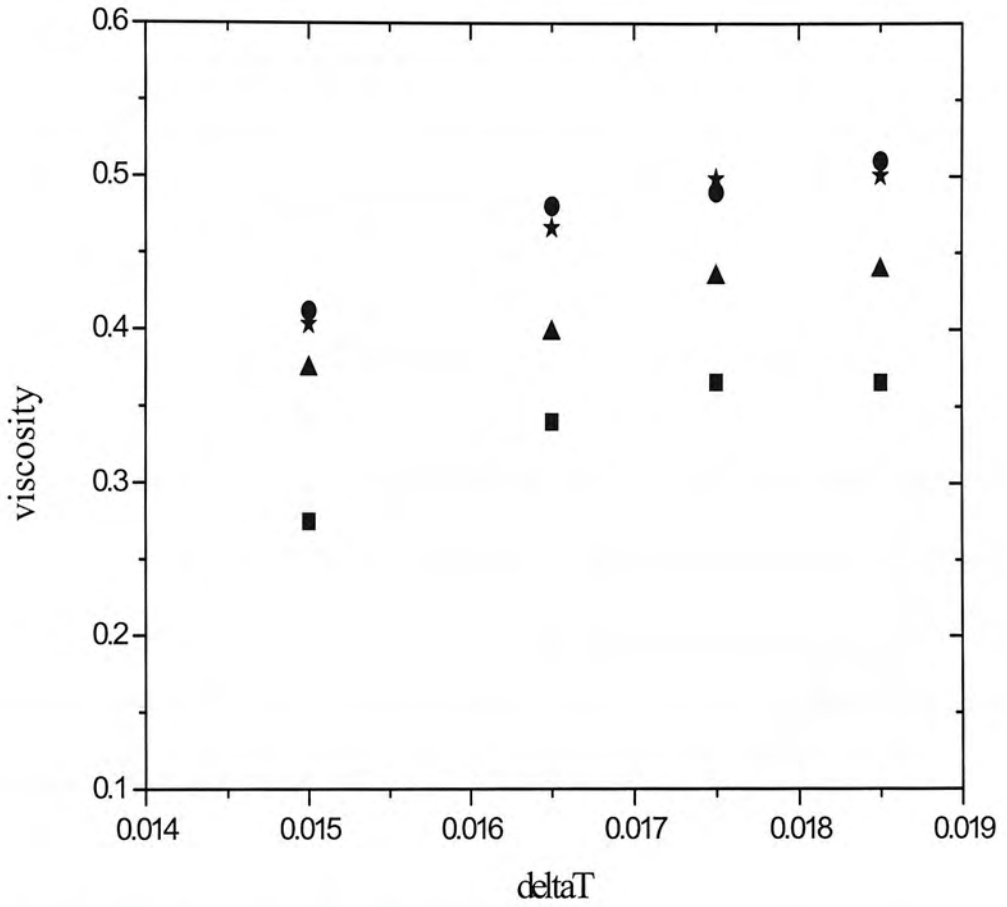

Figure 4.5. Viscosity fluctuation as a function of temperature difference (deltaT)

■ sub-volume size 4,4,4, ▲ sub-volume size 6,4,4, ★ sub-volume size 12,4,4, ● sub-volume size 29,4,4

The viscosity constant regions in the above studies were selected for bench mark studies and further experiments.

4.4. Validation of Galilean invariance artefact removal

The removal of Galilean invariance artefact, g, from the momentum equation can be demonstrated by examining the relaxation of a shear wave with transverse velocity in an open system (Salem *et al.* 1986). The lattice is initialized with a particular density and temperature and an initial velocity field is given by

$$u_0(x,t=0) = u_T e_y + u_L \sin(ky) e_x \tag{4.14}$$

where k is the wave number of the perturbation. Having a non-zero streaming speed in the direction of the perturbation will allow g to be measured directly from the evolution of the perturbation. There is no flow velocity in the z-direction. The evolution of this perturbation in time is given by the lattice Navier-Stokes equation for incompressible constant density and temperature flows

$$\frac{\partial u}{\partial t} + gu.\nabla u = \gamma \nabla^2 u \tag{4.15}$$

Substituting equation 4.14 for u in the above equation, it can be calculated analytically. The following solution can be derived.

$$u(x,t) = u_T e_y + u_L e^{-iku_T gt - \gamma k^2 t} \sin(ky) e_x \tag{4.16}$$

Where, we could see the time evolution of the phase and modulus of $u(t)$ directly measure the g-factor and the kinematic viscosity γ. The presence of viscosity in the flow causes the shear to be destroyed. Eventually only the transverse flow remains.

Simulations were run on a 64 x 64 x 64 lattice with various values of density and temperature. Validation runs were done with $u_T = u_L = 0.1$ and a wave number of $k = 2\pi/64$ which corresponds to one wavelength of the perturbation exactly fitting into the lattice volume. All macroscopic flow velocities are in units of number of lattice nodes travelled per time step where a time step is the time required to update the entire state-space volume. The component of momentum in the x-direction was measured at every time step and this signal was then Fourier transformed and the component with wave number k was extracted, all other Fourier components being noise. Phase and modulus of the remainder was calculated. Representative plots of the phase and modulus are shown in Figure 4.6 and 4.7.

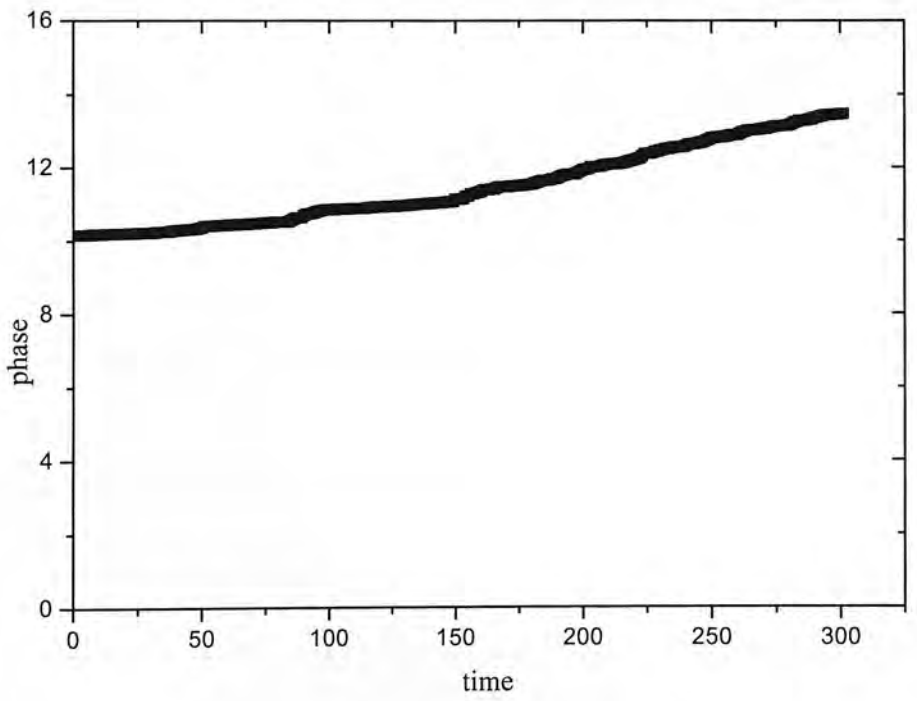

Figure 4.6.Phase of the shear perturbation as a function of time.

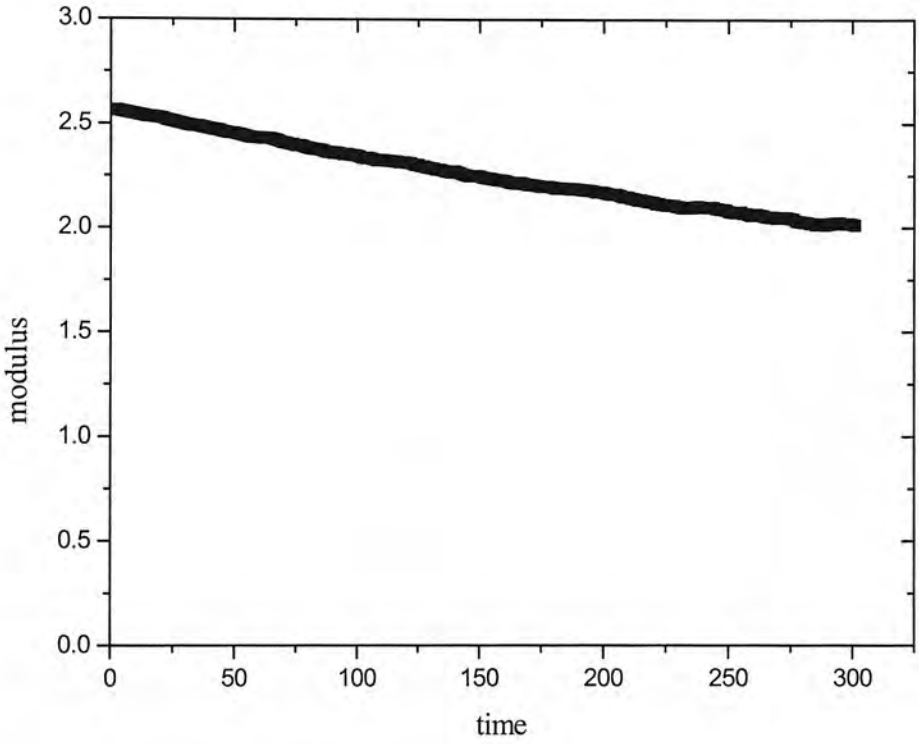

Figure 4.7. Modulus of the shear perturbation as a function of time.

The slope of the phase evolution is equal to gku_T in figure 4.6 and the slope of the modulus as function of time is equal to γk^2 in figure 4.7. Since k and u_T are input parameters it was possible to calculate g and γ from these slopes. The slope in figure 4.6 yield $g = 1.028 \pm 0.02$. It is evident from this result that this model achieves macroscopic Galilean invariance. Measured value of the Galilean invariance factor, g, and kinematic viscosity γ are shown in the below table 4.2.

density(ρ)	z	kinematic viscosity	g
10	8	0.269 ± 0.003	1.102 ± 0.02
12	8	0.256 ± 0.002	1.028 ± 0.03

Table 4.2. Simulation results for Galilean invariance factor.

4.5 Benchmarks

As this model is developed as new, it is planned to carry out further simulations to validate this model and check consistency. We examine some fluid dynamics experiments with the goal of further demonstrating the accuracy of the current implementation of the model of Teixeira. By simulating certain standard fluid dynamics experiments such as flow between parallel plates and flow past a circular cylinder, quantitative comparison of various flow properties with experimental results are possible. This provides further validation of the algorithm.

4.5.1 Poiseuille Flow

The work described in this section is to use the multi speed lattice gas method for a well-known flow: flow between two parallel plates known as Poiseuille flow and this type of flow is used for the experimental determination of the viscosity.

A lattice was formed of dimensions X= 354, Z =58, Y=6 and the nodes are linked between nearest neighbours according to a regular FCHC lattice. The longest side is considered as the flow direction. The lattice is initialized with particles of density ρ =5 and temperature related variable z = 8. Periodic boundary conditions are applied to the channel walls. The selection of bounce back conditions ensures that the average speed at each point of the channel walls is zero. With the x-direction being aligned to the length of the channel, the Navier-Stokes equation for this flow simplifies to

$$\frac{\partial}{\partial t}u_x = -\frac{1}{\rho}\frac{\partial}{\partial x}p + \upsilon\frac{\partial^2}{\partial y^2}u_x \qquad (4.17)$$

In a steady state condition, the flow is zero at the walls and reaches a maximum in the centre. The solution is

$$u_x(y) = u_0(1 - \frac{y^2}{a^2}) \qquad (4.18)$$

Where a is the half-height of the channel centred around $y = 0$. At equilibrium the velocity should attain a parabolic profile throughout the channel. From this result, a viscosity measurement can be obtained.

The simulation was started with the fluid at rest. Once the equilibrium was reached the data was accumulated for another 2000 time steps to assure the clean profile and measurements. A sample velocity distribution is shown in Fig 4.8. In the figure we show both the theoretical and simulation result and the channel flow gives the expected parabolic profile to a good degree of accuracy.

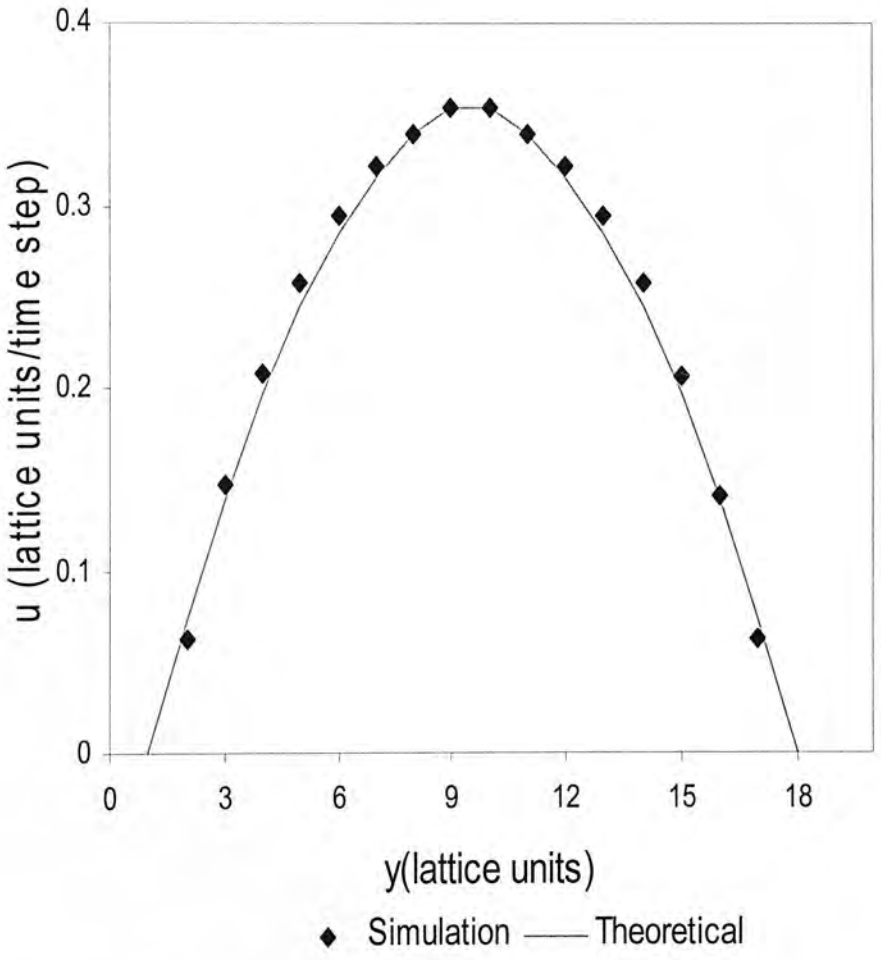

Figure 4.8. Flow distribution across a channel:Comparison of simulation with theoretical Poiseuille flow profile for three speed model.

A number of experiments for various densities ρ and temperatures z for the viscosity measurement are shown in Table 4.3.

density	z	kinematic viscosity
	2	0.503
5	5	0.442
	8	0.429
	2	0.361
8	5	0.343
	8	0.330
	2	0.328
10	5	0.286
	8	0.272
	2	0.311
12	5	0.264
	8	0.266

Table 4.3. Simulation results for viscosity measurements.

We see that as the temperature is increased (z is decreased) the kinematic viscosity also increases. This is the same trend observed for gases such as air. Furthermore the density dependence of the viscosity measurements is illustrated graphically in Figure

4.9. This also demonstrates the correct behaviour for gases with kinematic viscosity decreasing monotonically as the density is increased.

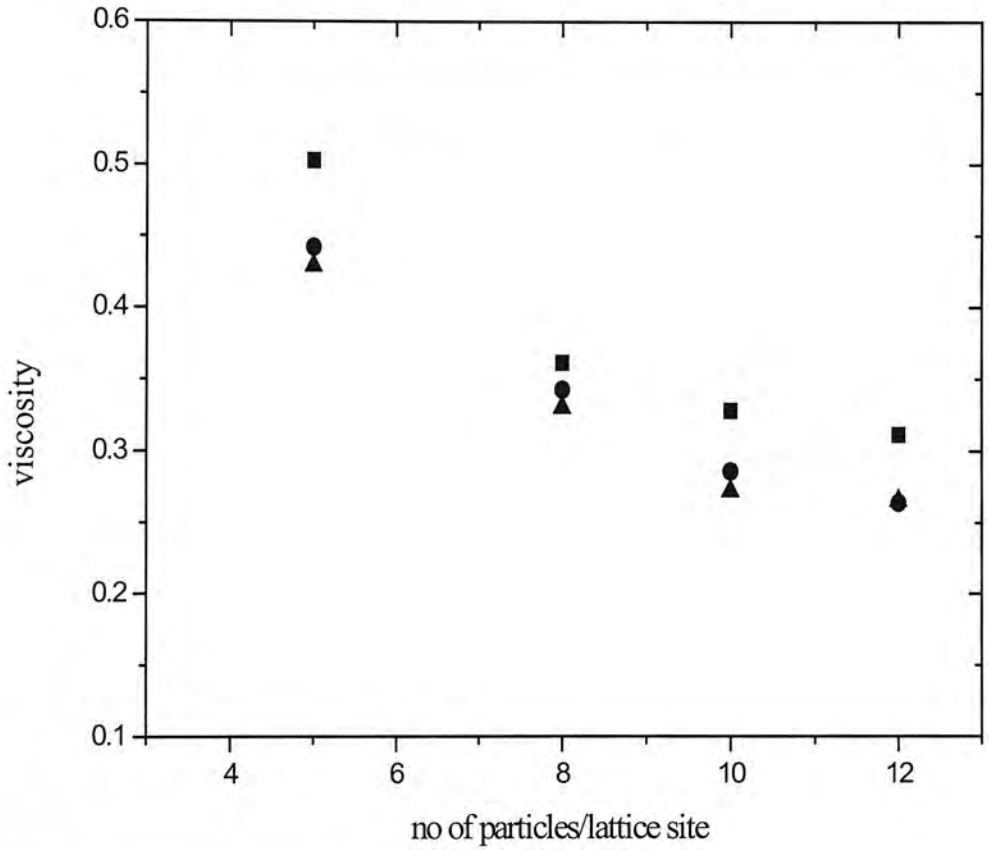

Figure 4.9. Simulation results of kinematic viscosity as a function of density.

z=8 (▲), z=5 (●), z=2 (■)

If the density becomes too large then collisions are actually inhibited because hole sites are needed for a collision to occur. We see evidence of this in Figure 4.9 for the high z (low temperature) flow where the viscosity has started to flatten out at high

densities. At low temperatures most of the particles reside in the low speed sites which inhibit energy exchange collisions into or out of these energies.

Calculations of the flow kinematic viscosity are compared with shear wave experiment and Teixeira results are shown in figure 4.10. The results are similar to what the Teixeira model described even though the exact method employed in his study is not known. We see that the viscosity measurements agree with each other. This is further strong evidence that the algorithm exhibits correct hydrodynamic behaviour as expected.

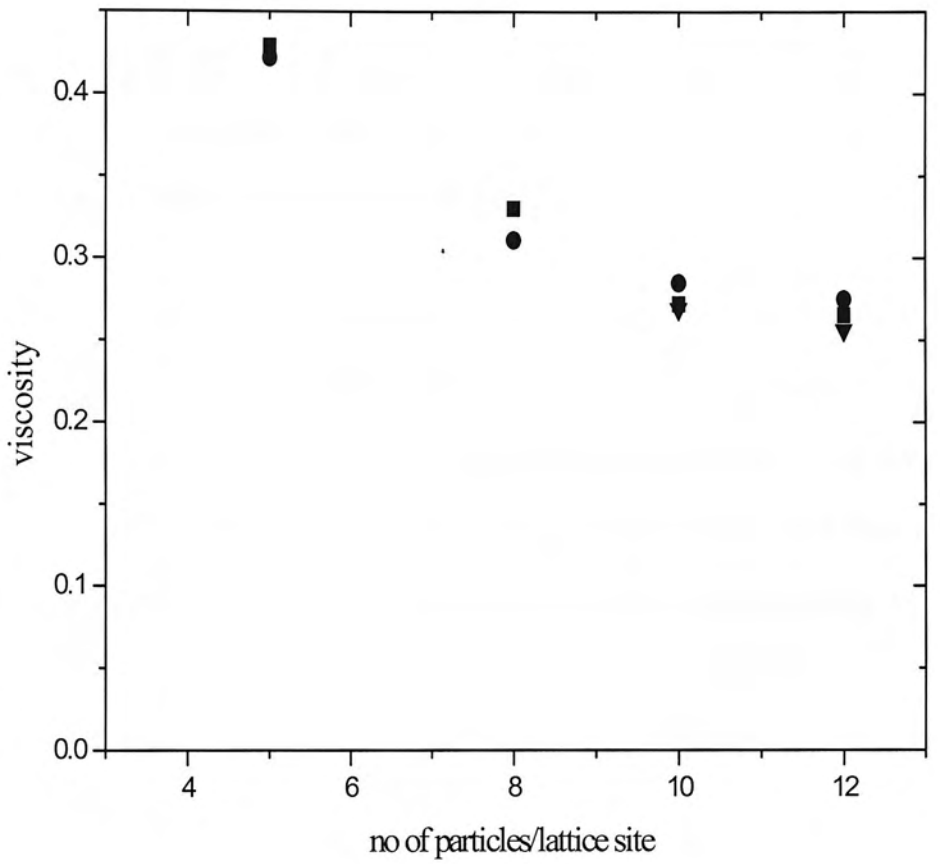

Figure 4.10. Kinematic viscosity as a function of density for z=8.

Simulation results (■), Teixeira results (●), data from shear wave measurement (▼)

4.5.2 Flow past a circular cylinder

Our GI-LGA model is used to investigate a most popular fluid dynamic experiment of the flow past circular cylinder to validate the system further. Cylinder was created in the LGA coding by assigning the nodes corresponding to the cylinder dimensions as a solid boundary. By setting the initial density and temperatures as constants, flow velocity is varied to obtain different Reynolds numbers.

Reynolds number is one of the important concepts in the fluid dynamics. It is a dimensionless number and it is defined as the ratio of inertial to viscous force. It quantifies the contribution of these forces in particular flow regime. Since viscous forces are dominant in laminar flow, the Reynolds number is small. Turbulent flow occurs at high Reynolds numbers. The Reynolds number can be calculated by the following

$$\mathrm{Re} = \frac{ud}{\upsilon}$$

where d is the diameter of the cylinder in lattice unit , u is the fluid velocity and υ is the kinematic viscosity of the fluid.

Random simulations were carried out with different lattice size. The lattice sizes were chosen from those lattice sizes reported in the literature and the GI-LGA model of Teixeira to facilitate the comparison of the results. The main flow property that was varied to get different Reynolds numbers was the flow velocity. The cylinder diameter also changed slightly in some cases.

A summary of the flow parameters for cylinder runs and system geometry for each case is given in Table 4.4. The system geometry is given as lattice units. The x direction is the length of the simulation volume which is the flow direction. The z and y directions represent the height and the width of the lattice size respectively.

Lattice Size			Diameter	Blockage ratio (%)	Re	C_d
x	z	y	d	d /z		
384	256	8	40	15.6	16	2.68
384	256	8	40	15.6	19.4	2.44
384	344	8	40	11.6	27.77	1.96
1280	512	8	44	8.6	29.45	1.88
384	256	8	40	15.6	31.52	1.80
1280	512	8	42	8.2	35.44	1.71
1280	512	8	48	9.4	41.79	1.61

Table 4.4. Summary of flow parameters (lattice units) for cylinder runs with Re < 45. Distances are measured in lattice units.

Simulations were run. Once the steady state had been reached, the drag on the cylinder was calculated to determine the drag coefficient

$$C_d = \frac{F_{cyl}}{A_{CS} \cdot \frac{1}{2} \rho u^2} \tag{4.19}$$

Where F_{cyl} the total is force on the cylinder and A_{CS} is the frontal cross-section of the cylinder which is equal to twice the radius multiplied by the cylinder length.

The force deposited to the wall by one particle is the amount of momentum imparted to the wall by the particle over the duration of the collision. To find the total force on the wall, we take twice the value of the component of momentum directed into the wall for particles that collide with the wall since the particles interact with solid boundaries by bouncing back from them.

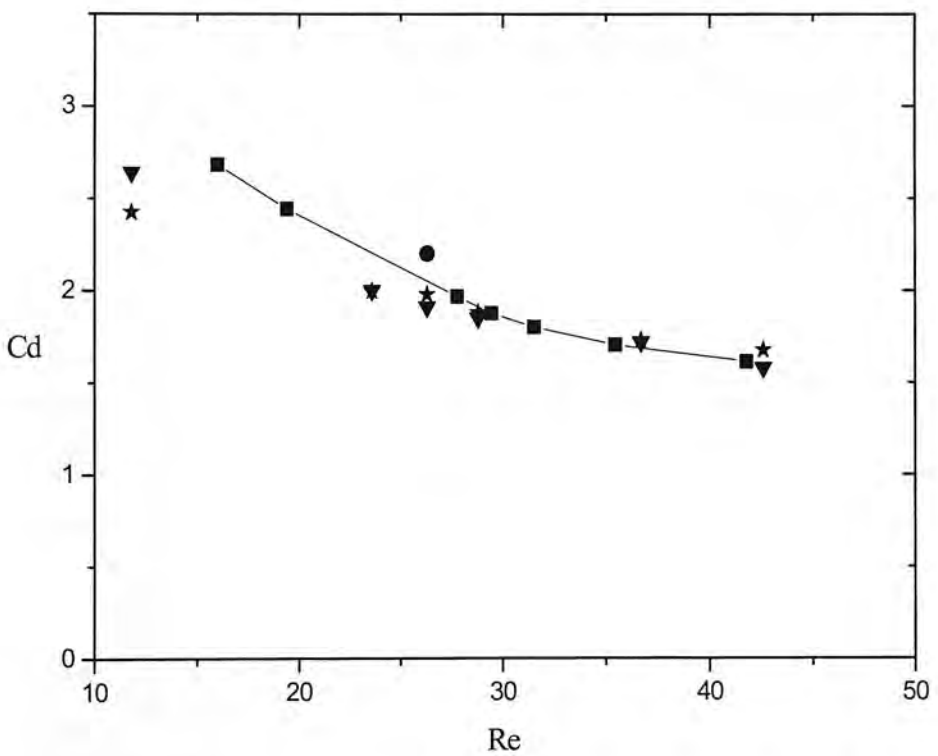

Figure 4.11. C_d Vs Re .simulation results (■), experimental results (▼), Teixeira results (□), CFD result (●) .The line connects the simulation results for clarity

The drag coefficient as a function of the Reynolds number is plotted in figure 4.11 along with the comparison of the literature results. Our results are comparable with

the experimental results of Tritton 1959 and CFD results of Karniadakis 1988 and with numerical simulations by Teixeira 1992. Quantitative agreement between our data and the literature results is satisfactory for Re > 25. There is a small discrepancy between our results and the literature results for low Reynolds number. One possibility for the disagreement at lower Re could be the influence of surface roughness for smaller radius cylinder and this issue concerns the degree to which we can delineate a continuously curving cylinder in a discrete lattice.

It might appear that the surface of a simulation cylinder of relatively small diameter is significantly rougher than a true cylindrical surface, since it is restricted to be defined by the lattice nodes. This was the smallest radius that was used in the cylinder experiments and so it represents the case with the largest surface roughness effect.

The second key geometrical consideration which is also of vital importance in wind tunnel experiments is the "blockage" or the ratio of the frontal projection area of the object to the total cross section area of the tunnel. The only effective way to reduce blockage is to actually simulate a larger physical volume. In this respect the result for Re=41.79 was carried out with the lowest blockage ratio and shows very good agreement with the experiment.

Summary

A three-speed GI-LGA model has been successfully implemented to accurately describe the hydrodynamic behaviour by removing the Galilean invariance artefact g. It is validated through a shear wave experiment. We have investigated the influence of sub-volume size and temperature difference on viscosity to choose the optimum parameters for the simulations.

An application of this model to the flow between two flat plates demonstrated the expected fluid dynamic behaviour. Flow around a cylinder compared well with literature results in measurement of the drag coefficient.

This GI-LGA model is applied to non-creeping single phase flow as flow at significant Reynolds number can now be studied correctly.

Chapter 5
New LGA model of non-creeping flow

Introduction

Even though the basic LGA models suffer some inherent shortcomings in non-creeping flow simulations, they are very good simulation tools for fluid flows in complex geometries. They have been used by many researchers in variety of problems in fluid mechanics. Stauffer *et al* (1991) summarized some of the basic fluid mechanics problems as well as flow through porous media applications. Apart from describing macroscopic phenomena, LGA methods also give microscopic detail. This property is very helpful to understand the volume-averaged parameters which are used in large-scale simulations of flow through porous media.

Existing literature on LGA methods for fluid flow through porous packed beds gives very limited information in marking the applicability of different flow regimes. There are no studies in literature, to our knowledge, on non creeping flows through random sphere packing using LGA methods. In this study we have attempted our single phase LGA model, which was validated and demonstrated to show gaining Galilean invariance, to simulate flow through a bed of non-overlapping randomly packed spherical particles. In this chapter, we start with a synopsis of different flow regimes and the details of implementation of GI-LGA for flow through random packing of spheres. This is then followed by results of our study and analysing the flow regimes that is characterised by the simulation results which are compared with the literature.

5.1 Review of flow regimes

Different types of flow patterns or regimes occur in porous media. Different types of forces that act on the particles and column wall contribute to the formation of different flow patterns. A comprehensive review on fluid flow regimes in porous media was published by Dybbs *et al.* 1975. The resistance to the flow of fluids through porous media was studied experimentally by Fand *et al.* 1987. In general, the flow regimes that are identified in fluid mechanics are termed as Darcy, Forchheimer, and turbulent flows. The predominant force which characterise each of these regimes will fall into one of the following category: viscous, inertial or turbulent forces. The following regimes can be defined based on the above forces:

(1) In the Darcy regime, the flow is dominated by viscous forces. Here, the pressure gradient is proportional to the flow rate.

(2) The viscous-inertial flow regime in which the relationship between the pressure gradient and the flow rate becomes non-linear. This is characterized by the laminar wake oscillations followed by the formation of vortices. This is termed as Forchheimer flow.

(3) A highly unsteady and chaotic regime that qualitatively resembles turbulent flow.

In addition to the flow regimes described above, another flow behaviour pattern was described based on Reynolds number values. Bear (1972) identified that Darcy's law does not hold true below a particular value of Reynolds number. The flow in this regime is referred as pre-Darcy flow. A considerable amount of research has been

conducted to obtain information on the flow resistance in both Darcy and Forchheimer regimes.

5.1.1 Darcy flow

Henry Darcy, in 1856, derived the following empirical relationship for relatively low-velocity one dimensional flow through porous media

$$P' = \frac{\mu}{K} u \tag{5.1}$$

Where P' is the pressure gradient, μ the dynamic viscosity, u is the fluid velocity and K is a constant called permeability.

Darcy's equation, also known as the Darcy's law, is applicable only to a restricted interval of the Reynolds number. The lower and upper bounds of the Darcy regime is shown in figure 5.1.

5.1.2 Forchheimer flow

Forchheimer (1901) suggested a non-linear relationship between the pressure gradient and fluid bulk velocity when viscous and inertia forces coexist and his proposed equation is

$$P' = au + bu^2 \tag{5.2}$$

Where a and b are constants and u is the fluid velocity. It is governed by the sum of two terms; one proportional to u and the other to u^2 that takes into account both the viscous and inertial effects of the flow.

Ergun (1952) expanded the above equation by relating the above terms to other elements influencing the flow like properties of the fluid, fractional void volume, orientation, size, shape of the porous matrix and dependence upon the flow rate. He concluded that the pressure gradient in a fixed bed can be equated to the sum of the following two terms; one related to the dissipation of viscous energy and the other related to the dissipation of kinetic energy. His proposed equation is

$$P' = A\frac{(1-\phi)^2}{\phi^3}\frac{\mu\upsilon}{d^2} + B\frac{(1-\phi)}{\phi^3}\frac{\rho\upsilon^2}{d} \tag{5.3}$$

Where A and B are dimensionless constants, μ is the dynamic viscosity of the fluid, ρ is the fluid density, d is the mean equivalent diameter of the porous matrix and ϕ is the porosity.

Irmay (1965) averaged the Navier-Stokes hydrodynamic viscous flow equation by using statistical methods to derive a non-linear equation applicable to Forchheimer regime and the derived expression is

$$P' = A\frac{(1-\phi)^2}{\phi^3}\frac{\mu\upsilon}{d^2} + B\frac{(1-\phi)}{\phi^3}\frac{\rho\upsilon^2}{d} + \frac{\rho}{\phi}\frac{d\upsilon}{dt} \tag{5.4}$$

The last term in the above equation accounts for unsteady flow and its value become 0 when the flow achieved steady state. So Ergun's and Irmay's equation are identical for steady state flows.

5.1.3 Dimensionless Expressions

In order to determine and define the transitions of flow to different regime in the simulation data, we need appropriate parameters. Ergun's expression for resistance to flow through packed columns is shown in equation 5.3. It can be derived in the following form which makes it a dimensionless parameter.

$$P' \frac{d^2}{\mu \upsilon} = A \frac{(1-\phi)^2}{\phi^3} + B \frac{(1-\phi)}{\phi^3} \mathrm{Re} \qquad (5.5)$$

The equation 5.3 can also be non-dimensionalized by appropriately inserting the actual flow Reynolds number based on the interstitial fluid velocity in the formula.

$$P' \frac{K}{\mu \upsilon} = 1 + \frac{B}{\sqrt{A}} \frac{\upsilon}{\phi} \frac{\rho \sqrt{\frac{K}{\phi}}}{\mu} = 1 + \frac{B}{\sqrt{A}} \mathrm{Re}_k \qquad (5.6)$$

It may be noted from the above expressions that the relevant non-dimensional group that governs the resistance to fluid flow through packed columns is either the Darcian Reynolds number based on particle diameter, Re, or the actual flow Reynolds number, Re_k, based on the interstitial fluid velocity which is $\upsilon^f = \upsilon / \phi$. Though both Reynolds numbers have been in use for fluid dynamic calculations, some would prefer the actual flow Reynolds number because of its weaker dependence on the porosity of the medium ϕ (Ifiyenia *et al.*1994). From the above expression the dimensionless pressure drop = $(P' \frac{K}{\mu \upsilon^f \varphi})$ and the actual flow Reynolds number, $\mathrm{Re}_k = \frac{\rho \sqrt{\frac{K}{\phi}}}{\mu} \upsilon^f$ can be calculated. Here ϕ and P' represent porosity and pressure drop respectively.

The dimensionless pressure drop as a function of Reynolds number for different flow regimes is shown in figure 5.1. Both Forchheimer and turbulent flows should have the same functional dependence on the Reynolds number. But the slope of the curve should be different for both flow regimes.

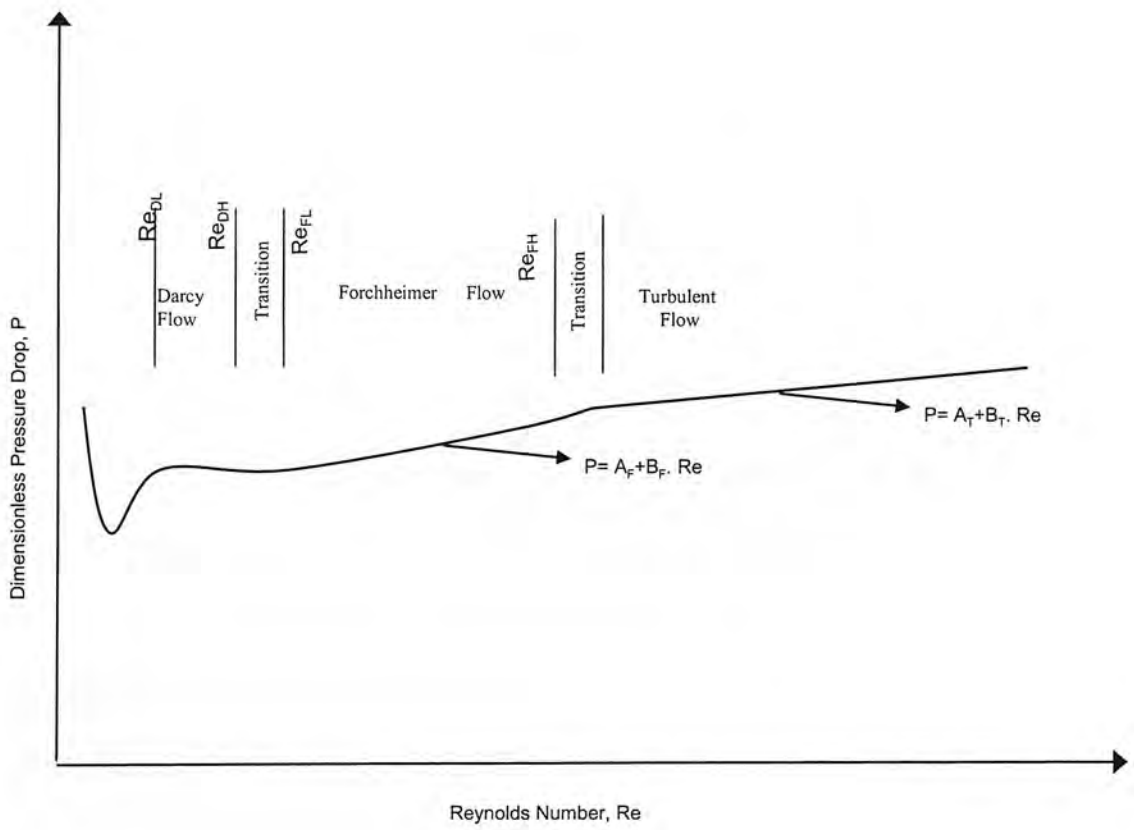

Figure 5.1. Flow regimes for fluid flow through porous media (after Ifiyenia *et al.* 1994).

In the Darcy regime, lower and upper bounds of Reynolds number will be designated by Re_{DL} and Re_{DH}. The lower and upper bounds of Re of Forchheimer flow is represented in the graph as Re_{FL} and Re_{FH}. The region between Re_{DH} and Re_{FL} is a transition region where the flow changes from Darcy to Forchheimer regime.

Beyond Re_{FH} there is another transition region which leads to the beginning of turbulent flow, designated herein as the "post- Forchheimer regime".

5.2 GI-LGA model of fluid flow in random sphere packing

In this part of the study, we experimented our GI-LGA model to simulate fluid flow in a bed of non-overlapping spheres. This non-overlapping sphere bed consists of uniform spheres and represents the model for porous media. The details of design and implementation are described in the next section.

5.2.1 Lattice configuration

We have coded a program for generating random packing of spheres using c++. It is based the algorithm of Nolan *et al* (1992) who created a program for random packing of hard spheres. His algorithm has features common with compressed gas model (Finney, 1976) and sequential dropping and rolling of spheres (Tory *et al.* 1968). This simulation can randomly pack hard spheres in a cylinder for gravitationally stable lattices ranging from random loose packing to random close packing. This model predicts the packing densities ranged from a minimum of 0.509 to a maximum of 0.638 and we have achieved the packing density of 0.57. A three dimensional view of the granular bed is illustrated in Figure 5.2.

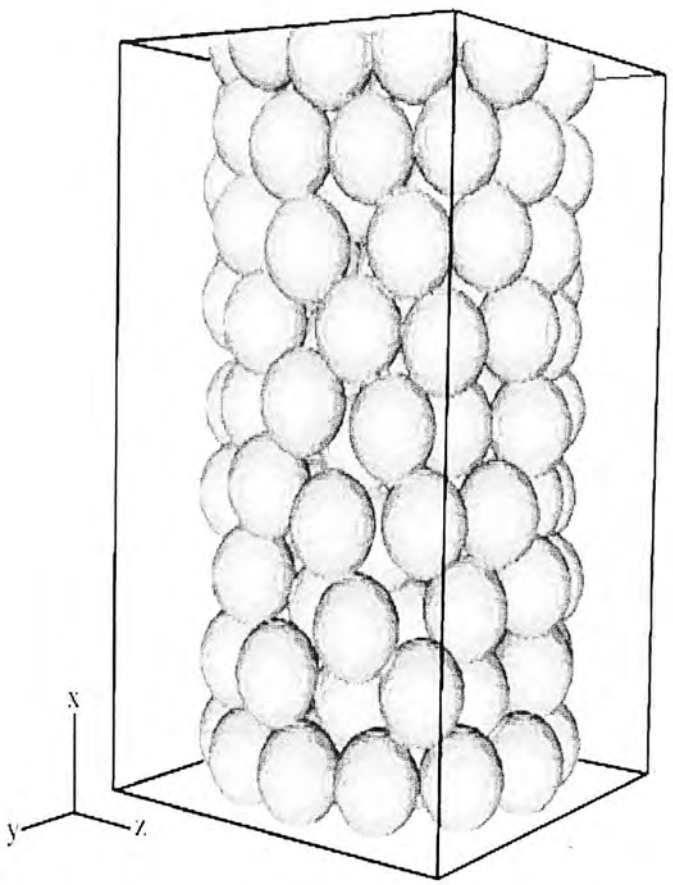

Figure 5.2. A three dimensional geometric view of a granular bed.

Example of the cross sectional view of this random packing is shown in figure 5.3. The empty circles represent the packing of spheres as regions with zero velocity (This figure also contains interstitial fluid flow).

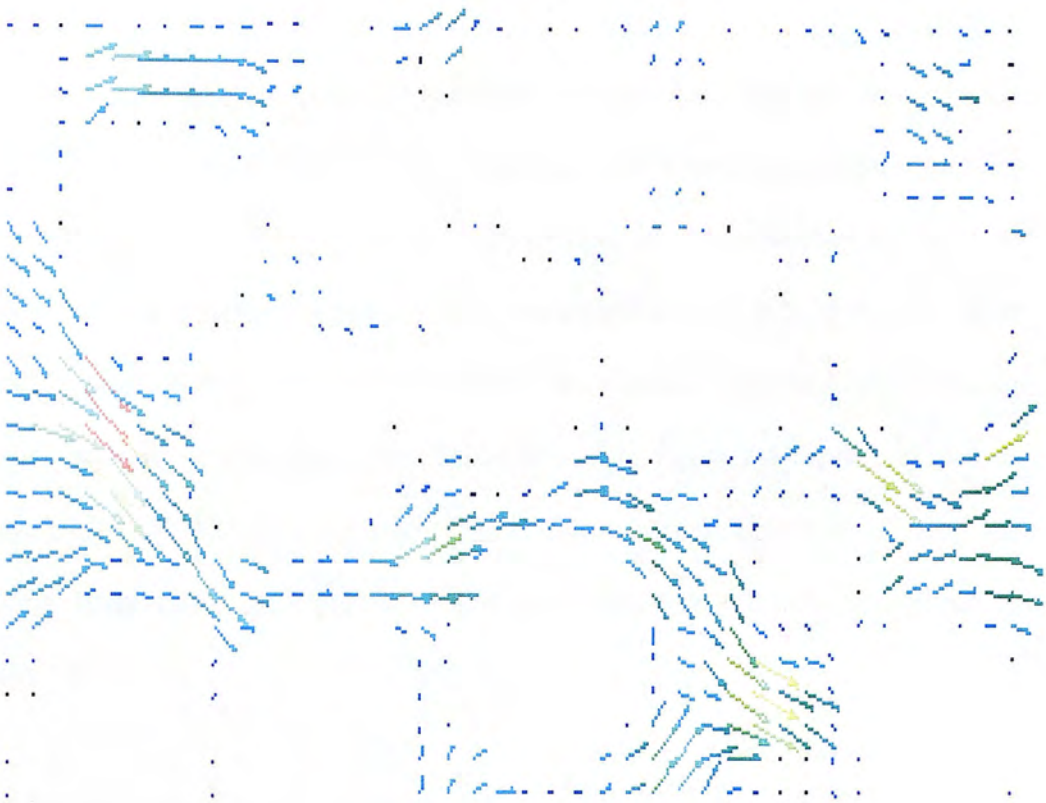

Figure 5.3. Cross sectional view of packed sphere bed.

The programs used in simulations are generally of those developed for the initial multi-speed GI-LGA model and the implementation details were similar as discussed in previous chapter. Additional coding was added to accommodate the sphere packing where it is necessary.

5.2.2 Implementation

In this simulation, a lattice with dimension of x =200, y=120, z =200 and a sphere diameter of 20 lattice units were used. The simulation is started with one level of flipping and the flow rate is calculated from an average over 100 time steps. Once it reached steady state, the sampling was done.

Flow rate as a function of time step is plotted in figure 5.4. This plot demonstrates how the simulation starts from the initial condition until it reaches the steady state for a single flipping. Multiple simulations were carried out by increasing the force of flipping to obtain a higher flow rate. This is explained in detail in section 3.3.5. With increasing level of flipping there is a change in momentum states of a set of number of lattice particles at each time step. In the following figure 5.4 the steady state is achieved after about 400 time steps where the sampling was done. During the sampling 10 blocks of data each over 100 time steps were accumulated to get an average value.

The pressure gradient is also calculated in the same manner for each level of flipping during the above simulations. Pressure gradient, ΔP was calculated during the simulation by accumulating the z-component of the momentum transfer to the solid surfaces. It is described by the following expression (Humby *et al.*2002)

$$\Delta P = \frac{1}{w_{xy}} \sum_{i \in s} m_i (c_{zi} - c_{zi'})$$

Here the summation is the overall particles impinging upon the solid surfaces. c_{zi} and $c_{zi'}$ are the z component of the velocities before and after collision with the solid surface. w_{xy} is the simulation domain normal to the direction of flow.

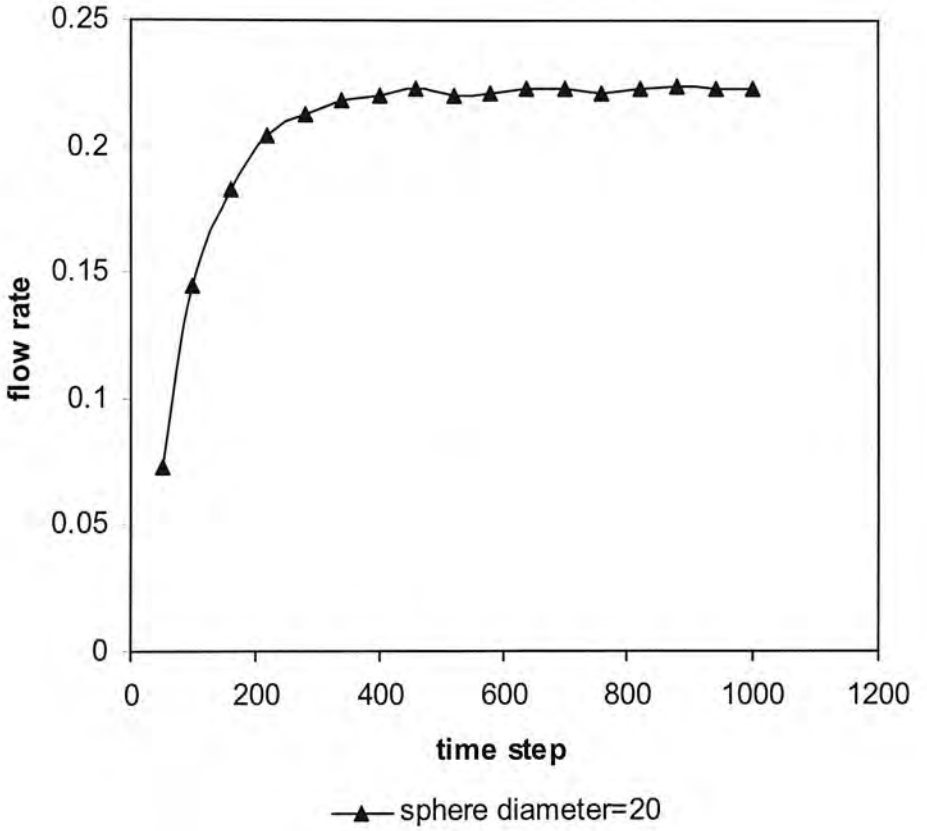

Figure 5.4. Volumetric flow rate as a function of time step.

5.2.3 Simulation results for various sphere packing

Several random spheres packing were tested to check the results are independent of the configuration of randomly packed spheres.

The following three different randomly packed beds of spheres have been generated and simulations were done for each packing as described above:

1) 42 spheres with lattice size x = 32, y= 80 ,z = 80
2) 83 spheres with lattice size x = 80, y= 48 ,z = 80
3) 200 spheres with lattice size x = 112, y= 80, z = 80.

All the above measurements are given in lattice units. A sphere diameter of 16 lattice units was used in all the packing. A plot of pressure gradient versus velocity is presented in figure 5.5.

There was no significant variation in the results for these three packing configurations. The results appear to be independent of the size of the domain relative to the number of spheres. The sphere packing contains 83 spheres was selected as a representative model for all further studies in this chapter.

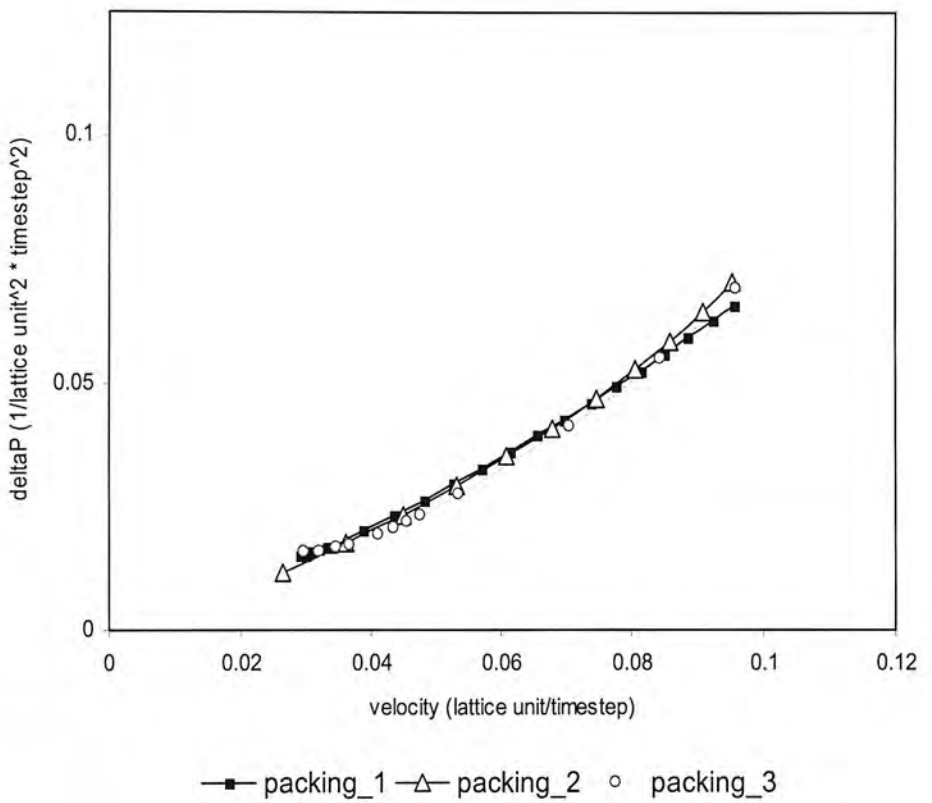

Figure 5.5. deltaP versus velocity for various sphere packing configurations.

5.2.4 Simulation results for various sphere diameters

Uniform sphere packing with various diameters were tested to achieve suitable level of discretization. The simulations were started with the volume size of x = 80, y= 48,

z = 80 with sphere diameter of 16 lattice units. Then the sphere diameter is varied from 16 lattice units up to 60 lattice units.

The sizes of the simulation domains for the various sphere diameters are listed below:

x	y	z	sphere diameter
80	48	80	16
100	60	100	20
130	78	130	26
180	108	180	36
200	120	200	40
300	180	300	60

Each point in the plot was an average of five to six simulation results to reduce the error margin. The velocity and ΔP were calculated in each simulation. A total of more than 100 simulations were carried out in this study. The results of ΔP versus velocity are presented in figure 5.6. When we increased the sphere diameter from 40 lattice units up to 60 lattice units, we could observe that there is no significant variation in the results. Therefore, we have used the lattice size with the sphere diameter of 40 lattice unit as a standard simulation for all the results analysis and discussion.

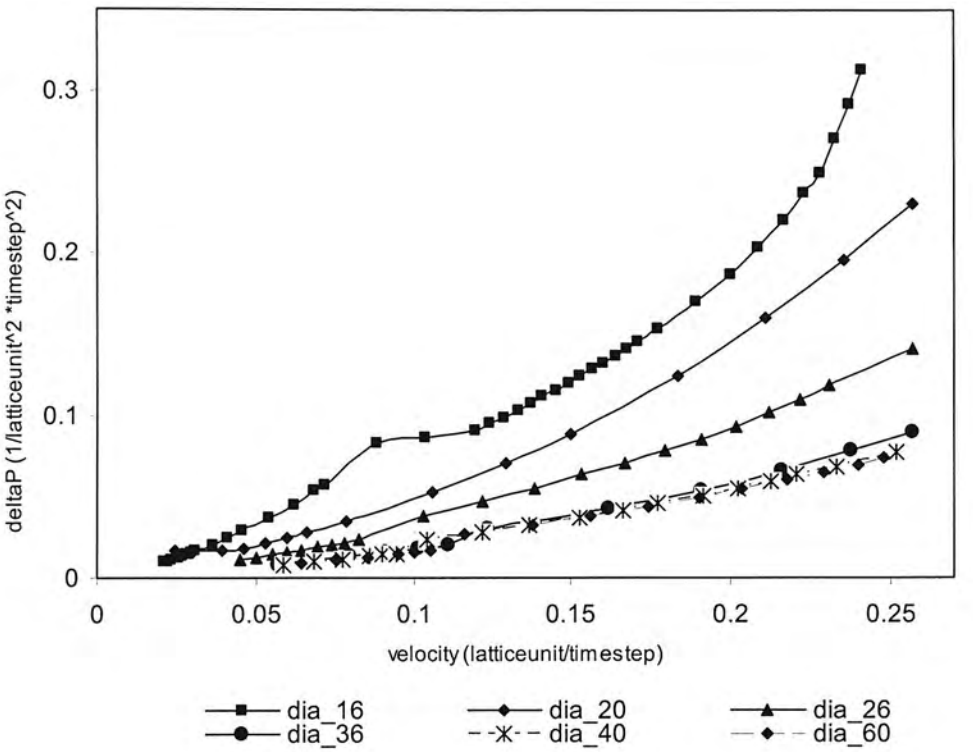

Figure 5.6. deltaP versus velocity for various sphere size (lattice unit) – from 16 to 60.

5.3 Flow regime analysis

To analyse the flow regime, further simulations were carried out with lattice domain size of x=200, y=120, z=200 which contains 83 spheres of 40 lattice units sphere diameter. Dimensionless pressure drop and the actual flow Reynolds number were calculated and plotted in figure 5.7.

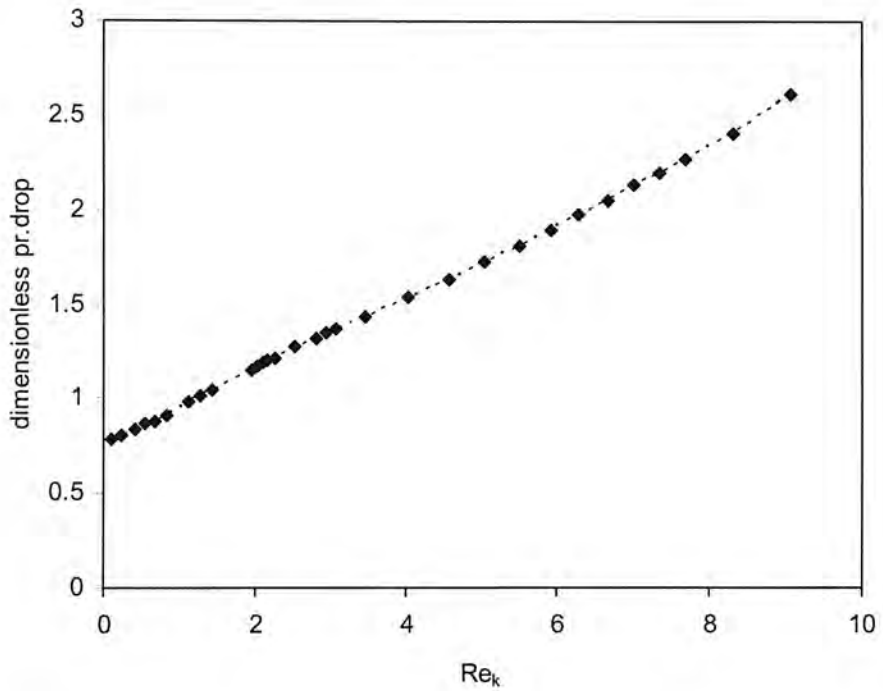

Figure 5.7. dimensionless pressure drop versus actual flow Reynolds number for entire regime.

The above plot is split into different flow regime to facilitate the analysis.

Darcy regime is presented in figure 5.8. In this regime, a range of Reynolds numbers for which the dimensionless pressure drop is proportional to Re. From this part the porous medium permeability was determined. Darcy flow was observed with the lower bound of Re_{DL} is 0.23 and the upper bound of Re_{DH} is 1.43. These limits were determined by the changes occurring in the slope of the plot.

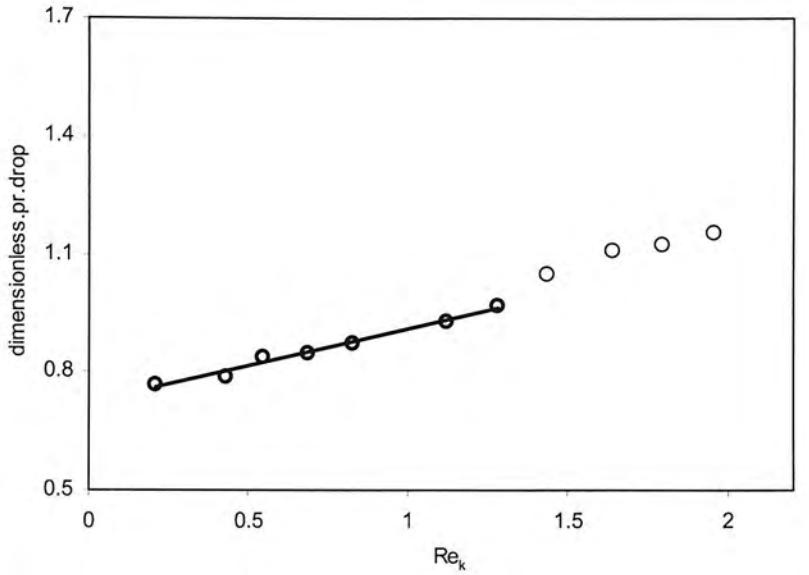

Figure 5.8. dimensionless pressure drop Vs actual flow Reynolds number for Darcy regime.

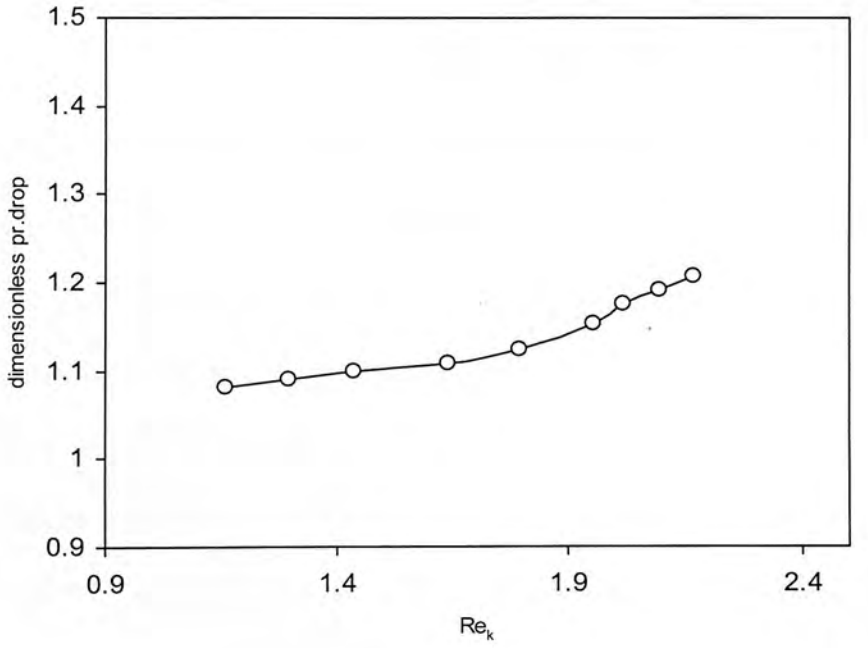

Figure 5.9. dimensionless pressure drop Vs actual flow Reynolds number for transition from Darcy to Forchheimer regime.

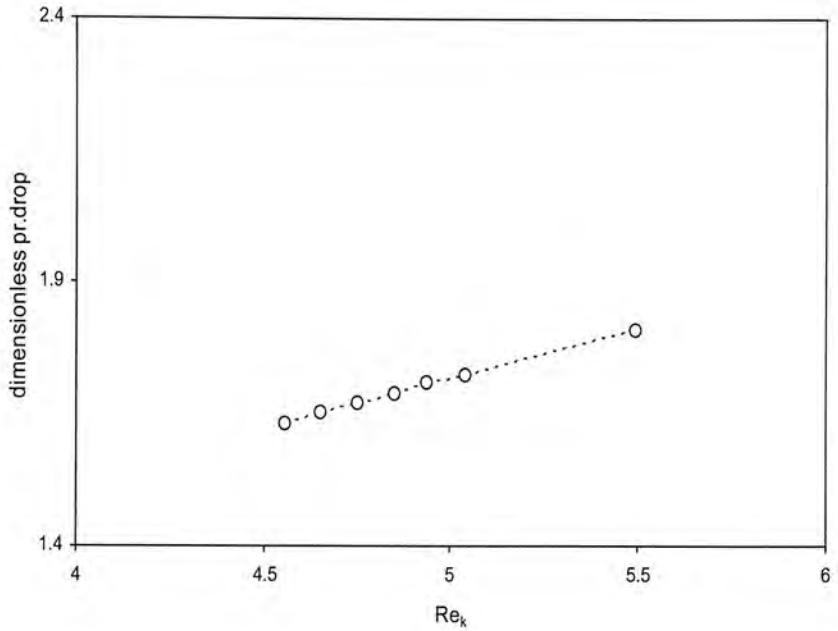

Figure 5.10. dimensionless pressure drop Vs actual flow Reynolds number for transition from Forchheimer to turbulent regime.

The region between Re_{DH} and Re_{FL} shown, in figure 5.1, is a transition region from Darcy to Forchheimer. The corresponding flow regime obtained from our study is demonstrated in figure 5.9. It occurs between the Re_k of 1.43 and 1.79. As the flow continues, there is appreciable change is seen in the slope of the plot.

The regime corresponds to Forchheimer flow is shown in figure 5.17. The lower bound of Re_{FL} is > 1.79 and the upper bound of Re_{FH} < 4.5 is identified. In post-Forchheimer flow there is another transition regime and it shown in figure 5.10. As the flow continues in this regime it becomes turbulent flow. It is not as well demarcated and described as the previous transition regime from Darcy to

Forchheimer. We have identified the turbulent flow regime for which $Re_k > 5.04$ and it is shown in figure 5.18.

5.4 Discussion

There are no results found in the literature which used GI-LGA methods for the simulation of flow in a random sphere pack which restrict the scope for direct comparison of our results. However, there are few results found in the literature from studies of flow through random sphere packing by experimental work and numerical simulation based on volume-of-fluid method.

Ergun (1952) summarized the important factors that influence the flow of fluids through packed columns. From his experimental studies he concluded that there was no evidence of variance of the coefficient of the viscous and kinetic energy term with porosity in equation. Macdonald *et al (*1979) reviewed the experimental study results of Gupte (Rumpf and Gupte, 1971) which measured the dependence of the permeability on the porosity using spherical glass beads packed in a uniformly random manner. In the above experimental data was analysed with Ergun's equation in his review paper and concluded that Ergun equation appears to be accurate and also in order to get a better fit to the data points, he used $\phi^{3.6}$ instead of ϕ^3 in the equation. Fand *et al* (1987), in two different studies, examined the resistance of fluid flow through random packing experiments. One of his studies was using uniform sphere diameter packing with porosity of ~0.36. He used particle based Reynolds number for the pressure drop calculations.

Ifiyenia *et al* (1994) summarized the recalculated correlations of Fand *et al* (1987), Macdonald *et al* (1979) and Ergun (1952). The details are presented in table 5.1. Mousavi *et al* (2006) studied fluid flow through random packing of non-overlapping spheres by CFD approach using volume-of-fluid method. He has given plots for the dimensionless pressure drop versus Reynolds number for two-post Darcy regimes in his study. We have calculated the correlation coefficients based on these plots and included in the table 5.1 for comparison.

We have plotted our simulation results along with the results from the above studies in figure 5.11 and compared.

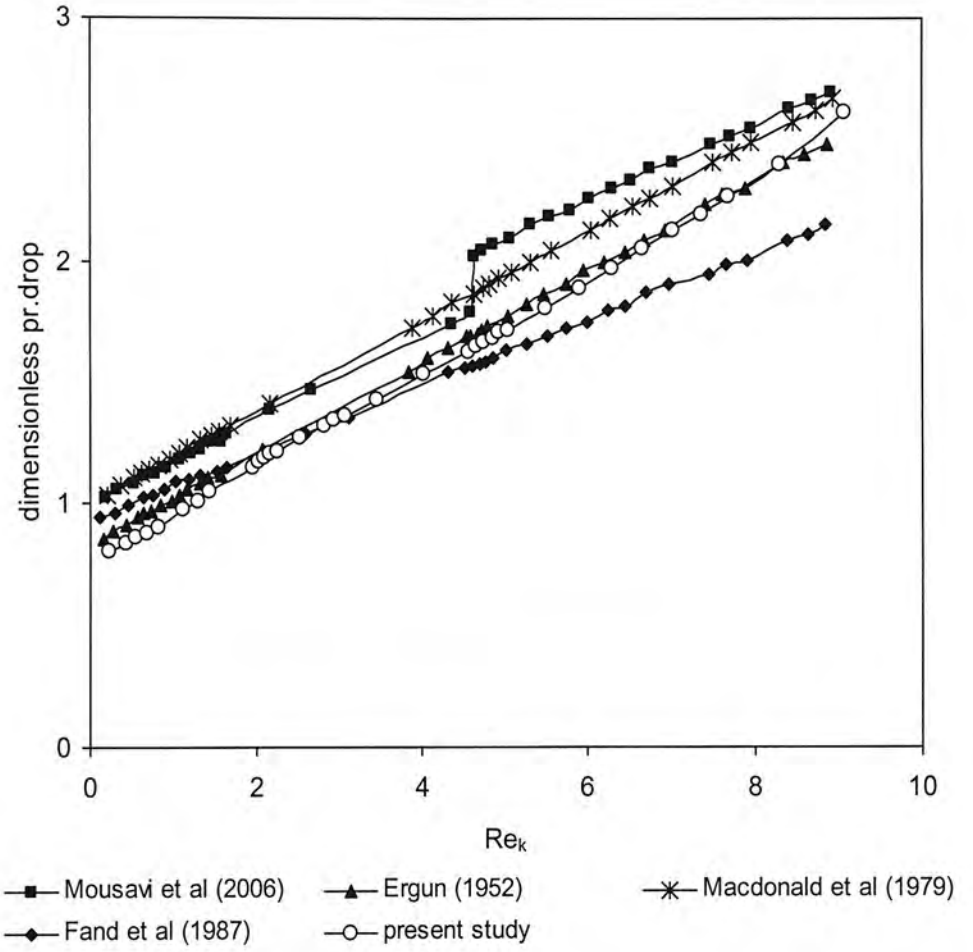

Figure 5.11. dimensionless pressure drop Vs actual flow Reynolds number.

For clarity, individual regimes are plotted separately along with literature results and discussed below.

Plots for Darcy regime is shown in figure 5.12. From the figure, our results are in good agreement with other results. It may be noted that our results are in very good agreement with Ergun (1952) results. Simulation results of Mousavi *et al* (2006) are closer to Macdonald *et al* (1979). We don't have enough data to plot the full flow regime from the Fand *et al* (1987) results. So comparison can not be made.

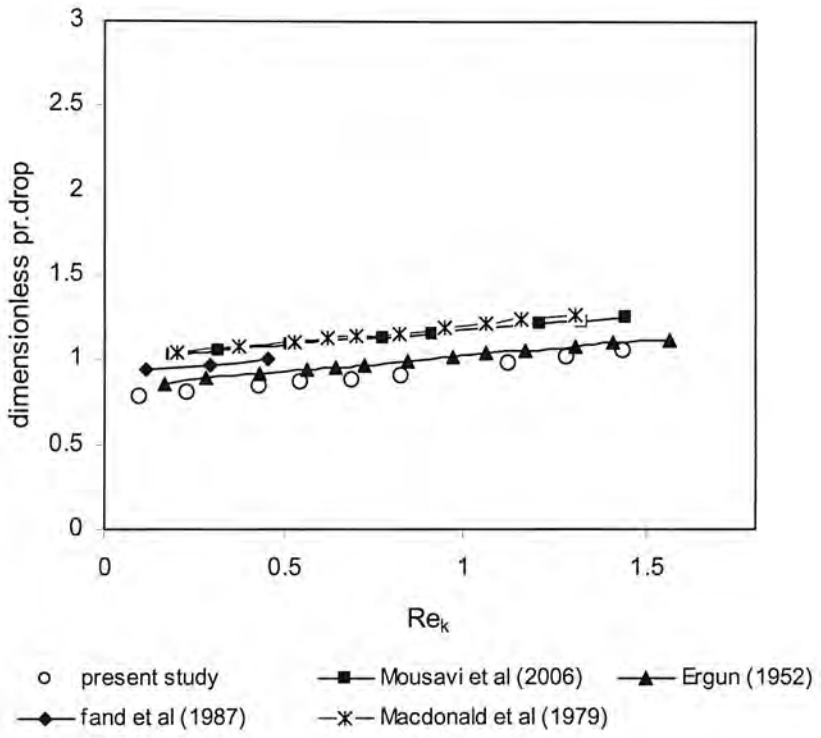

Figure 5.12. dimensionless pressure drop as a function of actual flow Reynolds number for Darcy Regime.

The plots transition from Darcy to Forchheimer regime is given in figure 5.13. It is noted from the figure, though there is a slight separation of plots, still our simulation results are close to the experimental result of Ergun (1952). As with previous regime, the simulations of Mousavi *et al* (2006) are closer to Macdonald *et al* (1979).

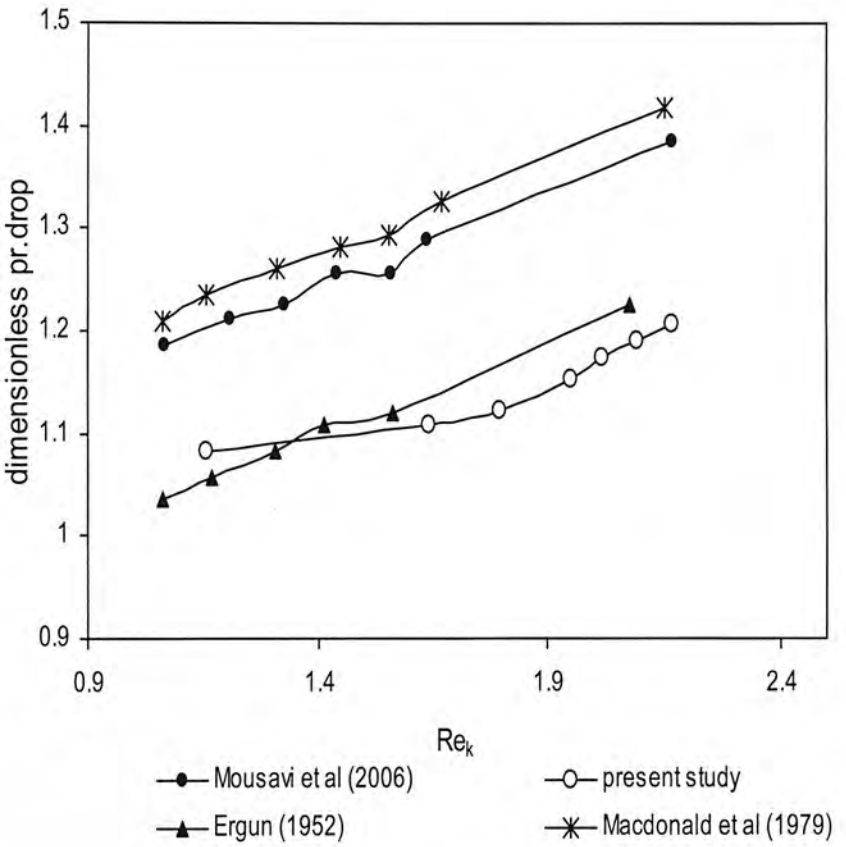

Figure 5.13. Plot of dimensionless pressure drop as a function of actual flow Reynolds number for transition from Laminar to Forchheimer regime.

The plot for the Forchheimer regime is shown in figure 5.14. The results are closer to the range of experimental results of Ergun (1952) and Fand *et al* (1987).

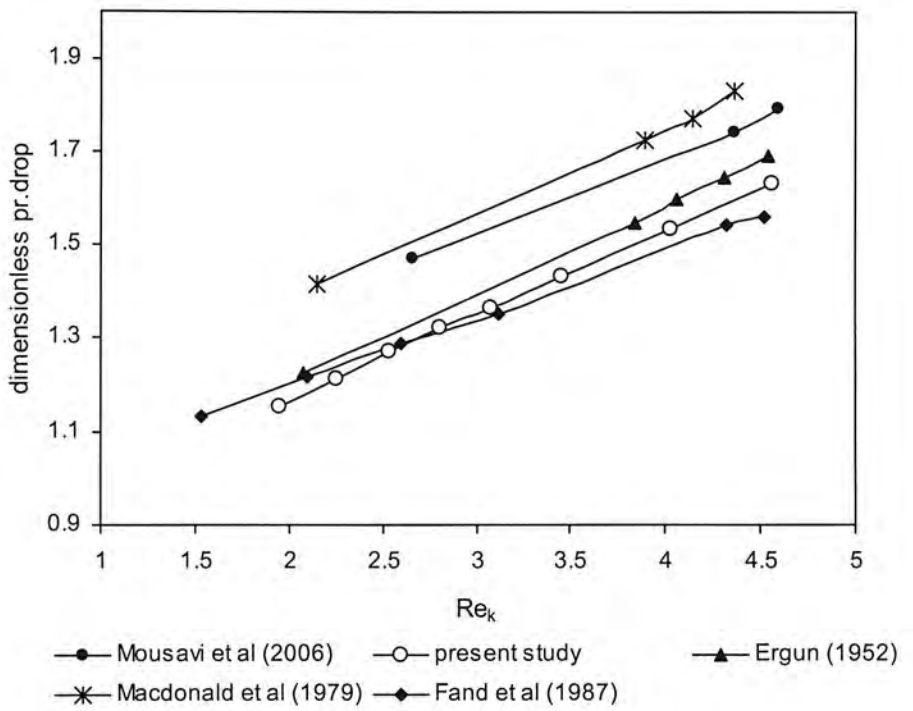

Figure 5.14. Plot of dimensionless pressure drop as a function of actual flow Reynolds number for Forchheimer flow.

Figure 5.15 shows plots for the transition from Forchheimer to turbulent regime. Our results comparable and are closer to the experimental results of Ergun (1952). An anomalous jump is noted in Mousavi *et al* (2006) simulation results for which there is no obvious explanation. There is no data available for Fand *et al*(1987).

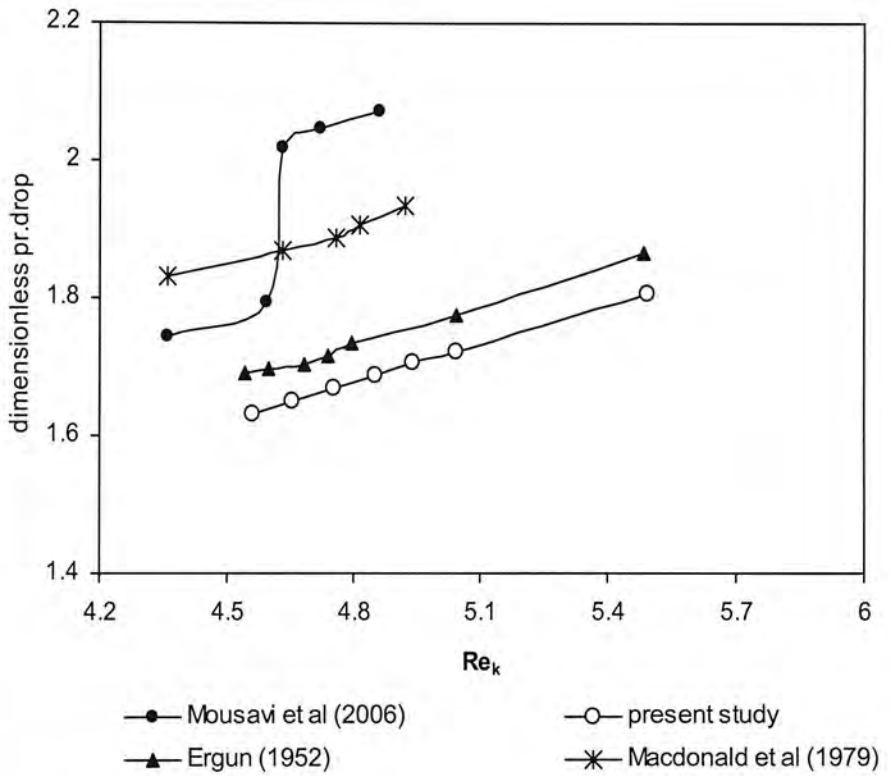

Figure 5.15. Plot of dimensionless pressure drop as a function of actual flow Reynolds number for transition from Forchheimer to turbulent regime.

The results for the turbulent regime are shown in figure 5.16. In this regime, the same trend continues with good agreement between Ergun (1952) and our simulation results. Mousavi *et al* (2006) reports a higher pressure drop in the turbulent region than Macdonald *et al* (1979).

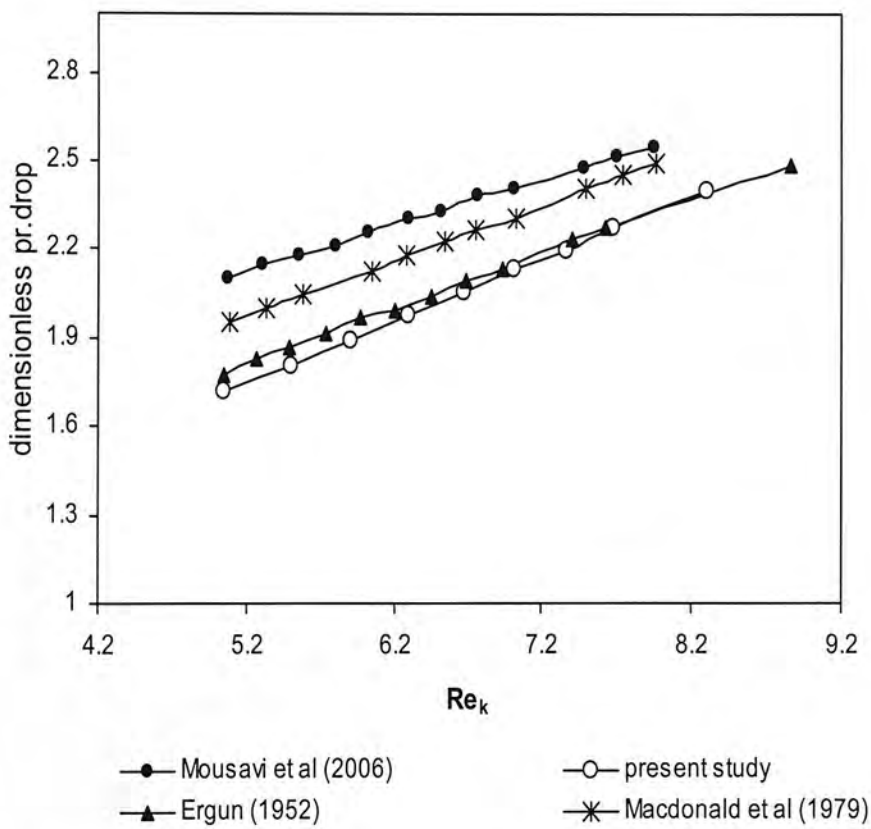

Figure 5.16. Plot of dimensionless pressure drop as a function of actual flow Reynolds number for turbulent regime.

5.4.1 Pressure drop equations

As we have seen earlier, the pressure drop may be expressed as a non-dimensionalised function of the Reynolds number (Ifiyenia *et al.* 1994 and Mousavi

et al 2006). The pressure drop coefficients calculated from our studies are summarised below in table 5.1.

The results are presented separately for the Forchhemier regime, the turbulent regime and then over the whole set of data for comparison with other authors. For the individual regimes, only the measurements of Fand and the simulations of Mousavi are available for comparison.

Figure 5.17 shows the best fit for the Forchheimer regime.

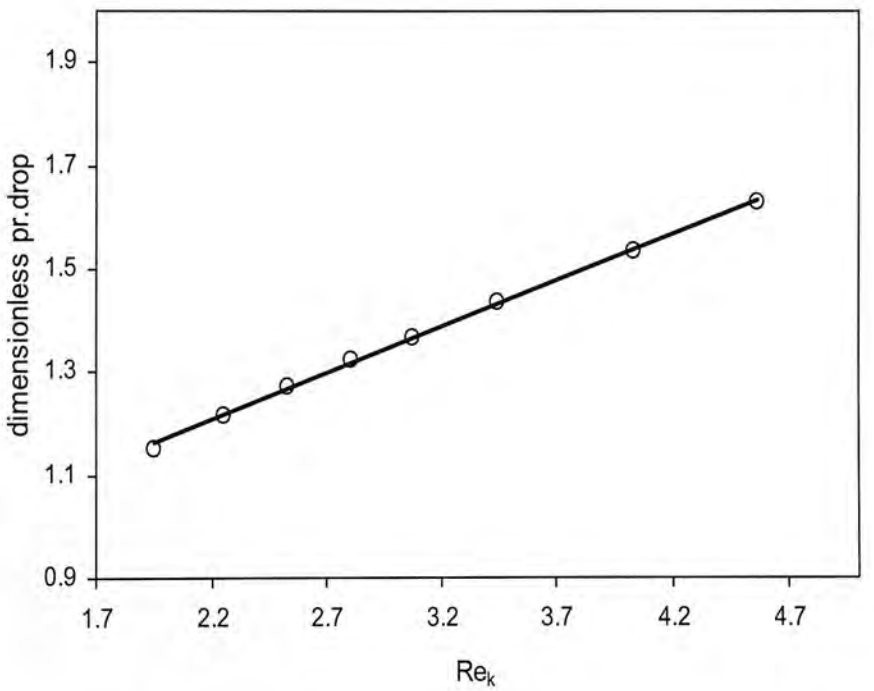

Figure 5.17. Plot of dimensionless pressure drop as a function of actual flow Reynolds number for Forchheimer regime.

The equation given for this regime is then,

$$\frac{P'K}{\mu\upsilon} = 0.826 + 0.176\,\mathrm{Re}_k$$

The R^2 value for this fit is 0.9999. The slope is 20% higher than the experimental work of Fand *et al* (1987) and 7% higher than the numerical study of Mousavi *et al* (2006). The intercept is 10-20% lower than from their results as this would be expected from the previous plots.

The turbulent regime (Figure 5.18) also achieves a high correlation of $R^2 = 0.9997$.

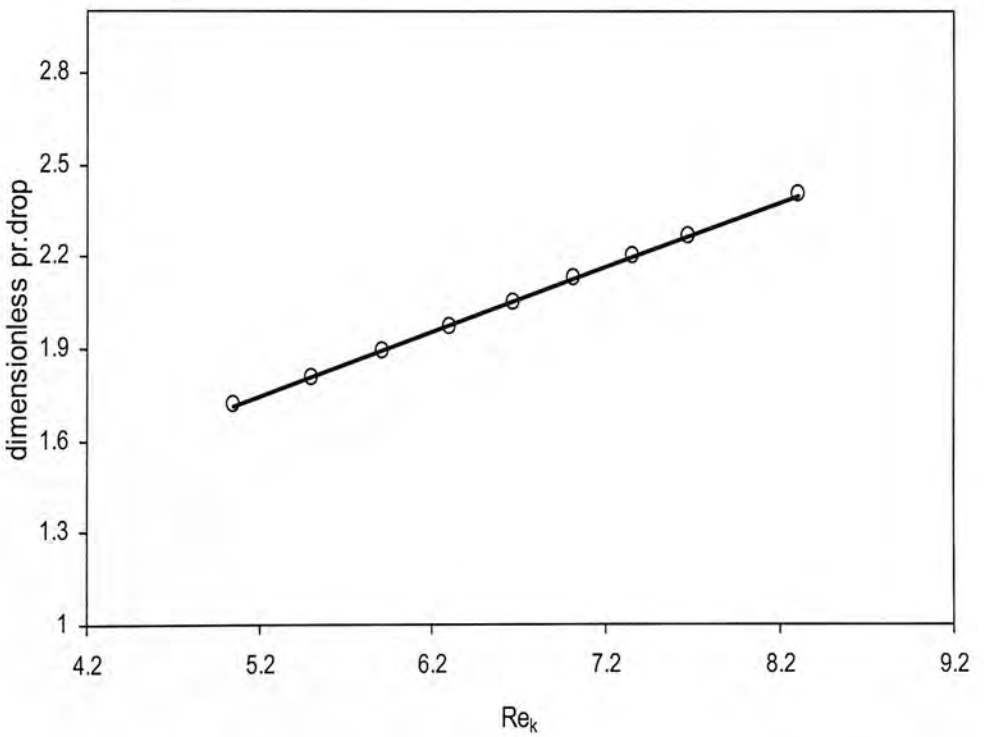

Figure 5.18. Plot of dimensionless pressure drop as a function of actual flow Reynolds number for Turbulent regime.

The equation for this regime is given by

$$\frac{P'K}{\mu\upsilon} = 0.653 + 0.2102\,\mathrm{Re}_k$$

The slope of the equation is 25% - 40% higher than those of either Fand *et al* (1987) or Mousavi *et al* (2006) and the intercept is 40- 50% lower than with their results.

Over the complete range of results (figure 5.19) the following equation is obtained with a correlation of R^2= 0.9979.

$$\frac{P'K}{\mu\upsilon} = 0.756 + 0.196\,\mathrm{Re}_k$$

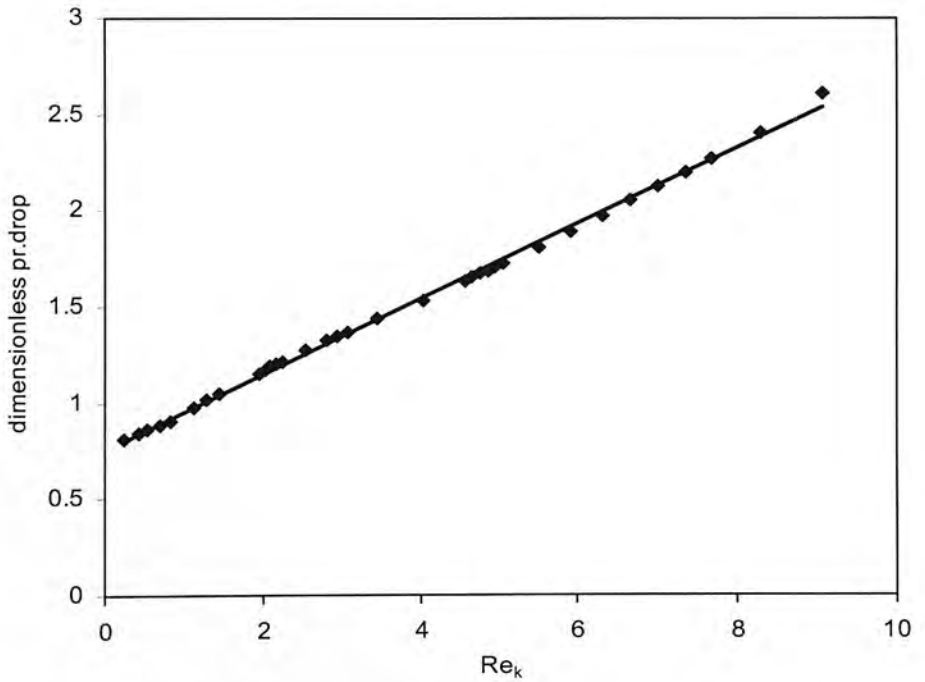

Figure 5.19. Plot of dimensionless pressure drop as a function of actual flow Reynolds number for entire regime.

The slope is in excellent agreement with the experimental results of both Ergun (1952) and Macdonald *et al* (1979) and the intercept agrees well with that of Ergun but is 25% lower than that of Macdonald. This suggests that there is some zero pressure anomaly between the Macdonald results and the Ergun results. It is not clear why the experiments of Fand *et al* (1987) result in such a low increase in pressure drop with increasing Reynolds number.

Table 5.1 Correlations for dimensionless pressure drop versus Reynolds number for flow through porous media

Type of study	Forchheimer flow	Turbulent flow	complete range
(i) Present study	$\frac{P'K}{\mu\upsilon} = 0.826 + 0.176\,\mathrm{Re}_k$ $1.79 < \mathrm{Re}_k < 4.5$	$\frac{P'K}{\mu\upsilon} = 0.6523 + 0.2103\,\mathrm{Re}_k$ $\mathrm{Re}_k > 5.04$	$\frac{P'K}{\mu\upsilon} = 0.756 + 0.196\,\mathrm{Re}_k$
(ii) Experimental work by Ergun *et al.* (1952) data only for complete range:			$\frac{P'K}{\mu\upsilon} = 0.83 + 0.19\,\mathrm{Re}_k$; $0.08 < \mathrm{Re}_k < 196$
(iii) Numerical work by Mousavi *et al* (2006)	$\frac{P'K}{\mu\upsilon} = 1.0316 + 0.164\,\mathrm{Re}_k$; $1.64 < \mathrm{Re}_k < 4.59$	$\frac{P'K}{\mu\upsilon} = 1.31 + 0.156\,\mathrm{Re}_k$ $\mathrm{Re}_k > 5.07$	
(iv) Experimental work by Macdonald *et al.* (1979) data only for complete range:			$\frac{P'K}{\mu\upsilon} = 1.00 + 0.19\,\mathrm{Re}_k$ $0.003 < \mathrm{Re}_k < 32.7$
(v) Experimental work by Fand *et al.* (1987)	$\frac{P'K}{\mu\upsilon} = 0.93 + 0.14\,\mathrm{Re}_k$; $0.57 < \mathrm{Re}_k < 9.00$	$\frac{P'K}{\mu\upsilon} = 1.14 + 0.12\,\mathrm{Re}_k$; $\mathrm{Re}_k > 13.5$	

Summary

Study of flow through random packing of non-overlapping sphere packing was investigated. In this chapter we have successfully studied flow through porous media using the GI-LGA method. The pressure drop of flow through the granular bed at various Reynolds number was investigated. The results were comparable with literature and found to be in good agreement with those reported in Ergun et al. This method appears most promising for simulating flow through porous media.

Chapter 6
Ab initio Prediction of Interstitial Flow

Introduction

The flow of fluid in porous media at the pore level has long been of interest for a variety of reasons. The nature of the macroscale flow models such as the Forchheimer equation is implicitly linked to the interstitial fluid flow. Similarly mass and heat transfer between porous media is intimately linked to the interstitial fluid flow. Another example is dispersion in porous media. It is for this reason that many have sought to understand the nature of fluid flow in porous media at the pore level using a wide variety of experimental methods as outlined in Chapter 2. Unfortunately, these methods cannot be applied to any porous medium – most are restricted to transparent media whilst those that can be applied to non-transparent media such as NMR are restricted in terms of their resolution and flow velocities, not to mention the need for sophisticated apparatus. Provided some representation of the porous medium is available, however, mesoscale simulation such as being developed here can be applied to any porous medium. I have, therefore, chosen as the second demonstration of the new model to study the interstitial flow within a model porous medium.

The porous medium considered here is a packed bed of equisized spheres. This has been considered as there is considerable experimental understanding of the interstitial flow in such media which can be used to validate at least qualitatively the predictions obtained here. It also offers the prospect that if there are any new findings

from this work, they can be tested, albeit by others, in the future. The chapter is laid out as follows.

6.1 Model and simulation details

The study reported here is concerned with elucidating the interstitial flow in the same random packing of spheres considered in the previous chapter. The size of the domain is 200 by 120 by 200 lattice units and the diameter of the solid particles is 40 lattice units. Flow was allowed to achieve steady state in the system and then the samples were taken. The sampling of velocity measurements and the illustration of how the steady state is achieved are discussed in the previous chapter. The snapshots define values of velocity using a colour coded vector map: regions of high velocity are seen as red and regions of low velocity as dark blue. The snapshots show spherical particles as circular areas of zero velocity because they do not contain LGA fluid particles. By averaging over a small number of sites, smooth results are obtained and the details are presented in the following section.

Because of computational resource limitations, consideration was restricted to five Reynolds Numbers – $\mathrm{Re}_k = 1.12$, $\mathrm{Re}_k = 2.1$, $\mathrm{Re}_k = 3.45$, $\mathrm{Re}_k = 4.8$ and $\mathrm{Re}_k = 6.1$ – one in each of the main flow regimes identified in Chapter 5.

As in the previous chapter, the simulations were initially run until the pressure drop across the medium reached a steady state at which point data sampling was begun and these data were then treated as described in the following section.

6.2 Visualisation of Interstitial flow field

Visualisation of the interstitial flow field is the most basic approach to elucidating in a qualitative way how the flow field varies with Reynolds Number. As will be outlined below, knowledge of this flow field also provides the basis for more quantitative analysis of the variation of the flow field with Reynolds Number. The interstitial flow field has, therefore, been determined for the five Reynolds numbers considered here.

6.2.1 Effect of time-step and sub-volume averaging

By the very nature of LGA, averaging of the results from a simulation over time and/or space is required to obtain meaningful velocity fields. The most appropriate size of the spatial sub-volume and time period used in this averaging is not known *a priori* but must, instead, be estimated by establishing the combination of the two that leads to velocity field invariance (*i.e.* no change in the velocity field with further increase in either parameter) whilst allowing the resolution of the flow field features of interest. The most appropriate averaging parameters will vary with the flow conditions. For example, under creeping flow conditions where the flow is steady and laminar, the temporal averaging period can be longer at the expense of a larger averaging sub-domain to increase the level of spatial resolution for a fixed computational effort. At Reynolds Numbers where the interstitial flow field is unsteady, on the other hand, the temporal period will necessarily need to be short, allowing a reduction in the spatial sub-domain size. This will necessitate a high density lattice for the same level of spatial resolution as in the creeping flow situation.

As an example of the analysis undertaken to determine the most appropriate averaging parameters, Figure 6.1 to 6.3 shows the computed velocity field in a plane through the packing at $\mathrm{Re}_k = 2.12$ which is the transition regime from laminar to Forchheimer. These figures are for the average of 10 timestep and three different sizes of the spatial averaging sub-volume. They have been plotted by importing the data into the Star-CCM+ visualisation package (CD-Adapco).

This figure shows that the interstitial velocity field obtained using the smallest spatial averaging sub-domain size is not well represented compared to the two larger sub-domain sizes considered. The most appropriate averaging sub-volume size for the averaging time period used can be selected by identifying the minimum value of the sub-volume size (4 x 4 x 4) beyond which, for example, the maximum velocity in the domain ceases to change significantly.

Figure 6.4 suggests that the sub-volume size (4 x 4x 4) is the most appropriate for the case where the averaging time step = 10. The same process is repeated for various averaging time steps to estimate the most appropriate averaging parameters for a given Reynolds Number. Using this approach, the most appropriate averaging parameters estimated here for the various flow regimes are given in Table 6.1.

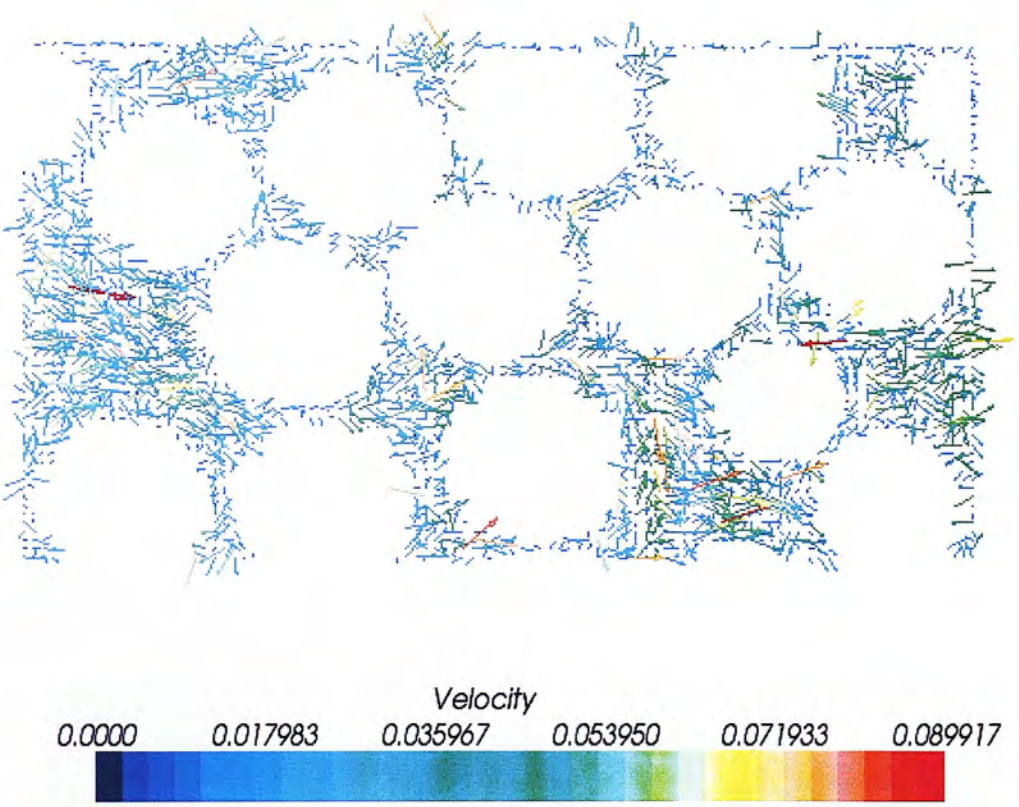

Figure 6.1. Interstitial flow field in a plane of a sub-volume of the packed bed as determined by averaging the GI-LGA results over an average of 10 time steps and spatial sub-volumes of 2 x 2 x 2. The white regions in which no arrows appear are occupied by solid

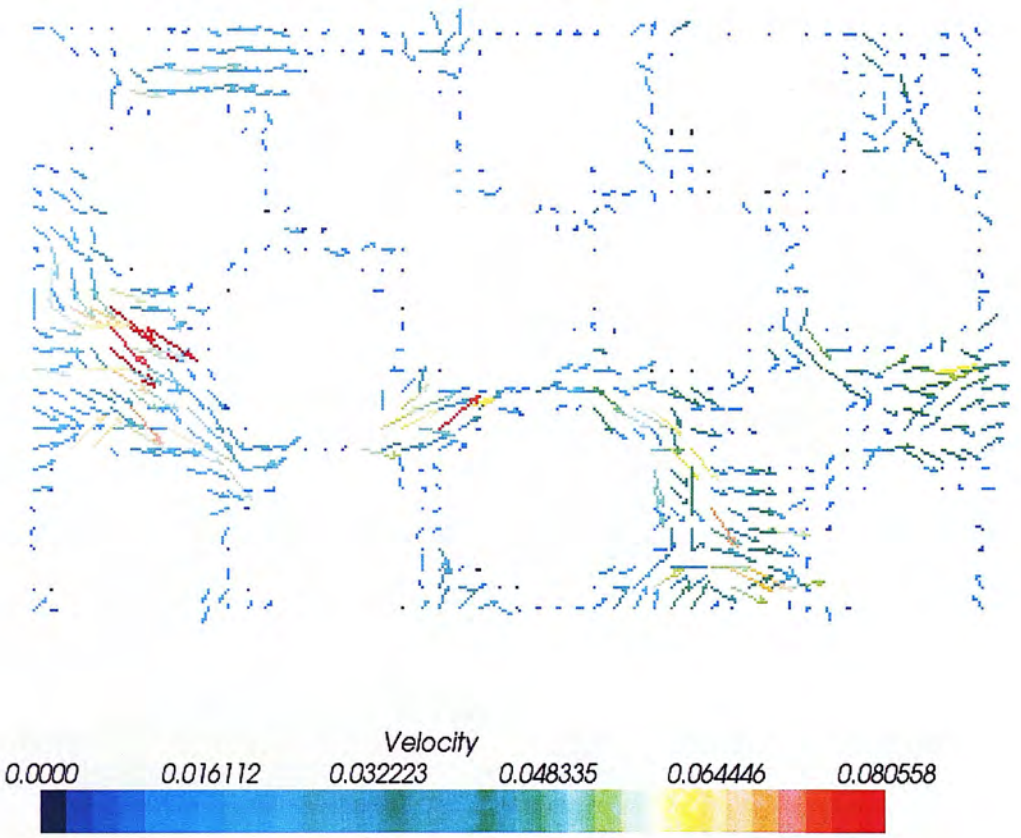

Figure 6.2. Interstitial flow field in a plane of a sub-volume of the packed bed as determined by averaging the GI-LGA results over an average of 10 time steps and spatial sub-volumes of 4 x 4 x 4. The white regions in which no arrows appear are occupied by solid

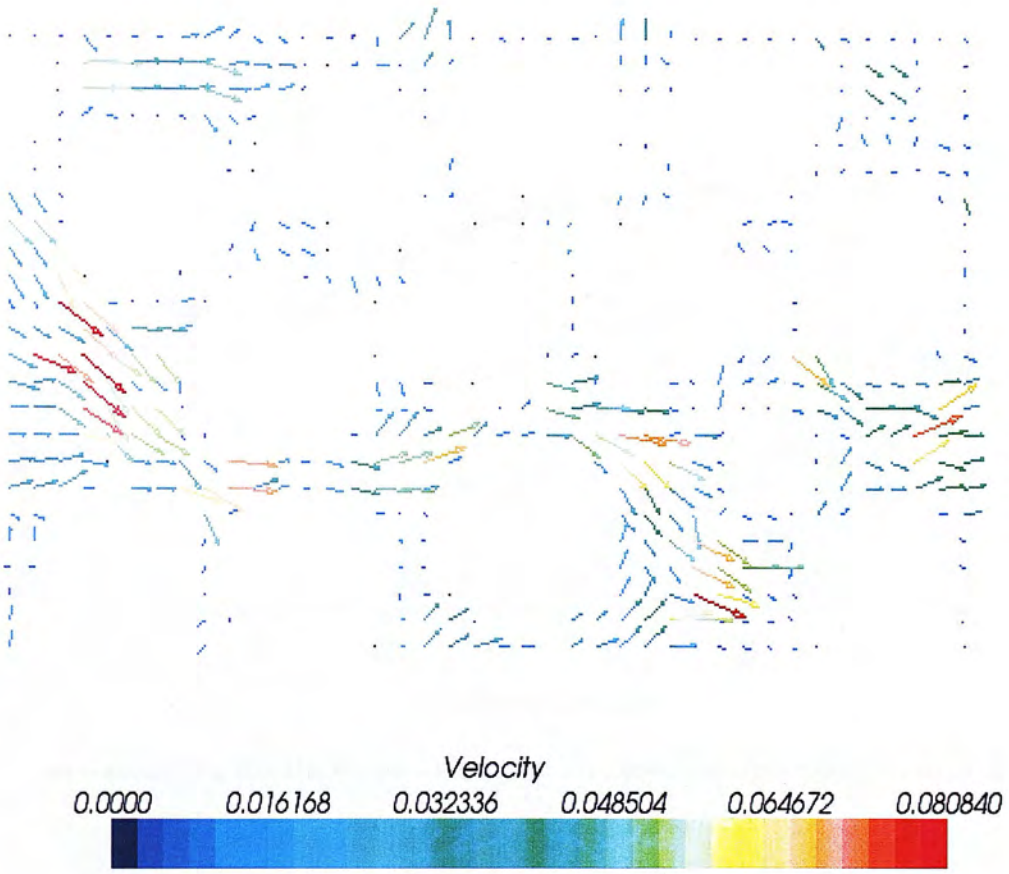

Figure 6.3. Interstitial flow field in a plane of a sub-volume of the packed bed as determined by averaging the GI-LGA results over an average of 10 time steps and spatial sub-volumes of 5 x 5 x 5. The white regions in which no arrows appear are occupied by solid

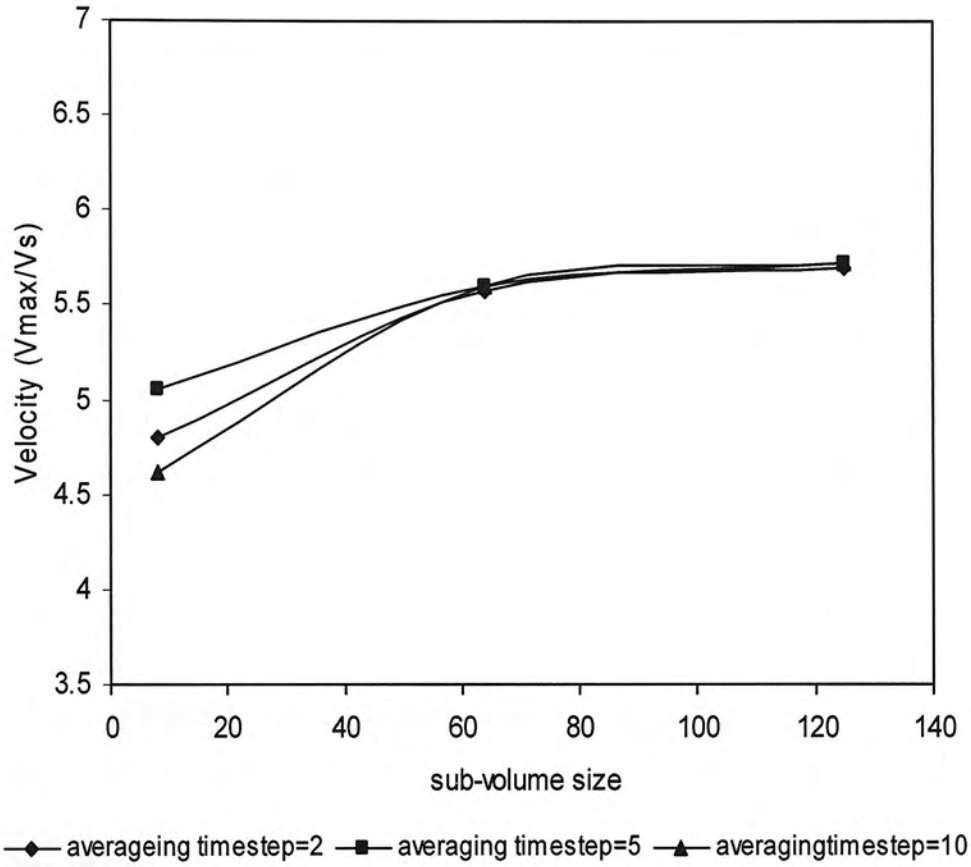

Figure 6.4. Velocity versus sub-volume size for various time step averaging. The sub-volume size is (2x2x2, 4x4x4, 5x5x5) and the time step averaging is 2,5,10.

Regimes	sub-volume size	time step
(a) Laminar	5	10
(b)Transition from Laminar to Forchheimer	4	10
(c)Forchheimer	2	5
(d) Transition from Forchheimer to Turbulent	2	5
(e)Turbulent	2	5

Table 6.1. Averaging parameters for various flow regimes.

6.3 Backflows

Recirculation 'behind' particles in the packing due to boundary layer separation is one example of where the local velocity is in a direction opposite to that of the superficial velocity (*i.e.* backflow).

Stationary backflows are thought to be associated with the approach of the upper end or exit from the Forchheimer regime (Hlushkoua *et al.* 2006). In the turbulent regime, backflows will exist because of the presence of coherent structures such as non-stationary vortices.

The identification of individual vortices within the interstitial flow field is challenging in general (Jeong *et al.* 1995), and even more so within the complex pore spaces being considered here. A commonly used method for identifying vortices is to determine the vorticity field (Hussain *et al.* 1987; Jeong *et al.* 1995) where the vorticity is defined by

$$\boldsymbol{\omega} = \nabla \times \mathbf{v} \tag{6.1}$$

This approach has been used here as part of the effort to elucidate the nature of the vortices in the upper reaches of the Forchheimer regime and beyond.

6.4 Flow regimes as a function of Reynolds number

The nature of the flow around spheres changes as the Reynolds number of the flow increases. In general, the higher the Reynolds number, the more complex is the flow. In this section we describe the nature of the flow for different Reynolds numbers in a range between Laminar to Turbulent flow.

In the velocity vector plots the colour scale is fixed to the largest Reynolds number for the comparison. For the vorticity plots colour scale that ranges from 0 to the maximum for each Reynolds number. This will allow a clearer identification the vortices in each regime.

6.4.1 Darcy Regime

Snapshots of the velocity field for various time steps and the corresponding vorticity plots are shown in this section. Figures 6.5 and 6.6 show the snapshot of the velocity field in the Darcy regime. From these plots we can see the vectors are always same and it is an evidence of steady flow in a stationary system.

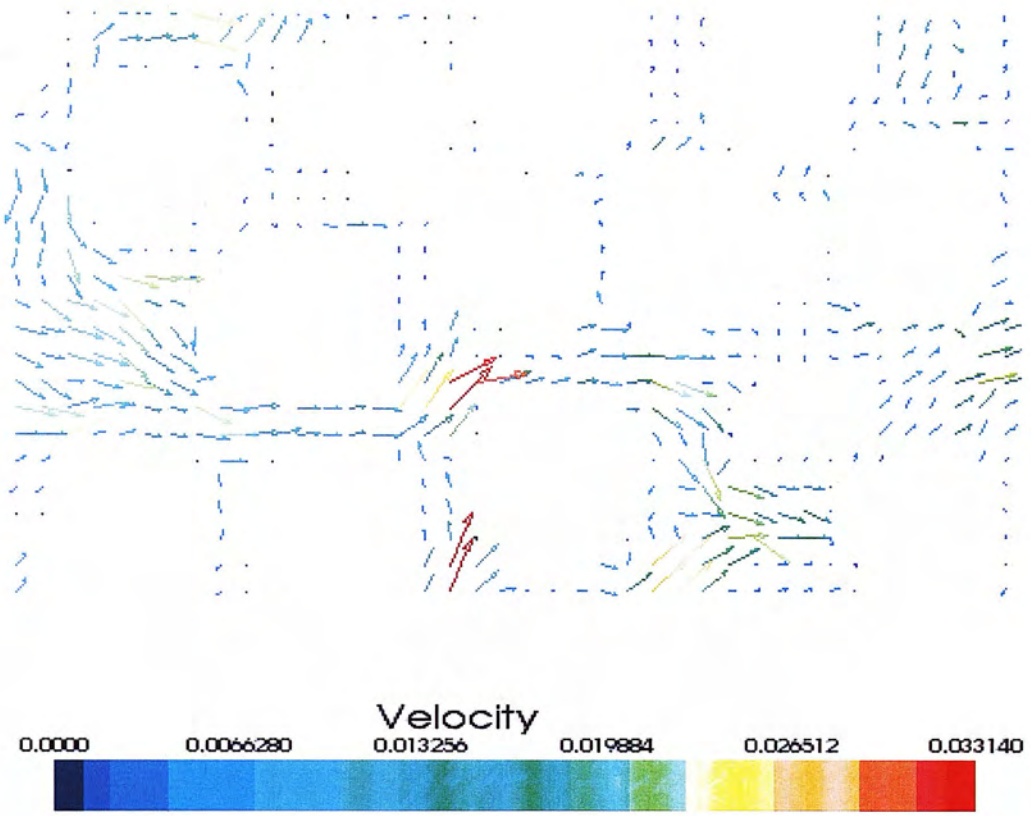

Figure 6.5. Vector plot of interstitial flow field in Darcy regime by averaging the GI-LGA results over an average of 500 -510 time steps and the spatial sub-volume is 5 x 5 x 5. The white regions in which no arrows appear are occupied by solid.

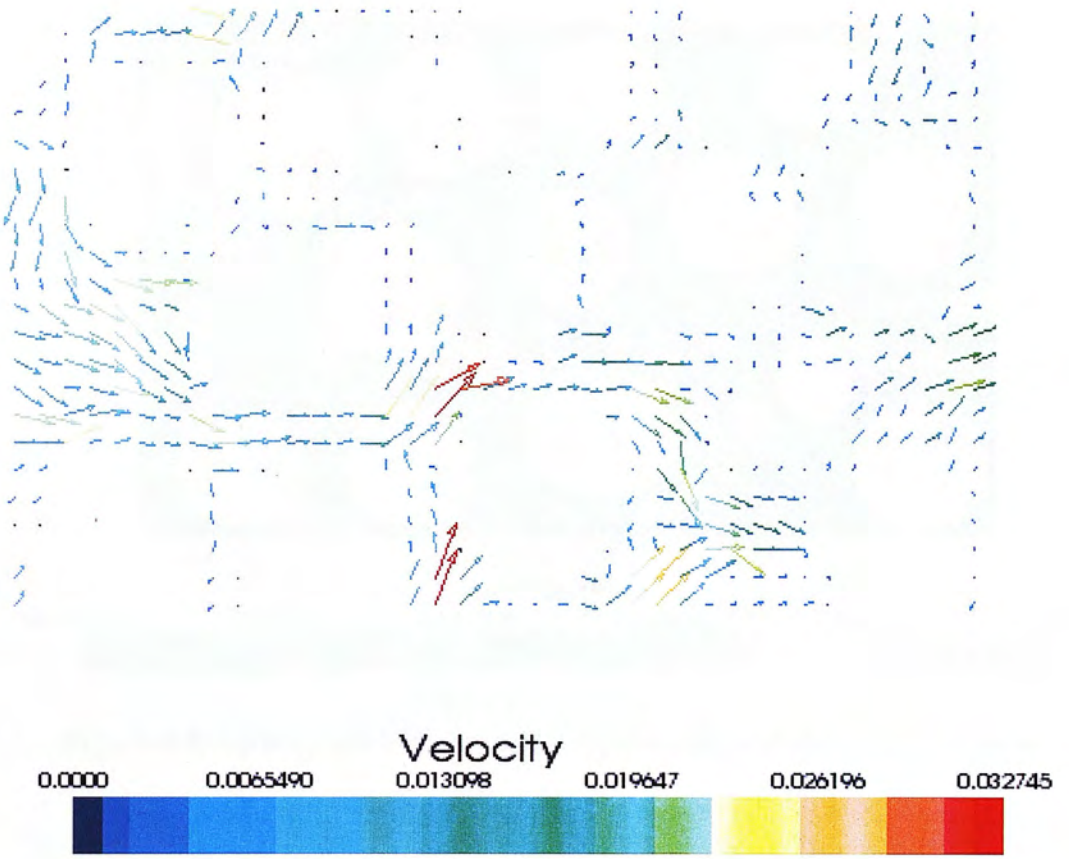

Figure 6.6. Vector plot of interstitial flow field in Darcy regime by averaging the GI-LGA results over an average of 600 -610 time steps and the spatial sub-volume is 5 x 5 x 5. The white regions in which no arrows appear are occupied by solid.

In figure 6.7 and 6.8, the vorticity values are plotted. Vorticity here is attached to the surfaces and the values are identical to within 1% (Max ~ 0.0031448). This demonstrates a steady state of flow which corresponds to Darcy regime.

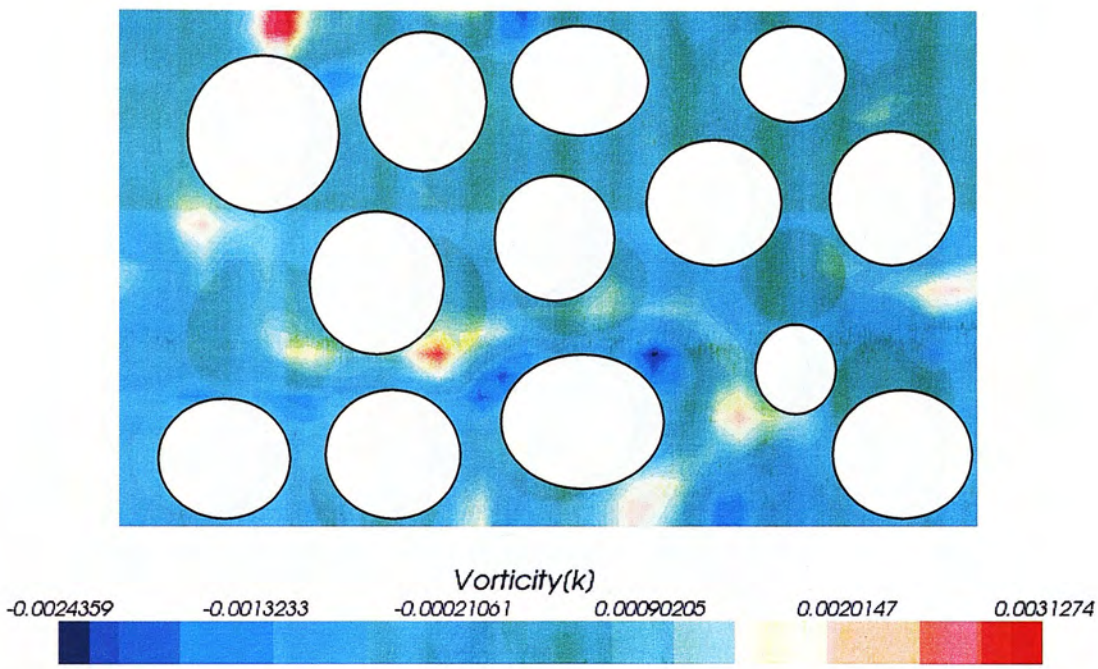

Figure 6.7. Vorticity plot in Darcy regime; an average of 500 -510 time steps.

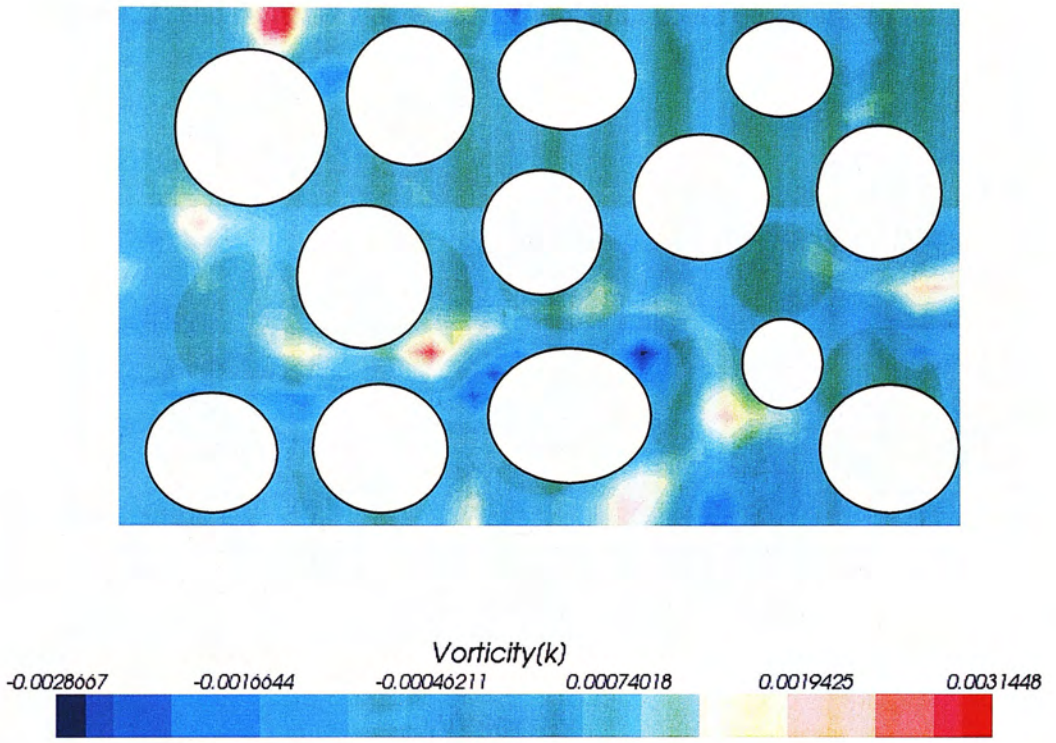

Figure 6.8. Vorticity plot in Darcy regime; an average of 600 -610 time steps.

6.4.2 Transition from Laminar to Forchheimer

Figures 6.9 and 6.10 show the snapshots of the velocity field and the corresponding vorticity plot in the transition from the Laminar to the Forchheimer regime. In this transition regime we can see that the vorticity magnitude is higher than before (max ~ 0.0066423) and there is evidence of recirculation zones beginning to form.

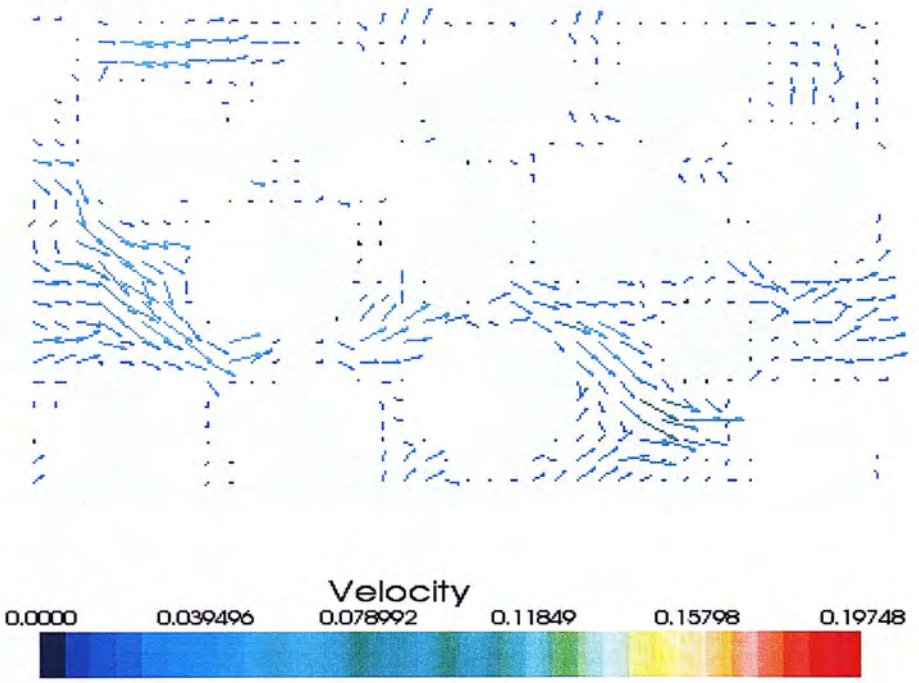

Figure 6.9. Vector plot of interstitial flow field in transition from Laminar to Forchheimer regime by averaging the GI-LGA results over an average of 400 - 405 time steps and the spatial sub-volume is 4 x 4 x 4. The white regions in which no arrows appear are occupied by solid.

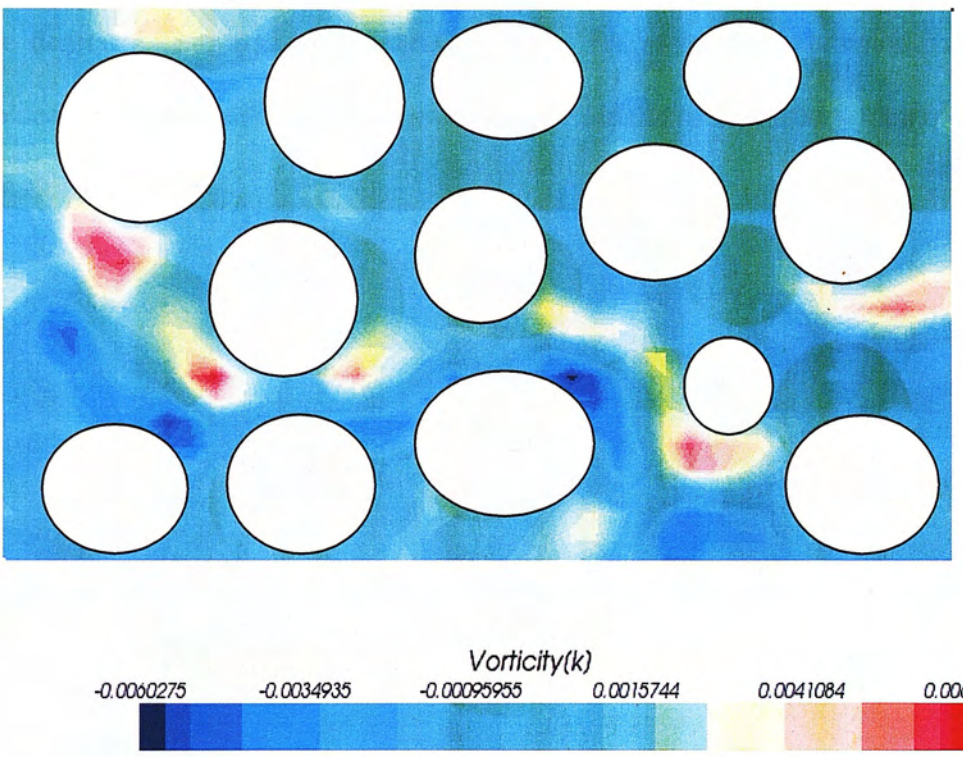

Figure 6.10. Vorticity plot in Transition from Laminar to Forchheimer regime; an average of 400 -405 time steps

6.4.3 Forchheimer regime

Figures 6.11 and 6.12 show the snapshots of the velocity field and the corresponding vorticity plot in the Forchheimer regime. In this regime, vorticity magnitude is higher than the above transition regime (max ~0.015746) and the flow remains attached. The nature of the flow in this regime has recirculation zones. In order to see the stationary vortices, one further image is taken at a later time is shown in Figure 6.13, to demonstrate that all of the vortices are of the same magnitude and in the same place. In figures 6.12 and 6.13, arrows are represented to show examples of the stationary vertices.

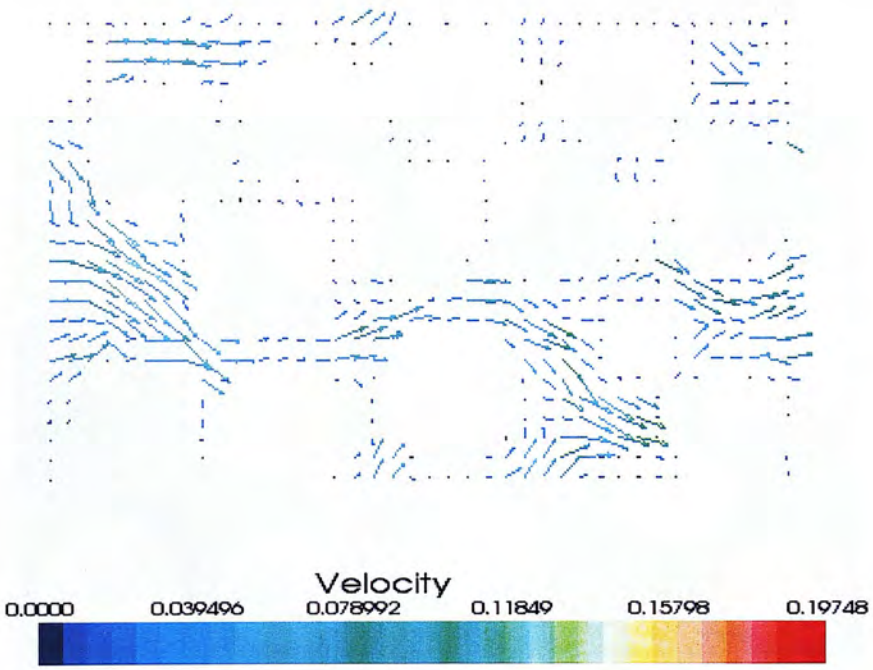

Figure 6.11. Vector plot of interstitial flow field in Forchheimer regime by averaging the GI-LGA results over an average of 400 -405 time steps and the spatial sub-volume is 2 x 2 x 2. The white regions in which no arrows appear are occupied by solid

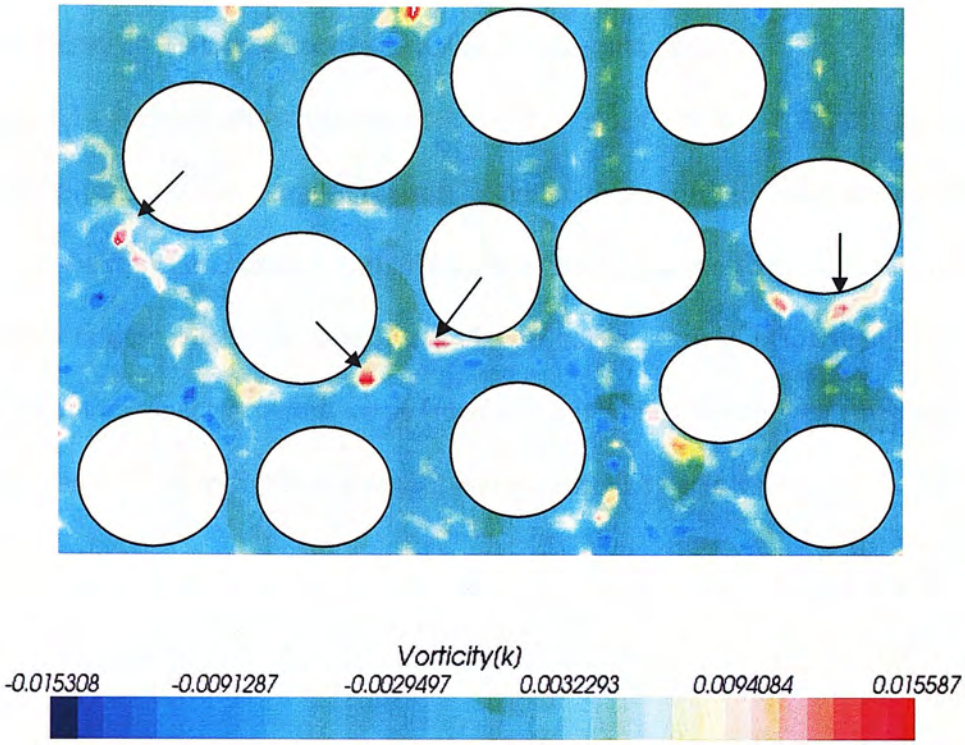

Figure 6.12. Vorticity plot in Forchheimer regime; an average of 400 - 405 time steps.

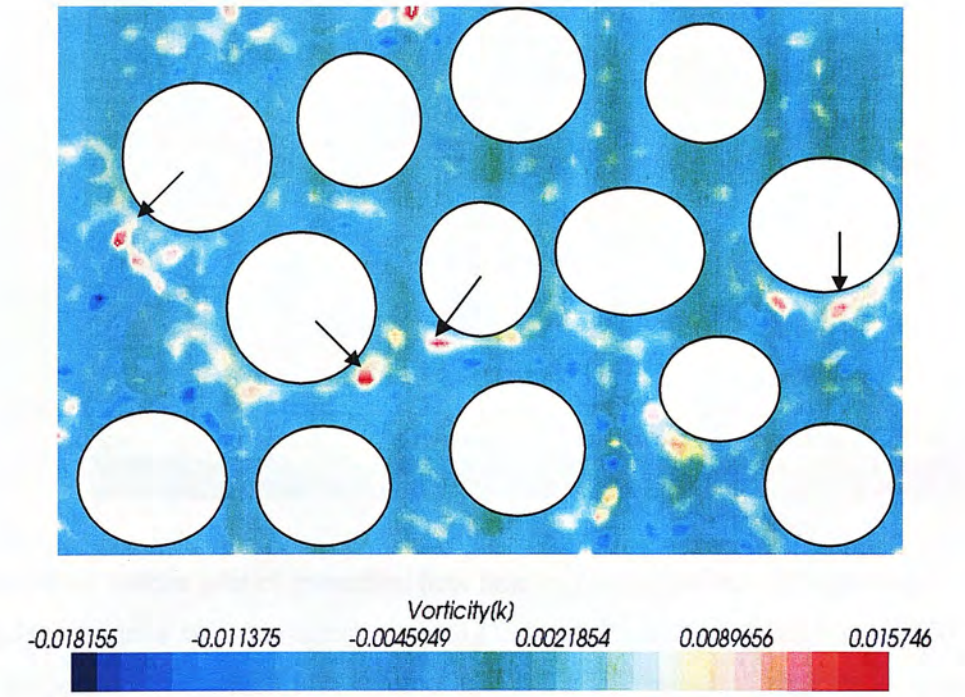

Figure 6.13. Vorticity plot in Forchheimer regime; an average of 600 - 605 time steps.

6.4.4 Transition from Forchheimer to Turbulent regime

Figures 6.14 and 6.15 show the snapshots of the velocity field and the corresponding vorticity plot in the Forchheimer regime. In this regime, vorticity magnitude is higher than the above regime (max ~ 0.025968). We found that the flow became unsteady and there is evidence of stronger recirculation zones. Also the flow consisted of a series of interconnected vortex loops (recirculation zones) which were shed from the spheres can be seen in figure 6.16 and it is represented by arrows.

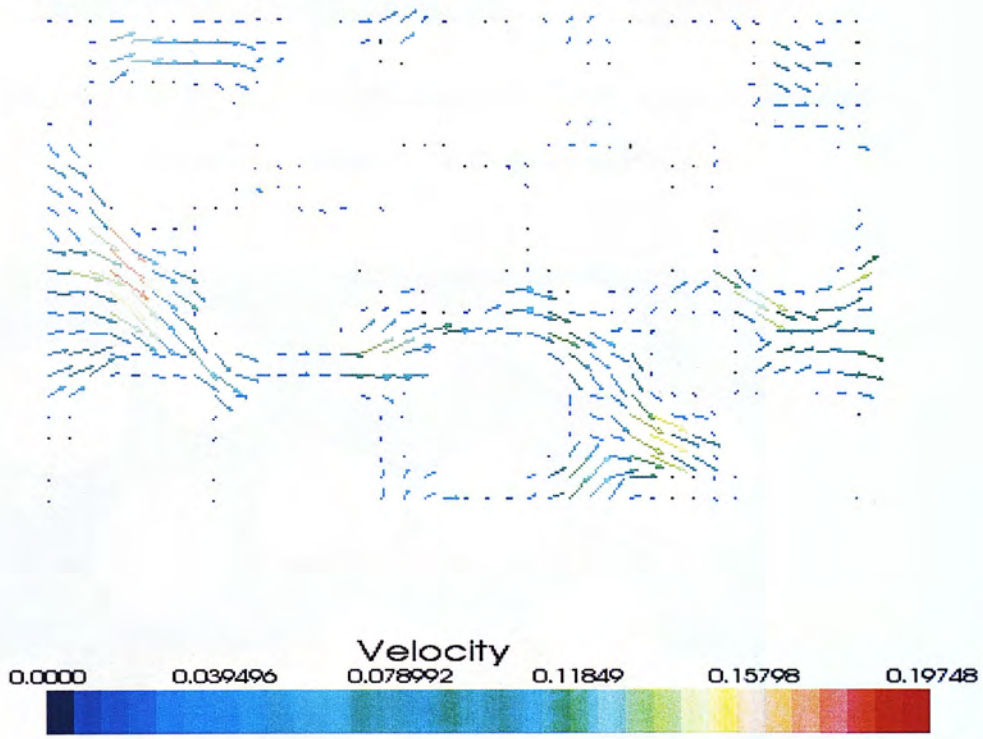

Figure 6.14. Vector plot of interstitial flow field in Transition from Forchheimer to Turbulent regime by averaging the GI-LGA results over an average of 400 -405 time steps and the spatial sub-volume is 2 x 2 x 2. The white regions in which no arrows appear are occupied by solid.

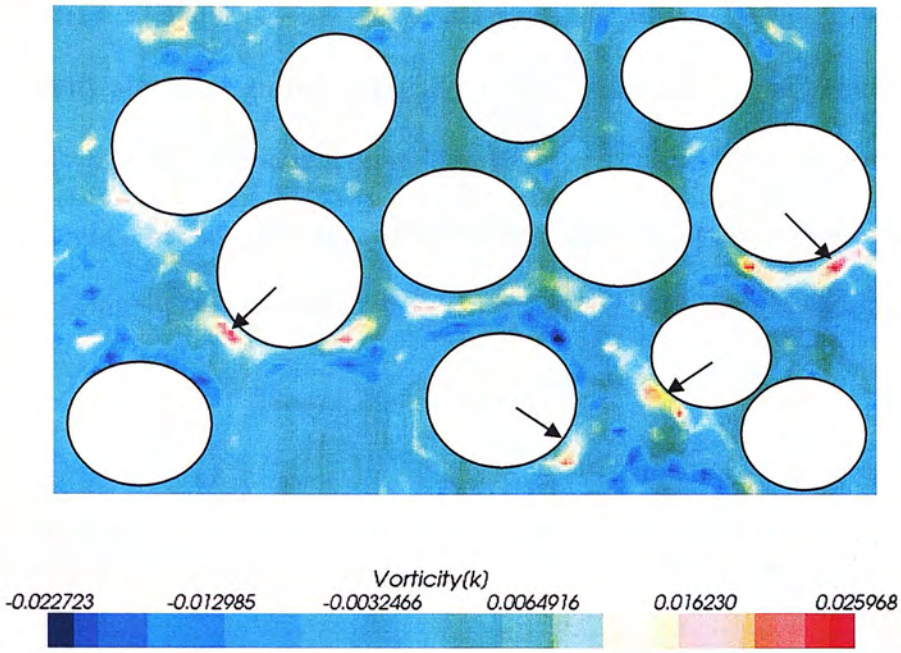

Figure 6.15. Vorticity plot in Transition from Forchheimer to Turbulent regime; an average of 400 -405 time steps.

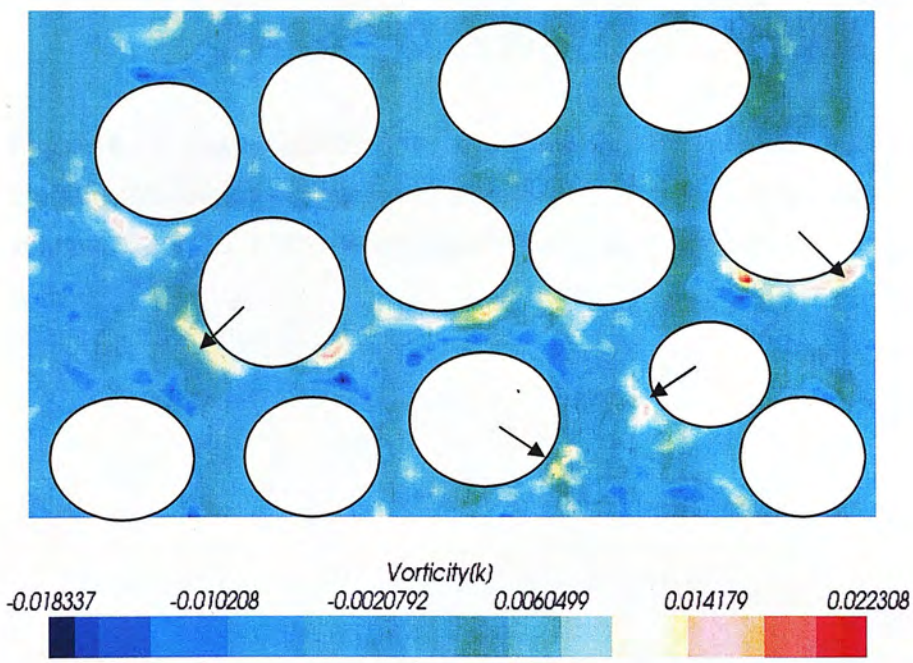

Figure 6.16. Vorticity plot in Transition from Forchheimer to Turbulent regime; an average of 600 -605 time steps.

6.4.5 Turbulent region

Figures 6.17 and 6.18 show the snapshots of the velocity field and the corresponding vorticity plot in the turbulent regime. In this regime, the vorticity magnitude is again higher than the previous regime. Some of the vortices have become non-stationary and exhibit vortex shedding. This can be seen in figure 6.19. This changing vortex field is highlighted by arrows and demonstrates that the flow is no longer stationary.

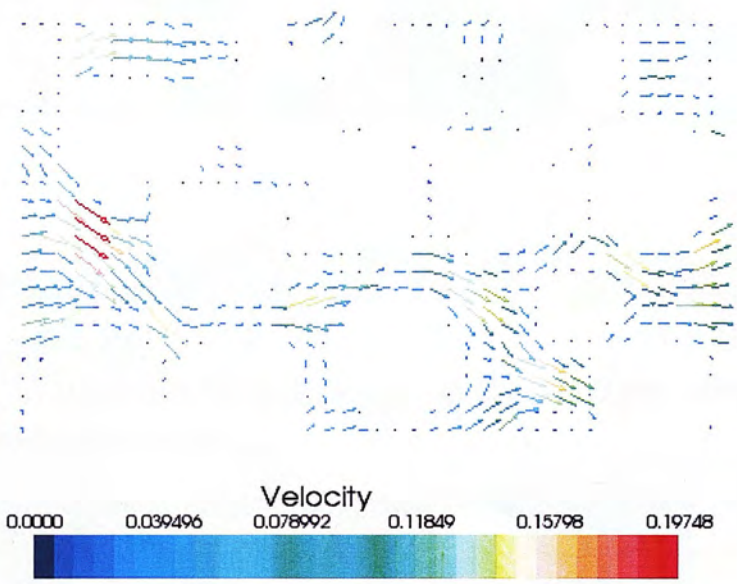

Figure 6.17. Vector plot of interstitial flow field in Turbulent regime by averaging the GI-LGA results over an average of 400 -405 time steps and the spatial sub-volume is 2 x 2 x 2. The white regions in which no arrows appear are occupied by solid.

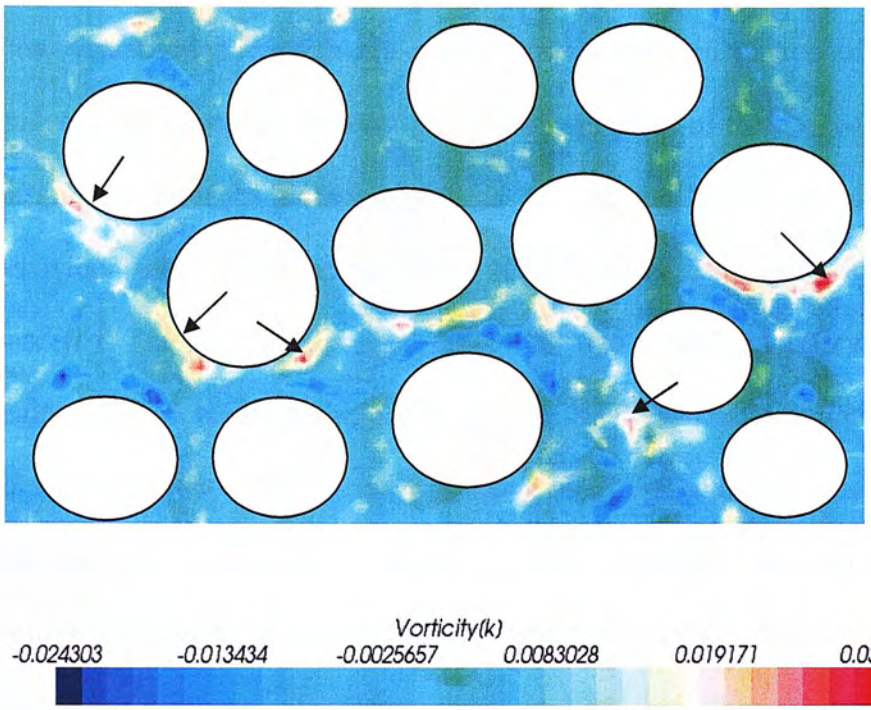

Figure 6.18. Vorticity plot in Turbulent regime; an average of 400 -405 time steps. Arrows represent vortex shedding.

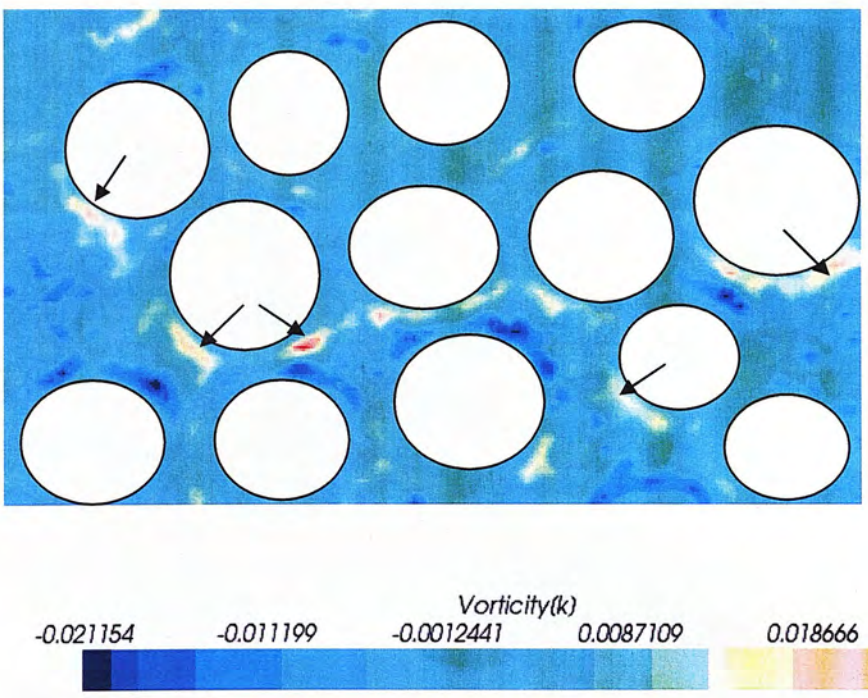

Figure 6.19. Vorticity plot in Turbulent regime; an average of 600 -605 time steps. Arrows represent vortex shedding.

Summary

Flow visualisation through the plane allows a detailed picture of the flow to be analysed and related to the structure of the void space of the packed bed and it gives insight into how the transport of fluid through the bed occurs. A range of flow behaviours is observed. In the Darcy regime, steady flow with no recirculation is observed. Trapped vortices appeared in the transition from Darcy to Forchheimer regime. The increased resistance to flow in the Forchheimer regime was due to the formation of the fixed vortices blocking the flow and this can be seen in the visualisations. Non-stationary vortices appeared in greater numbers during transition from Forchheimer to turbulent flow. The formation of these vortices and their subsequent frictional dissipation result in increased ratio of pressure drop with Reynolds numbers shown in Chapter5.

Chapter 7

Conclusions and Future work

7.1 Conclusions

Multiple speed lattice gas methods can be made to accurately and efficiently model a true continuum fluid. LGA models are good for the fundamental study of fluid flow problems in porous media. As we have seen earlier they suffer a significant disadvantage of lacking Galilean Invariance (GI) for non Darcy flows. Though LBM was developed as an extension of LGA to overcome some of its disadvantages, it has been postulated that further work on LGA methods could produce models to simulate a true continuum fluid very accurately and efficiently.

The main advantage of LGA is its unconditional stability with no necessity to use an approximation scheme to replicate the actual flow. Also another advantage of this model is the ease with which it can be parallel programmed; this reduces the simulation time and also makes large scale simulation possible.

We have identified several studies in the literature using LGA for single phase flows; all of them restricted to creeping flows. To our knowledge there are no previously published papers which extend LGA to the study of non-Darcy single phase flows. So the main aim of the present study was to develop a multiple speed LGA model for simulating single phase flow in porous media where previously only single speed models existed. The following problems have been addressed.

1] Examination of the existing single speed LGA models and assessment of their suitability for non-Darcy flows.

2] Development of a model which gains GI invariance in simulations.

3] Extending this model to simulate flow through random sphere packing

4] Visualisation of the interstitial flow patterns from the Darcy to turbulent regimes.

The results reported in chapter 3 demonstrate that the 2D and 3D LGA fluid transport codes written for this study are capable of reproducing correct hydrodynamic behaviour of fluids. These single speed LGA models are restricted to relatively slow flows due to non-Galilean invariance.

The LGA model of Tiexeira is one of the most advanced in demonstrating Galilean invariance LGA (GI-LGA). But the details of implementation are not available in open literature, so I have implemented this model using C++. Galilean invariance artefact removal is demonstrated through a shear wave experiment. Application of this model is validated through various benchmark problems. Flow between two flat plates demonstrated the correct laminar parabolic profile. Flow around a cylinder compares well with literature results in measurement of the drag coefficient.

This GI-LGA model was extended to flow through porous media. The resistance of fluid flow through a porous medium composed of randomly packed spheres was investigated. The pressure drop of flow through the granular bed at interstitial Reynolds numbers between 0 - 9.5 was investigated. The simulation results are compared with literature results and show excellent agreement with the experimental measurements of Ergun *et al.* The agreement is superior to that of previous numerical studies.

Finally the data was used to elucidate the flow pattern within the pores. A range of flow behaviours is observed. In the Darcy regime, the flow is demonstrated to be stationary: steady flow with no recirculation is observed. Trapped vortices appear in the transition from Darcy to Forchheimer regime and these are demonstrated to be stationary. Non-stationary vortices are shown to appear during the transition from Forchheimer to turbulent flow.

7.2 Future work

A number of potential extensions of this study were identified throughout the thesis and are summarized below.

The GI-LGA model presented here has proved stable and robust in simulating the non-creeping single phase fluid flow in porous media. With less concerns nowadays for issues of the large computer memory required for LGA, the current work opens up potential for the LGA model as a method of modelling real fluids more accurately and efficiently. This study has a great scope for further works in the short and long term.

1] The current code can be executed in parallel programming to involve large scale simulations.

2] The current simulation tool could be extended to flow through random multi-sized spheres.

3] Tests against 'real' porous media would be a very good test of the method and a practical application. Reconstruction of the pore-space could be obtained with the aid of x-ray tomography or MRI experiments and the simulation of single/multiphase

flow through this complex pore space morphology could be done using this GI-LGA model. This will lead to the development of advanced numerical methods for the calculation of the transport coefficients.

4] Current study can be extended to multiphase fluid flow in porous media.

References

Adler, P.M., Stokes flow in fractical capillary networks, International Journal of Multiphase Flow, Vol 11:213-239, 1985.

Adler, P.M., Jacquin, C. G., and Quiblier, J. A., Flow in Simulated Porous Media, International Journal of Multiphase Flow, Vol 16:691-712, 1990.

Adler, P.M., and Berkowitz, B., Effective medium analysis of random lattices, Transport in porous media, Vol 40:145-151, 2000.

Alshare, A.A., Simon, T.W., and Strykowski, P. J., Simulations of flow and heat transfer in a serpentine heat exchanger having dispersed resistance with porous-continuum and continuum models, International journal of heat and mass transfer, Vol 53:1088-1099, 2010.

Ameri, S., Meloy, T.P., Aminian, K., and Drescher, S., Powder Technology., Vol.75:107-112, 1993.

Andrade, J.S., Shibusa, Y., Arai, Y., and Mcgreavy, C., A network model for diffusion and adsorption in compacted pellets of bidisperse grains, Chemical Engineeering Science, Vol 50: 1943-1951, 1995.

Appert.C. and Zaleski, S., A lattice Gas with a Liquid-Gas Transition, Physical Review. Letters. Vol 64:1-4, 1990.

Auzerais,F.M., Dunsmuir, J., Ferreol, B.B., Martys, N., Olson, J., Ramakrishnan, T. S., Rothman, D. H., and Schwartz, L. M., Transport in sandstone: A study based on three dimensional microtomography, Geophys. Res. Lett., Vol 23:705-708, 1996.

Avraam, D.G., and Payatakes, A. C., Flow regimes and relative permabilities during steady state two phase flow in porous media, Journal of Fluid mechanics, Vol 293: 207-236,1995.

Balasubramanian , K., Hayot. F., and Saam, W. F., Darcy law for lattice gas dynamics, Phys. Rev. A, Vol 36:2248-2253, 1987.

Bear, J., Dynamics of fluids in porous media, American Elsevier Pub. Co., 125-127, 1972.

Békri, S., Thovert, J. F., and Adler, P. M., Dissolution of porous media, Chem. Eng. Science, Vol.50:2765-2791, 1995.

Beyne, A.O.E. and Froment, G. F., The effect of pore blockage on the diffusivity in ZSM5: a percolation approach, Chemical Engineering journal, Vol: 82:281-290, 2001.

Biggs, M.J. and Humby, S. J.,Lattice-gas automata methods for engineering, Transactions of the IChemE, 76:162-174, 1998.

Biggs, M.J., Humby, S.J., Buts, A., and Tüzün, U., Explicit numerical simulation of suspension flow with deposition in porous media, Chemical Engineering Science, 58:1271-1288, 2003.

Boon, J.P., Dab, D., Kapral, R., and Lawniczak, A., Lattice gas automata for reactive systems, Phys. Rep., Vol 273:55, 1996.

Brosa, U., and Stauffer, D., Simulation of flow Through a Two-Dimensional Random Porous Medium, J. Stat. Phys., Vol 63:405-409, 1991.

Brosa and Stauffer,D., Vectorized multisite coding for hydrodynamic cellular automata, Journal of Statistical Physics, Vol 57:399–403,1989.

Bryant, S.L., Mellor, D. W., and Cade, C. A., Physically representative network models of transport in porous media, AIChE Journal, Vol 39:387-396, 1993.

Buick, J.M., Lattice Boltzmann methods in interfacial wave modelling, PhD thesis, The University of Edinburgh, 1997.

Burganos, V.N., and Payatakes, A. C., Knudsen diffusion in random and correlated networks of constricted pores, Chemical Engineering Science, 47:1383–1400, 1992.

Burganos, V.N., and Payatakes, A.C., Knudsen diffusion in random and correlated networks of constricted pores, Chemical Engineering Science, 47:1383–1400,1992.

Chen.S., Lee, M., Zhao, K. H., and Doolen, G. D., A lattice gas model with temperature, Physica D, Vol 37:42-59, 1989.

Chen S., Diemer, K., Doolen, G. D., Eggert, K., Fu, C., Gutman, S., and Travis, B.J.,Lattice gas automata for flow through porous media. Physica D Vol 47:72–84, 1991.

Chen, S., G.D.Doolen, K.Eggert, D.Grunau and E.Y.Loh, Discrete Models of Fluid Dynamics World Scientific, Singapore, 1991.

Chen S, Diemer,K., Doolen, G.D., Eggert, K, Fu,C., Gutman, S., Travis, BJ., Lattice gas automata for flow through porous media. Physica D, Vol 47:72–84, 1991.

Chen,S.Y., Chen, H. D., Doolen, G.D., Gutman, S., and Lee, M., A lattice gas model for thermohydrodynamics, J. Stat. Phys. Vol 62:1121,1991b.

Chen,S., Dawson.S.P., Doolen,G.D., Janecky,D.R., Lawniczak,A., Lattice methods and their applications to reacting systems, Computers & Chemical Engineering, Vol 19:7617-646, 1995.

Chen.S., and Doolen, G. D., Lattice Boltzmann method for fluid flows, Annual Review of Fluid Mechanics, Vol 30:329-364, 1998.

Constantinides, G.N., Payatakes, A.C., Effects of precursor wetting films in immiscible displacement through porous media, Transport in porous media, Vol 38:291-317, 2000.

Craft, B.C, and Hawkins, M.F., Applied Petroleum Reservoir Engineering, 210-218, Englewood Cliffs, New Jersey, 1997.

Dadvar, M., Sohrabi, M., Sahimi, M., Pore network model of deactivation of immobilized glucose isomerase in packed-bed reactors - I: Two-dimensional simulations, Chemical Engineering Science, Vol 56:2803-2819, 2001.

Dadvar, M., and Sahimi,M., Pore network model of deactivation of immobilized glucose isomerase in packed-bed reactors II: three-dimensional simulation, Chemical Engineering Science ,Vol 57:939-952, 2002.

Darcy, H., Les Fontaines publiques de la ville de Dijon, Paris, 1856, (English translation).

Davis, J. A., and Jones, S.C., Displacement mechanisms of micelle solutions, J. Pet. Technol., Vol 20:1415-1428, 1968.

d'Humières, D., Lallemand, P., and Frisch, U., Lattice gas models for 3-D hydrodynamics, Europhys. Lett., Vol 2:291-297,1986.

d'Humières, D. and Lallemand, P., Lattice gas automata for fluid mechanics, Physica A., Vol 140:26-335, 1986a.

d'Humières, D and Lallemand, P., Numerical simulations of hydrodynamics with lattice gas automata in two dimensions, Complex Systems Vol 1:599–632,1987.

Dong, H., and Blunt, M.J., Pore-network extraction from micro-computerized-tomography images , Physical Review E , Vol 80:307 -318, 2009.

Dullien, F.A.L., Zarcone,C., MacDonald, I.F., Collins,A., and Brochard, R.D.E., The Effects of Surface Roughness on the Capillary Pressure Curve in Glass Bead Packs, Journal of Colloid Interface Science, Vol127:363-372,1989.

Dullien, F.A.L., Zarcone.C., MacDonald I.F., Collins.A., and Brochard, R.D.E., The Effects of Surface Roughness on the Capillary Pressure Curve in Glass Bead Packs, Journal of Colloid Interface Science, 127: 363-372,1989.

Dullien, F.A.L., Characterization of porous media –pore level, Transport in porous media, Vol.6:581-606, 1991.

Dullien, F.A.L., 'Porous Media - Fluid Transport and Pore Structure', Academic Press Inc., London-UK, 1992.

Dupuy,J., and Dianoux, A., Microscopic Structure and Dynamics of Liquids, 1978.
Dybbs and Edwards,R., Measurement of fluid velocity inside porous media with a laser anemometer, Phys. Fluids, Vol 18:913–914,1975.

Eissler, W., Drtina, P., and Frohn, A., Cellular automata simulation of flow around chains of cylinders, Int. J. Num. Meth. Engineering., Vol.34, pp773-791,1992.
Ergun.S., Fluid flow through packed column, Chemical Engineering progress, Vol 48:89-94, 1952.

Fand,R.M., Kim, B.Y.K., Lam, A.C.C., and Phan, R.T., Resistance to flow of fluids through simple and complex porous media whose matrices are composed of randomly packed spheres, Journal of fluids engineering, Vol 109:268-274, 1987.

Fang, H.P., Wan, R.Z., Gong, X.J., Lu, H.J., and Li, S.Y., Dynamics of single-file water chains inside nanoscale channels: physics, biological significance and applications, Journal of Physics D-Applied Physics, Vol.41, article no:103002, 2008.

Ferreol,B., and Rothman, D.H., Lattice–Boltzmann simulations of flow through Fontainebleau sandstone. Transport in Porous Media Vol .20, pp. 3–20,1995.

Finney. J.L., Fine structure in randomly packed, dense clusters of hard spheres, Mater. Sci. Eng. Vol 23:199 -205, 1976.

Forchheimer, P., Wasserbewegung Durch Bodeen. Z Ver Deutsch Ing, Vol 45, 1782 – 1788, 1901, (English translation).

Frisch, U., Hasslacher,B and Pomeau,Y, Lattice gas automata for the Navier-Stokes equations. Phys.Review Letters,.Vol 56:1505–1508, 1986.

Frisch, U., d'Humières, D., Hasslacher, B., Lallemand, P., Pomeau, Y., and Rivet, J-P., Lattice Gas hydrodynamics in two and three dimensions, Complex Systems, Vol 1: 649 -707, 1987.

Frisch, U., and Orzag, S.A., Turbulence: Challenges for theory and experiment, Physics Today, pp24-32, 1990.

Gao.Y and Sharma, M.M., LGA model for fluid-flow in heterogeneous porous-media. Transp. Porous Media, Vol 17:1–17, 1994.

Goldsztein, GH, Solute transport in porous media. Media with capillaries as voids, Journal of applied mathematics, Vol 68 : 1203-1222, 2007.

Graham, D.R., and Higdon, J.J.L., Oscillatory forcing of flow through porous media. Part 1. Steady flow, Journal of fluid mechanics, Vol 465:213-235, 2002.

Grayson,P., Tajkhorshid, E., Schulten,K., Mechanisms of selectivity in channels and enzymes studied with interactive molecular dynamics, Biophysical Journal, Vol 85:36-48, 2003.

Gupte, A. R., Ph.D Dissertation, Karlsruhe, 1970.

Hall, M.J., and Hiatt, J.P., Measurements of pore scale flows within and exiting ceramic foams', Experiments in Fluids, Vol 20:433-440, 1996.

Hardy, J., de Pazzis, O., and Pomeau, Y., Molecular Dynamics of a Classical Lattice Gas Transport Properties and Time Correlation Functions, Physics Review A. Vol 13:1949-1961,1976.

Hayot, F., and Lakshmi, M.R., Cylinder wake in lattice gas hydrodynamics, Physica D., Vol 40: 415-420,1989.

Hénon, M., Isometric collision rules for the four-dimensional FCHC lattice gas, *Complex Systems*, Vol.1 pp475-494,1987.

Herzyk,P., Goodfellow, J.M., and Neidle, S., Molecular dynamics simulations of dinucleoside and dinucleoside drug crystal hydrates, Journal of biomolecular structure and dynamics, Vol 9:363-38, 1991.

Hlushkoua.D and Tallarek,U., Transition from creeping via viscous-inertial to turbulent flow in fixed beds, Journal of Chromatography A, Vol 1126: 70-85, 2006.

Holm, R., van Dijke, M.I.J., and Geiger, S., Three-Phase Flow Modelling Using Pore-Scale Capillary Pressures and Relative Permabilities for Mixed-Wet Media at the Continuum-Scale, Transport in porous media, Vol81 :423-442, 2010.

Horton, N,A., and Pokrajac,D., Onset of turbulence in a regular porous medium: An experimental study, Physics of Fluids, Vol. 21, paper 045104, 2009.

Hughes,B.D. and Sahimi,M., Random walks on the Bethe Lattice, J.Stat.Physics, Hughes Vol . 29, pp 781 - 794, 1982.

Humby,SJ., Biggs,MJ., & Tuzun,U., Explicit numerical simulation of fluids in reconstructed porous media. Chemical Engineering Science, Vol 57:1955–1968, 2002.

Hussain, A.K.M.F., and Hayakawa, Eduction of large-scale organized structures in a turbulent plane wake', Journal of Fluid Mechanics, Vol 180:193-229, 1987.

Ifiyenia.K., and J.Yuxiang, Flow through porous media of packed spheres saturated with water, Journal of Fluids Engineering, Vol 116:164-170, 1994.

Indakm, A.O., and Sahimi,M., Computer simulation of particle transport processes in flow through porous media, Chemcial Engineering Science, Vol 46:1977-1993, 1991.
Irmay.S., Theoretical model of flow through porous media, Symp.Transfer of water in porous media, Vol 29:36-43, 1965.

Jeong, J., and Hussain, F., On the identification of a vortex, Journal of Fluid Mechanics, Vol 285:69-94, 1995.

Jerauld, G.R.,.Hatfield, J.C., Scriven, L.E., and Davis, H.T., Percolation and conduction on Voronoi and triangular networks: a case study in topological disorder, J. Phys. C.: Solid State Phys., Vol17:1519-1529, 1984.

Jeulin, D., Introduction to Numerical Methods for the Simulation of Multi-phase and Complex Flows, ed. T.M.M. Verheggen, Springer-Verlag, Berlin, 1992.

Kadanoff, L.P., McNamara, G.R., and Zanetti, G., A poiseuille viscometer for lattice gas automata, Complex Systems, Vol 1:791-803, 1987.

Karapiperis, T., Cellular automaton model of precipitation/dissolution coupled with solute transport, J. Stat. Phys., Vol 81:165-174 J., Stat. Phys., Vol.81 pp165 1995.

Karniadakis.G., Numerical Simulations of forced convection heat transfer from a cylinder in crossflow, Int.J.Heat.Mass.Transfer Vol 31:107-118, 1988.

Kim,S.M., and Ghiaasiaan, S.M., Numerical modelling of laminar pulsating flow in porous media, Journal of fluids engineering, Vol 131: pages: 041203 -1-9,2009.

Kirsh, V.A., Stokes flow past periodic rows of porous cylinders , Theoretical foundations of Chemical Engineering, Vol 40:465-471, 2006.

Kohring,G.A., Effect of finite grain-size on the simulation of flow through porous-media. J. Phys. II 1 2 , pp. 87–90,1991a.

Kohring,G.A., Calculation of permeability of porous-media using hydrodynamic cellular automata. J. Stat. Phys. 63 1–2 , pp. 411–418,1991b.

Kohring, G.A., The cellular automata approach to simulating fluid-flows in porous media. Physica A 186 1–2 , pp. 97–108, 1992.

Knackstedt, M.A., and Zhang, X., Direct evaluation of length scales and structural parameters associated with flow in porous media. Physical Review E 50:2134–2138, 1994.

Lavallée, P., Boon, J.P., and Noullez, A., in Discrete Kinetic Theory, Lattice Gas Dynamics and Foundations of Hydrodynamics, ed. R. Monaco, World Scientific, pp 206-214, 1989.

Lavallée, P., Boon, J.P., and Noullez, A., Boundaries in Lattice Gas Flows, Physica D., Vol.47:233-240, 1991.
Liao, K.H., and Scheidegger, A.E., Statistical models of flow through porous media, Industrial and Engineering Chemistry, Vol 61:137-145, 1969.

Liu,S., and Masliyah, J.H., Principles of Single-Phase flow through porous media, Journal of American Chemical Society, 227-286, 1996.

Lock, P.A., Jing, X.D., Zimmerman, R.W., and Schlueter, E.M., Predicting the permeability of sandstone from image analysis of pore structure, Journal of applied physics, Vol 92:6311-6319, 2002.

Macdonald,I.F., El-Sayed, M. S., Mow,K., and Dullien, F.A.L., Flow through Porous Media-the Ergun Equation Revisited, Ind. Eng. Chem. Fundam., Vol. 18:199 - 207, 1979.

Manwart.C, Aaltosalmi, U., Koponen, A., Hilfer,R., and Timonen,J., Lattice-Boltzmann and finite-difference simulations for the permeability for three-dimensional porous media, Physical Review E, Vol 66: pages: 016702 ;1-11, 2002.

Margolus, N., Toffoli, T., and Vichniac, G., Cellular-Automata Computers for Fluid Dynamics Modelling, Physical Review Letters. Vol.56:1694-1696, 1986.

McCarthy, J.F., Flow through arrays of cylinders: Lattice gas cellular automata simulations, Physics of Fluids, Vol 6:435-437, 1994.

McNamara, G. R., and Zanetti. G., Use of the Boltzmann equation to simulate lattice-gas automata, Physical Review Letters, Vol 61(20), 2332-2335, 1988.

Molvig. K., Donis, P., Myczkowski, J., and Vichniac, G., Removing the discrete artifacts in 3D lattice gas fluids, in Discrete Kinetic Theory, Lattice Gas Dynamics and Foundation of Hydrodynamics, R. Monaco, ed. (World Scientific, 1989), p. 409.

Molvig.K, Donis, P., Miller, R., Myczkowski,J., and Vichniac, G., Multi-Species Lattice-Gas Automata for Realistic Fluid Dynamics Cellular Automata and the Modeling of Complex Physical Systems, Springer proceedings in Physics,Vol 46:206-231, 1990 .

Molvig, K., Particle Interaction processing system, Patent no # 5432718, 1994.

Mousavi, S.M., Jafari,A., Yaghmaei,S., Vossoughi,M., and Sarkomaa,P., Computer simulation of fluid motion in a porous bed using a volume of fluid method: Application in heap leaching, Minerals Engineering, Vol 19: 1077-1083,2006.

Mujica .R., Lattice gas wind tunnel, MSc thesis, MIT,1991.

Nield 1991, The limitations of the Brinkman-Forchheimer equation in modeling flow in a saturated porous medium and at an interface, International Journal of Heat and Fluid Flow ,Volume 12:269-272, 1991.
Nitsche, L.C., and Brenner, H., Eulerian kinematics of flow through spatially periodic models of porous media, Archive for rational mechanics and analysis, Vol 107, Pages: 225-292, 1989.

Nolan,G.T., and Kavanagh,P.E., Computer simulation of random packing of hard spheres, Powder Tech, 72:149-155, 1992.

Ogata, H., and Amano, K., Fundamental solution method for two-dimensional Stokes flow problems with one-dimensional periodicity, Japan journal of Industrial and applied mechanics, Vol. 27:191-215, 2010.

Okabe, H., and Blunt, M. J., Prediction of permeability for porous media reconstructed using multiple-point statistics, Physical Review E, Vol 70:6135 -145, 2004.

Øren, P. E., and Bakke, S., Process based reconstruction of sandstones and prediction of transport properties, Transp. Porous Media, Vol 46:311–343, 2002.

Pereira. J. C. F., Malico,I., Hayashi, T. C., and Raposo, J. M. F., Experimental and numerical characterization of the transverse dispersion at the exit of a short ceramic foam inside a pipe, Int. J. Heat Mass Transfer , Vol 48: 1-14, 2005.

Quartarone, E., Mustarelli, P., and Magistris, A., Transport properties of porous PVDF membranes , Journal of physical chemistry B, Vol 106:10828-10833, 2002.

Ramaswamy, S., Gupta, M., Goel, A., Aaltosalmi, U., Kataja, M., Koponen, A., and Ramarao, B. V., Efficient simulation of flow and transport in porous media, Colloids and Surfaces A: Physicochemical and Engineering Aspects 241 (1):323–333, 2004.

Rapaport, D. C., Interactive molecular dynamics, Physica A, Vol: 240:246-254, 1997.

Rapaport, D. C., An introduction to molecular dynamics simulation, Computer Simulations of Surface and Interfaces,Vol: 114:59-73, 2003.

Rashidi, M., Peurrung, L., Tompson, A. F. B., and Kulp, T. J., Experimental analysis of pore-scale flow and transport in porous media, Advances in Water Resources, vol. 19:163-180, 1996.

Rivet,J.P., and Boon, J.P., Lattice Gas Hydrodynamics, Cambridge University Press, 2001.

Roache, P. J., Computational Fluid Dynamics, Hermosa Publishers, 1976.

Rothman, D.H., and Keller, J. M., Immiscible cellular-automaton fluids, Jounral of Stastical Physics, Vol 52:1119-1127, 1988.

Rothman, D. H., and Zaleski, S., Lattice-gas models of phase separation: Interfaces, phase transitions, and multiphase flow, Review of Modern Physics, Vol 66:1417-1479, 1994.

Rothman, D. H., and Zaleski, S., Lattice-gas automata: Simple models of complex hydrodynamics, Cambridge University Press, UK, 1997.

Roy, A.G., Buffin-Belanger, T., Lamarre, H., and Kirkbride, A. D., Size, shape and dynamics of large-scale turbulent flow structures in a gravel-bed river, Journal of Fluid Mechanics, vol. 500, pp. 1-27,2004.

Rumpf, A., Gupte, A.R ., Translation into English from Chem. Ing. Tech. 1971, vol. 43 pp.367.

Rybka, R., Cieplak, M., D'Ortona, U., Salin, D., and Banavar, J.R., Cellular-automata studies of circular couette flows and chaotic mixing, Physical Review E., Vol 48:757-766, 1993.

Saenger, E. H., Ciz, R., Kruger, O. S., Schmalholz, S. M., Gurevich, B., and Shapiro, S. A., Finite- difference modeling of wave propagation on microscale: A snapshot of the work in progress, Geophysics, Vol 72:293-300, 2007.

Saito, M. B., and de Lemos, M. J. S., A correlation for interfacial heat transfer coefficient for turbulent flow over an array of square rods, Journal of heat transfer transactions, Vol 128:444-452, 2006.

Sahimi, M., Gavalas, G. R., Tsotsis, T.T., Statistical and continuum models of fluid solid reactions in porous media, Chemical Engineering Science, Vol 45:1443-1502, 1990.

Sahimi, M., and Stauffer, D., Efficient simulation of flow and transport in porous media, Chem. Eng. Science, Vol 46:2225-2233, 1991.

Sahimi, M., Transport of macromolecules in porous media, Journal of Chemical physics, Vol: 96:4718-4728, 1992.

Sahimi, M., Flow phenomena in rocks: from continuum models to fractals, percolation, cellular automata, and simulated annealing, Rev. Mod. Phys., Vol 65:1393-1534, 1993.

Sahimi, M., Flow and Transport in Porous Media and Fractured Rock: From Classical Methods to Modern Approaches, John Wiley, Hoboken, N. J, 1995.

Salem.J., and Wolfram, S., Theory and Applications of Cellular Automata, S.Wolfram ed., 382 ,World Scientific, 1986.

Sangani, A.S., and Acrivos, A., Slow flow through a periodic array of spheres, Int. J. Multiphase Flow, Vol 8:343-360, 1982.

Schrandt,R and S.Ulam, On recursively defined geometrical objects and patterns of growth, Essays on cellular automata, pages 232-243, University of Illinois, Urbana, 1970.

Schwartz, L.M., Martys, N., Bentz, D. P., Garboczi, E. J., and Torquato, S., Cross-property relations and permeability estimation in model porous media, Phys. Rev. E 48(1993) 4584.

Shimomura, T., Doolen, G.D., Hasslacher, B., and Fu, C., Los Alamos Science, Special Issue pp201-210 (1987); reprinted in: 'Lattice Gas Methods for Partial Differential Equations', ed. Doolen et al., Addison-Wesley, Redwood City-USA, pp3-9, 1990.

Shiyi Chen, Karen Diemer, Gary D. Doolen, Kenneth Eggert, Castor Fu, Semion Gutman and Bryan J. Travis, Lattice gas automata for flow through porous media, Physica D: Nonlinear Phenomena, Vol 47:72-84,1991c.

Slichter,S.C, Theoretical investigations of the motion of ground water, U.S.Geological Survery, 19th Annual Report, Part2, pp295,1899.

Sokolovskii, R. O., Cates, M. E., and Sokolovska, T. G., Model fluid in a porous medium: Results for a Bethe lattice, Physical Review E, Vol 68,026124 :1 -13, 2003.

Spielman, L. A., and Goren, S.L., Progress in induced coalescence and a new theoretical framework for coalescence by porous media, Industrial and Engineering Chemistry, Vol 62:10-24 , 1970.

Stauffer,D., Computer simulations of cellular automata, J.Phys.A:Math.Gem, Vol 24: 909-927,1991.

Sterling, J. D., and Chen, S., Stability analysis of lattice boltzmann methods, Journal of Computational Physics, Vol 123:196-206, 1996.

Strigle, R. F., Jr., Packed TowerDesign and Applications: Random and Structured Packings, Gulf Publishing, Houston 1994.

Tanino, Y., Nepf, H. M., Lateral dispersion in random cylinder arrays at high Reynolds number, Journal of Fluid Mechanics, vol. 600: 339-371, 2008.

Tennekes, H., and Lumley, J. L., A First Course in Turbulence, The MIT Press, Cambridge, USA, 1972.

Teixeira, C.M., Continuum limit of Lattice gas fluid dynamics, PhD Thesis, 1992.

Thompson,P., and Robbins,M.,To Slip or Not to Slip?, Physics World, pp 35, 1990.

Torelli, L., and Scheidegger, A.E., Three-dimensional and branching-type models of flow through porous media, J. Hydro. Vol.15:23-35, 1972.
Tory, E. M., Cochraine, N.A., and Wadell, S. R., Anisotropy in Simulated Random Packing of Equal Spheres, Nature, Vol 220:1023-1024, 1968.

Tritton, D. J., Experiments on the flow past a circular cylinder at low Reynolds numbers, Journal of Fluid Mechanics Vol 6:547-567, 1959.

Vafai.K., and Kim, S.J., Fluid Mechanics of the Interface Region between a Porous Medium and a Fluid Layer: an Exact Solution, International Journal of Heat and Fluid Flow, Vol. 11: 254-256, 1990.

Vafai , On the limitations of the Brinkman-Forchheimer-extended Darcy equation, International Journal of Heat and Fluid Flow ,Vol 16: 11-15,1995.

Van Genabeek, O., and Rothman, D. H., Macroscopic manifestations of microscopic flows through porous media: Phenomenology from simulation, Annual Review of Earth and Planetary Sciences, Vol 24:63-87, 1996.

Wolf-Gladrow, D. A., Lattice gas cellular automata and lattice Boltzmann models: an introduction, Springer-Verlag, Heidelberg, 2000.

Wolfram, S.,'Lattice Gas Methods for Partial Differential Equations', Journal of Statistical. Physics., Vol 45: 471-526, 1986.

Wong, P., Statistical physics of sedimentary rock, Phys. Today, Vol 41: 24-25, 1998.

Worthing, R. A., Mozer, J., and Seeley, G., Stability of lattice Boltzmann methods in hydrodynamic regimes, Physical Review E, Vol 56: 2243-2253, 1997.

Yao, K., Habibian, M.T., and O'Melia, C.R., Water and wastewater filtration: Concepts and applications, Environ. Sci. Technol. Vol 5: 1105-1112, 1971.

Yevseyev, A. R., Nakoryakov, V. E., Romanov, N. N., Experimental investigation of a turbulent filtration flow, International Journal of Multiphase Flow, vol 17(1):103-118,1991.

Yanuka, M., Dullien,F.A.L., and Elrick, D. E., Percolation processes and porous media: Geometrical and topological model of porous media using a three-dimensional joint pore size distribution, J.Colloid Interface Sci, 112,24-41, 1986.

Zanetti, G. Hydrodynamics of Lattice-Gas Automata, Physical Review A. Vol 40:1539-1548, 1989.

Zick, A. A., Homsy, G.M., Stokes flow through periodic arrays of spheres, Journal of Fluid Mechanics, Vol 115:13-26, 1982.

List of Publications

In preparation

[1] GI- LGA model of non creeping single phase flow through a porous medium and hydrodynamic properties prediction

[2] Ab *initio* prediction of interstitial flow through random sphere packing.